



CENTER FOR INFRASTRUCTURE ENGINEERING STUDIES

SEISMIC UPGRADE OF BEAM- COLUMN SUBASSEMBLAGES WITH COMPOSITES

By

ANDREA PROTA

University of Missouri-Rolla

**CIES
02-29**

Disclaimer

The contents of this report reflect the views of the author(s), who are responsible for the facts and the accuracy of information presented herein. This document is disseminated under the sponsorship of the Center for Infrastructure Engineering Studies (CIES), University of Missouri -Rolla, in the interest of information exchange. CIES assumes no liability for the contents or use thereof.

The mission of CIES is to provide leadership in research and education for solving society's problems affecting the nation's infrastructure systems. CIES is the primary conduit for communication among those on the UMR campus interested in infrastructure studies and provides coordination for collaborative efforts. CIES activities include interdisciplinary research and development with projects tailored to address needs of federal agencies, state agencies, and private industry as well as technology transfer and continuing/distance education to the engineering community and industry.

Center for Infrastructure Engineering Studies (CIES)
University of Missouri-Rolla
223 Engineering Research Lab
1870 Miner Circle
Rolla, MO 65409-0710
Tel: (573) 341-6223; fax -6215
E-mail: cies@umr.edu
www.cies.umr.edu

**SEISMIC UPGRADE OF BEAM-COLUMN
SUBASSEMBLAGES WITH COMPOSITES**

by

ANDREA PROTA

A THESIS

Presented to the Faculty of the Graduate School of the

UNIVERSITY OF MISSOURI-ROLLA

In Partial Fulfillment of the Requirements for the Degree

MASTER OF SCIENCE IN CIVIL ENGINEERING

2001

Approved by

Dr. Antonio Nanni, Advisor

Dr. Pedro Silva

Dr. Lokeswarappa R. Dharani

Abstract

Many gravity load designed reinforced concrete frames are nowadays located in seismic areas. Their design carried out without seismic provisions generally results in an unsatisfactory response during earthquake events. The main issues related to the behavior of such structures are outlined in Chapter 1. Then, Chapter 2 discusses strengthening strategies suggested by the main seismic guidelines; different upgrade methodologies are also summarized distinguishing those based on traditional and composite materials, respectively. A brief summary of tests on interior connections is proposed with particular attention to used test setup.

Chapters 3 and 4 deal with the proposed upgrade technique based on the use of composites. The innovative aspect of combining FRP bars and laminates is underlined and developed tests are detailed. The technique is based on using near surface mounted (NSM) FRP rods providing flexural strengthening and lay-up laminates improving the confinement of columns and the strength of the joint. Test results are discussed in Chapter 5 and the influence of the FRP strengthening on strength and/or ductility is assessed. Overall, experimental results showed that such technique could become a promising and sound methodology for the upgrade of RC connections, provided that constructability issues are also addressed. Along with the discussion on global performance, the analysis of stresses in the joint is carried out in order to define failure criteria for the design of the connection upgrade.

TABLE OF CONTENTS

	Page
ABSTRACT	1
ACKNOWLEDGMENT	2
NOTATIONS	3
LIST OF FIGURES	4
LIST OF TABLES	12
SECTION	
1. INTRODUCTION AND BACKGROUND ON GLD SUBASSEMBLAGES	14
2. UPGRADE TECHNIQUES AND TESTS ON GLD SUBASSEMBLAGES	20
3. PROPOSED UPGRADE TECHNIQUE FOR GLD SUBASSEMBLAGES	30
4. TESTING CONFIGURATION AND RESULTS	55
5. DISCUSSION AND ANALYSIS OF THE SEISMIC UPGRADE OF GLD SUBASSEMBLAGES	73
6. CONCLUSIONS	
7. REFERENCES	99
APPENDICES	
A. SPECIMEN FABRICATION	A.1
B. TESTING	124
C. DIAGRAMS	154

Notation List

- A_{col} , gross area of the column cross section, mm^2 .
 A_g , area of the gross cross section, mm^2 .
 A_s , area of tension reinforcement, mm^2 .
 A'_s , area of compression reinforcement, mm^2 .
 b , width of the member, mm.
 C_c, C'_c , compression stress resultants of beams, kN.
 C_s, C'_s , compression stress resultants in the steel of beams, kN.
 d , distance from extreme compression fiber to centroid of tension reinforcement, mm.
 d_{max} , maximum gravel size in concrete, mm.
 d_v , longitudinal bar diameter, mm.
 d_t , diameter of the tie, mm.
 f'_c , compressive strength of concrete, MPa.
 f_b , average axial stresses in beam direction, MPa.
 f_v , average axial stresses in column direction, MPa.
 p_c , principal compression stress in the joint, MPa.
 p_t , principal tension stress in the joint, MPa.
 P , axial load on the column, kN.
 T, T' , the tensile stress resultants of beams, kN.
 v_j , nominal joint shear stress, MPa.
 V_1 , current shear applied to beam 1 at any cycle of loading, kN.
 V_2 , current shear applied to beam 2 at any cycle of loading, kN.
 V_{col} , average of column shears above and below the joint, kN.
 V_{jh} , horizontal joint shear force, kN.
 V_{jv} , vertical joint shear force, kN.
 V_v , gravity beam load, kN.
 ρ , ratio of tension reinforcement = A_s/bd .
 ρ' , ratio of compression reinforcement = A'_s/bd .
 D , bar size, mm.

List of Figures

Figure 1. 1 Concrete crushing and buckling of steel rebars

Figure 1. 2 Failure of an exterior joint

Figure 2. 1 Typical strengthening methods (Sugano, 1997)

Figure 2. 2 Test setup used by Beres et al. (1992)

Figure 2. 3 Test setup used by Durrani and Wigth (1985)

Figure 2. 4 Test setup used by Hakuto et al. (2000)

Figure 1. 3 Weak column-strong beam construction

Figure 3. 1 Laminates installed in different regions of the connection

Figure 3. 2 NSM rods in the columns (a) and joint (b)

Figure 3. 3 Geometry and reinforcement of the specimen

Figure 3. 4 Carbon FRP rods.

Figure 3. 5 Anchor detail on the top cross head

Figure 3. 6 Typical test setup

Figure 3. 7 Carbon FRP rods

Figure 3. 8 C1-30 fibers on the left; scheme of wet lay up system on the right

Figure 3. 9 Monitored debonding zones on specimens H2 and H2U

Figure 3. 10 Primer injection of bubbles by a syringe

Figure 3. 11 Front view of upgraded subassemblages

Figure 3. 12 Cross section of column

Figure 3. 13 Upgrade scheme type 4

Figure 3. 14 Cross section of beam

Figure 3. 15 Upgrade scheme type 5

Figure 4. 1 Test setup

Figure 4. 2 Scheme of loads application before inversion of beam shear

Figure 4. 3 Loads application after inversion of beam shear

Figure 4. 4 Alternatives for seismic load application (Park, 1994)

Figure 4. 5 Load history

Figure 4. 6 LVDT locations

Figure 4.7 Strain gages on the column wrapping

Figure 4. 8 Cracks at failure in the panel of subassemblage H2U

Figure 5. 16 Equilibrium of interior joint (Paulay and Priestley, 1992)

Figure 5. 2 Crushing of the diagonal strut at failure of specimen L3

Figure 5. 3 Kupfer and Gerstle curve : theoretical vs. experimental

Figure 5. 4 Confinement defect on the superior column of connection H2U

Figure 5. 5 Column shear vs. story drift angle at cracking of the joint (left hand side) and
at failure of the subassemblage (right hand side)

Figure A.1 Typical formworks: on the left H3, on the right H1

Figure A.2 Typical beam reinforcement

Figure A.3 Typical metallic reinforcement of the nodal zone

Figure A.4 Typical stirrup spacing of the column

Figure A.5 Wooden predisposition for NSMR: L3, L4, H3, H4, H5, M3

Figure A.6 View of the beam prior to concrete casting: L4

Figure A.7 Induced confinement defect in the column: H2U

Figure A.8 Concrete vibration: H1

Figure A.9 After casting: on the left H1, on the right H4

Figure A.10 Rounding of the corners prior to laminates application

Figure A.11 Rounded corner

Figure A.12 Primer application

Figure A.13 Filling of holes and imperfections by putty

Figure A.14 Impregnation of fibers by saturant

Figure A.15 Drilling through the panel prior to installation of NSM rods

Figure A.16 Joint prepared for the installation of NSM rods

Figure A.17 Blowing of the grooves

Figure A.18 Hand cleaning of the grooves

Figure A.19 Pouring of the first layer of concrete paste into the grooves

Figure A.20 Installation of NSM FRP rod

Figure A.21 Filling of the grooves after rod installation

Figure A.22 Finishing of the surface after installation of NSM rods

Figure A.23 Joint after installation of NSM rods has been completed

Figure A.24 NSM FRP rods as horizontal reinforcement of the panel

Figure A.25 NSM rods installed into the columns and the panel

Figure A.26 Application of carbon laminate as vertical reinforcement of the panel

Figure A.27 Completed upgrade of joints L4 and H4

Figure A.28 Curing of the primer prior to putty application

Figure A.29 Curing of putty prior application of saturant

Figure A.30 U-wrapping of beam around its bottom surface: joint H5

Figure A.31 View of the top surface of the beam: joint H5

Figure B.1 Restraint at the column end

Figure B.2 Test setup view from the inferior column

Figure B.3 Test setup view from the superior column

Figure B.4 LVDT transducers on both columns and beams

Figure B.5 Initiation of flexural cracks in the beam: joint L1

Figure B.6 Propagation of flexural cracks in the beam: joint L1

Figure B.7 Initiation of shear cracks in the panel: joint L1

Figure B.8 Initiation of flexural cracks in the columns: joint L1

Figure B.9 Propagation of shear cracks in the panel: joint L1

Figure B.10 Column failure: joint L1

Figure B.11 Lateral view of failed column: joint L1

Figure B.12 Crack pattern at failure: joint L1

Figure B.13 Flexural cracks in the beams: joint H1

Figure B.14 Initiation of shear cracks in the panel: joint H1

Figure B.15 Opening of flexural cracks in the columns: joint H1

Figure B.16 Lateral view of failed column: joint H1

Figure B.17 Failure of the columns: joint H1

Figure B.18 Crack pattern at failure: joint H1

Figure B.19 Initiation of shear cracks in the panel: joint L2

Figure B.20 Propagation of shear cracks in the panel: joint L2

Figure B.21 Tension failure of the columns: joint L2

Figure B.22 Top view of the failure regions: joint L2

Figure B.23 Lateral view of failed column: joint L2

Figure B.24 Initiation of diagonal cracks in the panel: joint H2

Figure B.25 Propagation of diagonal cracks in the nodal zone: joint H2

Figure B.26 Initiation of shear cracks in the panel: joint H2L

Figure B.27 Propagation of shear cracks in the panel: joint H2L

Figure B.28 Initiation of diagonal cracks in the nodal zone: joint H2U

Figure B.29 Shear cracks in the panel: joint H2U

Figure B.30 Panel damage: joint H2

Figure B.31 Completed upgrade of joints L4 and H4

Figure B.32 Bottom view of panel damage: joint H2

Figure B.33 Panel damage: joint H2U

Figure B.34 Tension failure of column: joint H2

Figure B.35 Tension failure of column: joint H2U

Figure B.36 Combined panel-column failure: joint H2

Figure B.37 Initiation of fibers breaking in column compression region: joint H2

Figure B.38 Shear failure of the panel: joint H2L

Figure B.39 Carbon fibers breaking in compression region of column: joint H2L

Figure B.40 Initiation of diagonal cracks in the panel: joint L3

Figure B.41 Propagation of shear cracks in the panel: joint L3

Figure B.42 Top view of shear failure of the panel: joint L3

Figure B.43 Shear failure of the panel: joint L3

Figure B.44 Shear failure of the panel: joint H3

Figure B.45 Damage due to panel shear failure: joint H3

Figure B.46 Panel shear failure: joint M3

Figure B.47 Top view of joint M3 at failure

Figure B.48 Separation at panel-superior column: joint L4

Figure B.49 Lateral view of the superior column at failure: joint L4

Figure B.50 Separation at panel-inferior column: joint L4

Figure B.51 Top view of joint L4 at failure

Figure B.52 View from the superior column at failure: joint H4

Figure B.53 Separation at panel-superior column: joint H4

Figure B.54 View from the inferior column at failure: joint H4

Figure B.55 Separation at panel-inferior column: joint H4

Figure B.56 View from the superior column at failure: joint H5

Figure B.57 Separation at interface panel-superior column: joint H5

Figure B.58 Joint H5 at failure

Figure C.1 Column shear-displacement: L1

Figure C.2 Column shear-story drift: L1

Figure C.3 Column shear-displacement: H1

Figure C.4 Column shear-story drift: H1

Figure C.5 Column shear-displacement: L2

Figure C.6 Column shear-story drift: L2

Figure C.7 Inferior column moment-laminate strain: L2

Figure C.8 Inferior column moment-laminate strain: L2

Figure C.9 Superior column moment-laminate strain: L2

Figure C.10 Superior column moment-laminate strain: L2

Figure C.11 Column shear-story drift: H2

Figure C.12 Inferior column moment-laminate strain: H2

Figure C.13 Inferior column moment-laminate strain: H2

Figure C.14 Superior column moment-laminate strain: H2

Figure C.15 Superior column moment-laminate strain: H2

Figure C.16 Column shear-displacement: H2U

Figure C.17 Column shear-story drift: H2U

Figure C.18 Inferior column moment-laminate strain: H2U

Figure C.19 Inferior column moment-laminate strain: H2U

Figure C.20 Superior column moment-laminate strain: H2U

Figure C.21 Superior column moment-laminate strain: H2U

Figure C.22 Column shear-displacement: L3

Figure C.23 Column shear-story drift: L3

Figure C.24 Inferior column moment-laminate strain: L3

Figure C.25 Inferior column moment-laminate strain: L3

Figure C.26 Superior column moment-laminate strain: L3

Figure C.27 Superior column moment-laminate strain: L3

Figure C.28 Column shear-displacement: H3

Figure C.29 Column shear-story drift: H3

Figure C.30 Column shear-displacement: M3

Figure C.31 Column shear-story drift: M3

Figure C.32 Inferior column moment-laminate strain: M3

Figure C.33 Inferior column moment-laminate strain: M3

Figure C.34 Superior column moment-laminate strain: M3

Figure C.35 Superior column moment-laminate strain: M3

Figure C.36 Column shear-displacement: L4

Figure C.37 Column shear-story drift: L4

Figure C.38 Inferior column moment-laminate strain: L4

Figure C.39 Inferior column moment-laminate strain: L4

Figure C.40 Superior column moment-laminate strain: L4

Figure C.41 Superior column moment-laminate strain: L4

Figure C.42 Column shear-displacement: H4

Figure C.43 Column shear-story drift: H4

Figure C.44 Inferior column moment-laminate strain: H4

Figure C.45 Inferior column moment-laminate strain: H4

Figure C.46 Superior column moment-laminate strain: H4

Figure C.47 Superior column moment-laminate strain: H4

Figure C.48 Column shear-story drift: comparison for series L connections

Figure C.49 Column shear-story drift: comparison for series H connections

Figure C.50 Column shear-story drift: comparison for type 1 connections

Figure C.51 Column shear-story drift: comparison for type 2 connections

Figure C.52 Column shear-story drift: comparison for type 3 connections

Figure C.53 Column shear-story drift: comparison for type 4 connections

List of Tables

Table 3. 1 Average compressive stress of the superior column

Table 3. 2 Compressive concrete strength of all specimens

Table 3. 3 Yield strength of reinforcing steel

Table 3. 4 Mechanical properties of C-Bar rods.

Table 3. 5 Mechanical properties of Galileo rods.

Table 3. 6 Tensile properties of used resins

Table 3. 7 Summary of upgrade schemes

Table 4. 1 Experimental outcomes for specimens L1 and H1

Table 4. 2 Strain measurements for specimen L2

Table 4. 3 Average crack width: specimen H2U

Table 4. 4 Experimental outcomes for specimens L2, H2 and H2U

Table 4. 5 Strain measurements for subassemblage H2

Table 4. 6 Strain measurements for subassemblage H2U

Table 4. 7 Strain measurements for subassemblage L3

Table 4. 8 Strain measurements for subassemblage M3

Table 4. 9 Experimental results for subassemblages L3, H3 and M3

Table 4. 10 Strain measurements for subassemblage L4

Table 4. 11 Experimental results for subassemblages L4 and H4

Table 4. 12 Strain measurements for subassemblage H4

Table 5. 1 Comparison between series L specimens

Table 5. 2 Comparison between series H specimens

Table 5. 3 Nominal shear stresses and column shear at cracking of the joint
and ultimate of the subassemblage

Table 5. 4 Principal stresses and column shear at cracking of the joint and ultimate of
the subassemblage

1. INTRODUCTION AND BACKGROUND ON RC GLD FRAMES

1.1 INTRODUCTION

The present thesis focuses on problems related to the seismic upgrade of reinforced concrete (RC), gravity load designed (GLD) frames and, in particular, on beam-column connections. ACI-ASCE 352 R defines them as interior, exterior or corner connections depending on their vertical and horizontal position within the structure. The work herein presented deals with interior RC subassemblages.

In order to strengthen such connections, an innovative technique based on the use of composites is proposed and validated by means of an experimental program. Composite materials, known as fiber reinforced polymers (FRP), have shown a great potential for the strengthening of reinforced concrete structures in the forms of:

- Lay-up laminates externally bonded to a concrete member to increase flexural and shear capacity as well as to provide concrete confinement [Alkhrdhaji et al. 1999], and
- Near surface mounted (NSM) reinforcement to increase flexural and shear strength [De Lorenzis et al. 2000].

The basic idea for the work of the present thesis was to evaluate the opportunities offered by using FRP laminates and NSM rods for strengthening RC GLD subassemblages in order to finally compile design and construction guidelines on their seismic retrofitting and upgrade with composite materials.

1.2 BACKGROUND ON RC GLD FRAMES

The upgrade of the seismic performance of existing RC GLD frames represents an important issue that involves economic and social aspects in different areas of the world

like, for example, Europe, USA and Japan. In fact, RC frames, designed without seismic provisions, are often characterized by an unsatisfactory structural behavior due to the low available ductility and the lack of a hierarchy of strength inducing global failure mechanisms.

The overall design of such GLD structures could be insufficient and some basic requirements (i.e., in plan and vertical regularity, or absence of any soft story) missed; very often constructive details could be poor (i.e. low percentage of stirrup, poor bond conditions). This results in critical zones (such as beam-column joints, footing zone of beam-column) with no ductile behavior, showing brittle failure modes (i.e. pull-out or buckling of bars, shear failure, etc.). Such constructive details can be pointed out as potential critical causes of brittle failure mechanisms, which are sensitive to the cyclic damage.

For beams, the major problem concerns the ends where brittle shear failure could occur under earthquake due to the superposition of shear forces (i.e., gravity and seismic loads) and to the low amount of steel reinforcement. The non-linear shear-bending interaction plays a major role in this type of mechanism that can lead to a small global ductility.

For what concerns columns, the lack of appropriate size and spacing of ties, which does not guarantee the required level of confinement, can cause the collapse of the column end, resulting in crushing of the not confined concrete, instability of the steel reinforcing bars in compression and pull out of those in tension. An example is shown in Figure 1.1, depicting a column damaged during the 1999 Turkish earthquake. In general, the design of columns only for vertical load lead to interior column with large cross

sectional area and amount of steel reinforcement inadequate to satisfy flexural and shear demand generated during an earthquake. This results in interior columns with high stiffness and low strength, and, in terms of global mechanisms, high potential for the formation of plastic hinges at the ends.

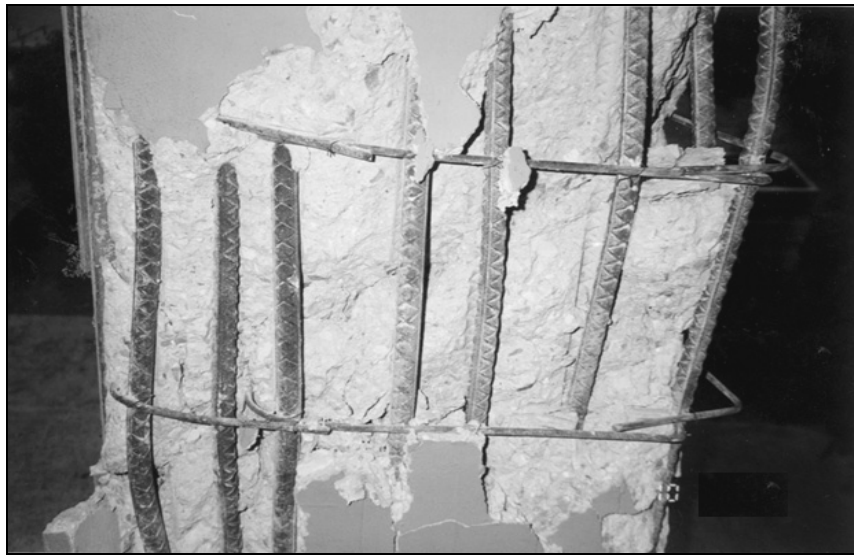


Figure 1. 1 Concrete crushing and buckling of steel rebars

A critical region in RC frames is the beam-column connection, where different constructive details can originate local failures, such as shear collapse of the joint due to the lack of transverse reinforcement. Figure 1.2 provides an example of such crisis occurred on an RC exterior joint during the 1999 Turkish earthquake.

In general, the lack of a design based on the strength hierarchy influences the global behavior of GLD frames and is responsible for the low dissipative capacity (Cosenza and Manfredi [1997], White and Mosalam [1997]). This typically results in a weak column-strong beam construction that, under a seismic event, yields most likely to the formation of local hinges in the columns. Such failure mode represents the lower bound of the hierarchy of strength because it is characterized by brittle and catastrophic

structural crisis (Bracci & al. [1992]). Figure 1.3 shows an example of such failure mode of the column occurring in presence of a stiffer beam or horizontal floor system.



Figure 1. 2 Failure of an exterior joint

The seismic upgrade of GLD structures should aim at strengthening its members, allowing more strength and/or ductility and energy dissipation. The final objective could be obtained selecting the local upgrade of members in order to achieve a ductile global behavior. As mentioned, the lower bound of the frame behavior pertains to column failure and it could represent a typical condition of such structures.

The upgrade of columns by providing them with higher confinement level and/or with more flexural reinforcement could cause the failure to occur in the nodal zone. Calvi et al. (2001) underlined that, in the case of interior connections, moving the crisis from the column to the joint can improve the global behavior of the frame, even though

the effects of the brittle shear crisis of the joint on the global behavior of the frame needs to be carefully evaluated.



Figure 1. 3 Weak column-strong beam construction

In order to move up along the hierarchy of strength, the panel should also be strengthened. The upgrade of both column and panel could allow moving from the previous intermediate level of the hierarchy of strength (i.e., shear failure of the joint) to its upper bound (i.e., crisis of the beams). Inducing such failure mode would be the best result of a seismic repair/strengthening. Formation of plastic beam hinges would mean that a ductile and very effectively energy dissipating mechanism be achieved.

The upgrade technique proposed within this context was developed in order to improve the evidenced local lacks of GLD frames, without neglecting the effects on their seismic global behavior. In order to validate such methodology, an experimental program was conducted. Before detailing on performed tests (in Chapter 3), an overview

is provided in following Chapter 2 on strengthening techniques already available in the literature and tests that other researchers conducted on RC GLD interior connections.

2. UPGRADE TECHNIQUES AND TESTS ON GLD SUBASSEMBLAGES

2.1 SEISMIC UPGRADE STRATEGIES

Different alternatives could be selected for seismic strengthening of deficient RC structures. In general, seismic upgrade is designed in order to increase the strength, or the ductility, or both strength and ductility; the effort toward the satisfaction of seismic performance can be achieved by different means, as summarized by Sugano [1997] and depicted in Figure 2.1.

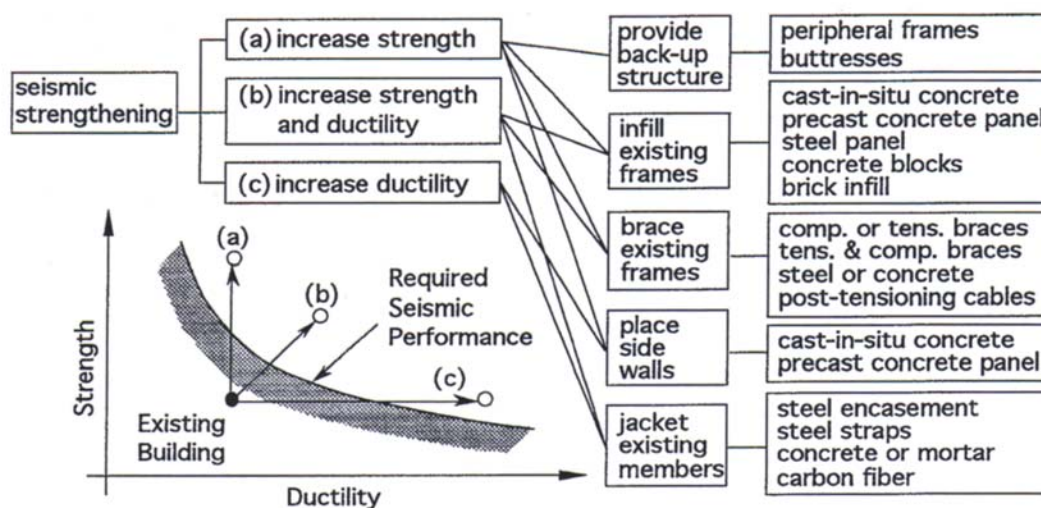


Figure 2. 1 Typical strengthening methods (Sugano, 1997)

Seismic guidelines, such as FEMA 273 [1997], outline the following strategies that engineers would pursue depending on specific structural properties and lacks:

- Local Modification of Components: this is the most economical approach to rehabilitation and it can be followed when only a few of the building's components do not provide satisfactory seismic performance. Such local modifications do not change the original configuration of the lateral-force resisting frame and are aimed at

- eliminate local lacks in order to achieve a desirable hierarchy of strength within the frame. The strengthening of a component influences the global mechanisms and could allow to move from potential brittle failure modes to mechanisms of crisis characterized by more ductility and energy dissipation capacity.
- Removal or Lessening of Existing Irregularities and Discontinuities: compared to the previous strategy, this is more invasive since it is based on demolition or reduction of structural portions determining stiffness, mass or strength irregularities, or discontinuities (i.e., soft or weak story, termination of a perimeter shear wall above the first story, etc.). Such approach is necessary in cases when the assessment of the deficient frame underlines unbalanced values of structural displacements or inelastic deformation demands.
 - Global Structural Stiffening: addition of new braced frames or shear walls are typical techniques used for seismic upgrade of structures characterized by elements with inadequate toughness under seismic lateral loads. In this cases, the most appropriate choice is to stiffen the structure in order to achieve a response with reduced lateral deformation.
 - Global Structural Strengthening: this is a strategy very effective for structures showing inelastic behavior at low levels of seismic shaking. This is due to their inadequate strength to withstand lateral loads generated by the ground motion. The addition of braced frames and shear walls can allow such frames to increase the level of carried loads corresponding to a given damage. Generally, the design philosophy of added structures aims at providing additions a lot stiffer than the original structure and then carrying the majority of lateral loads.

- **Mass Reduction:** this strategy has something in common with the above mentioned removal of existing portions. The reason for demolishing components or parts is to reduce the structural mass and then decrease the demand in terms of force and deformation which is due to a seismic event.
- **Seismic Isolation:** inserting bearings between superstructure and foundations represents an effective remedy in cases of stiff buildings with large mass and high values (i.e., historical, contents, equipment or functional value). In this way, seismic actions are concentrated on energy dissipating damping and the superstructure performs almost as a rigid body when earthquake comes.
- **Supplemental Energy Dissipation:** the insertion of energy dissipation devices is generally selected for relatively flexible structures with some inelastic deformation capacity. Such systems are mainly added as components of braced frames and, depending of specific characteristics, they provide static or dynamic stiffness to the structure. A careful assessment needs to be performed prior to installing these devices in order to check that the reduction of structural displacement does not result in a too huge increase of forces on the frame.

2. 2 LOCAL UPGRADE BY TRADITIONAL TECHNIQUES

Within the above mentioned set of possible strategies, the attention is herein focused on the local upgrade since this is the basic concept for the innovative technique discussed in following chapters. The scope of the present section is to summarize the main methodologies traditionally used for local strengthening of RC members in seismic areas.

- Reinforced Concrete Jacketing: this has been a common technique mainly for strengthening columns, even though applications on beams have also been performed (Alcocer [1993]). It is generally accomplished by encasing the member with a new RC jacket. In order to realize it, the surface of the upgraded member needs to be roughened and a new steel cage is placed around it; forms are then built prior to pouring new concrete. From a structural stand point, the main issue is related to the actual bond between new and existing structure: if concrete shrinks and some cavities are left at interface, no proper bond could be ensured (Corazao and Durrani [1989]). Also, the mass increase could worsen the overall seismic response of the frame. From a constructability stand point, such technique has a strong impact on occupants, requires minimum times for concrete curing and implies loss of room compared to original dimensions of the structural bone.

Tests have been performed in order to validate the structural benefits of such technique on RC members. Rodriguez and Park [1994] strengthened square columns 350 mm x 350 mm with a 100 mm thick concrete jacket reinforced with eight new bars bundled into the corners of the jacket and new square hoops. Stoppenhagen et al. [1995] adopted the same technique for strengthening of columns by encasing original members with new columns containing longitudinal and shear steel reinforcement. UNDP/UNIDO RER/79/015 [1983] recommended that, when RC jacketing is done on columns, appropriate details are also prescribed in order to guarantee the stress diffusion to beams and beam-column joints.

- Steel Profile Jacketing: another technique developed for column strengthening was based on placing four longitudinal steel angle profiles at each corner and then connecting

them together in a skeleton with transverse steel straps (UNDP/UNIDO [1983]). Even though a protection realized either with normal concrete or shotcrete generally completed the installation, corrosion and fire were still crucial issues for such technique, along with mass increase and difficulty on the perfect engagement of the old column in order to guarantee the collaboration of the new portion.

- Steel Encasement: the encasement of columns with welded steel plates between 4 mm and 6 mm thick has been used in order to increase the flexural strength, ductility and shear capacity of these members (Bracci et al. [1992]). Such plates had a small distance from the existing column and the resultant void was filled with non-shrinking concrete. In applications on rectangular columns four vertical steel plates have been connected by four welded angle profiles. Even though this technique does not imply too much increase of column size, durability and fire resistance problems, as well as issues related to stress transfer through adjacent members were still considered as weak aspects of such method (UNDP/UNIDO [1983]). Ghobarah et al. [1997] extended this technique to the upgrade of beam-column connections. They proposed to apply grouted corrugated steel jackets to both beam and column; steel angles anchored to concrete by anchor bolts and welded to steel jackets were also placed in order to resist lateral pressure. The writer does not feel comfortable with such proposal that prescribes complete wrapping of beams, which is in reality very hard to achieve due to the presence of floor system on the top surface.

2. 3 LOCAL UPGRADE BY USING FRP COMPOSITES

In the last years, FRP composites are entering the retrofit market and they are increasing their competitiveness over traditional materials: the high mechanical

properties, the easy and fast installation, low maintenance costs, and high resistance to corrosion and aggressive environments, and low weight make them very promising for seismic strengthening of RC elements and structures. At date, the majority of field applications are in the confinement of columns and bridge piers, even though some applications to beam-column joints or column-footing joints have been proposed. The effectiveness of this technique was assessed by Wang and Restrepo [2001] who used glass FRP laminates for wrapping circular columns.

Pantelides et al. [2000a] and Antonopulos et al. [2001] extended this technique to the strengthening of building exterior joints; also in this case the writer does not agree on upgrade solutions based on covering the top surface of beams as well as extending FRP laminates from the joint on the column: in both cases, the presence of a floor system would make the proposed scheme not applicable in the field. On the other hand, such issues are not present when discussing about bridge piers, since it is possible to work around them. Pantelides et al. [2000b] validated the effectiveness of carbon fiber laminates by an in-situ bridge test on column-cap beam joints wrapped with FRP laminates.

2. 4 TEST ON RC INTERIOR SUBASSEMBLAGES

The present section deals with tests on interior RC beam-column connections reported in literature and outlined beneath. Their analysis provided an important background for the design of the performed experimental program.

A series of tests on 20 interior beam-column subassemblages were performed by Beres et. al [1992]. Full-scale specimens with square columns 406 mm X 406 mm and

beams with dimensions 355 mm x 610 mm were built. Load application was based on a testing frame, showed in Figure 2.2. After gravity load were applied, seismic actions were cyclically generated by varying shear forces acting on the beams. For each level of load, three cycles were imposed, keeping constant the algebraic sum of beam forces and compressive axial force on the top column. Different constructive details characterized tested connections in order to assess the influence on the global behavior played by spliced and unspliced longitudinal column bars, joint reinforcement, discontinuous positive beam rebars, axial load level on columns, amount of column reinforcement and concrete strength. Since column ends were not moved and seismic loads were applied by beam shear variation, interstory drift (i.e., relative lateral displacement between two adjacent floors divided by the story height of the frame) was computed from displacement measured on beams.

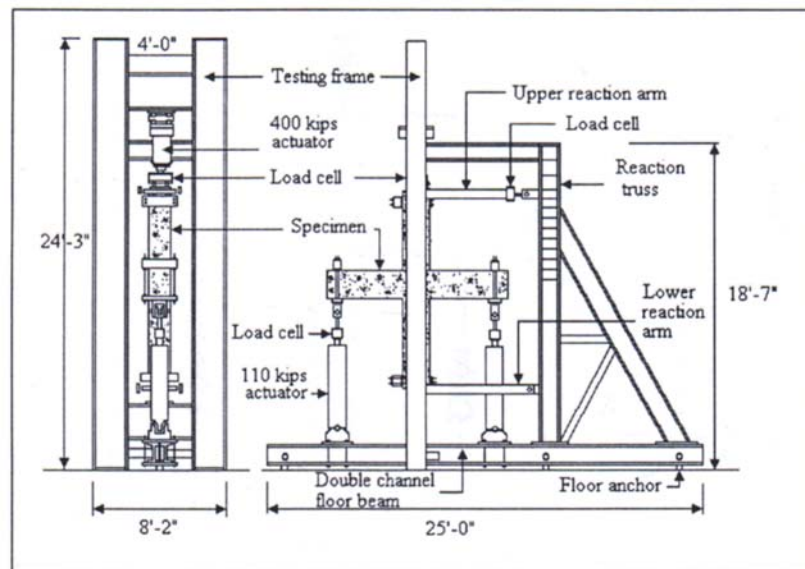


Figure 2. 2 Test setup used by Beres et al. (1992)

A similar setup was used by Tabata and Nakachi [1996] for tests on full-scale interior RC subassemblages characterized by square columns 400 mm x 400 mm and beams 300 mm wide and 400 mm high. Also in this case, columns were pinned at points of contraflexure, while beam ends were moved. Such load arrangement was adopted for testing interior RC connections also by Kamimura et. al [2000]; their analysis focused on half-scale subassemblages with square columns 250 mm x 250 mm and beams having dimensions 180 mm x 250 mm. The objective of their experimental study was to evaluate the influence of joint shear stress level on the global behavior. By means of same seismic load simulation Fu et a. [2000] tested ten cross shaped specimens with square columns 350 mm x 350 mm and beams 250 mm wide and 400 mm high; the main scope of such experiments was to recognize how much joint shear transfer mechanisms and level of axial load on columns could affect the overall performance of the connection.

Along with these above reported, other tests on interior RC subassemblages have been done by applying both vertical and lateral loads on the top of the column and just recording induced shear forces on beams. Durrani and Wigth [1985] investigated the effect of joint shear stress on the performance of interior connections by testing three specimens with square columns 360 mm x 360 mm and beams having width equal to 280 mm and height of 406 mm. Their test setup is shown in Figure 2.3: force links constrained beam ends to move only horizontally, while vertical and lateral load was applied near the top of the column. By means of the same loading scheme, Joh and Goto [2000] tested 6 half-size interior beam-column subassemblages. Their specimens had square columns 300 mm x 300 mm and beams 200 mm wide and 350 mm high. Their

objective was to investigate the influence that beam bar area and diameter could play on frame behavior. Pampanin et al. [2001] analyzed four half-size subassemblages with square column 200 mm x 200 mm and beams with dimensions 200 mm x 330 mm. They applied a cyclic horizontal load at the end of the superior column and introduced another parameter by varying the axial load level on the column during the test.

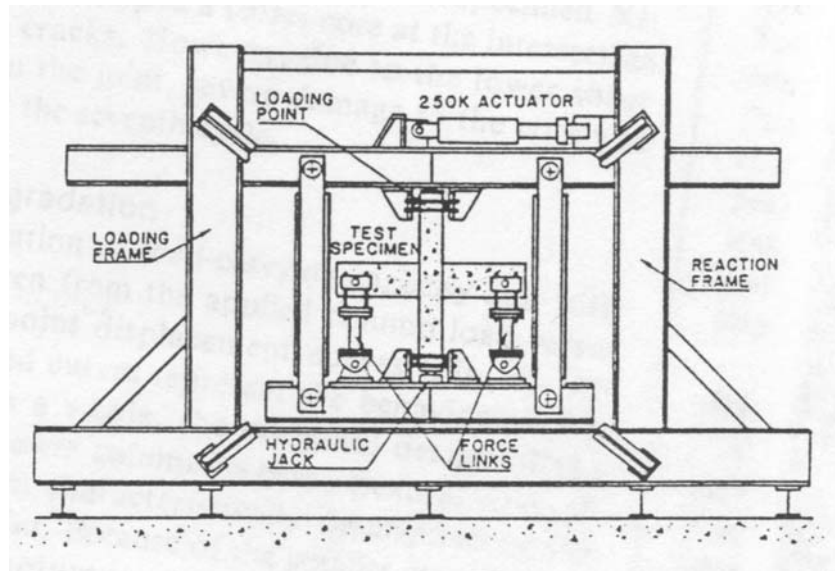


Figure 2. 3 Test setup used by Durrani and Wight (1985)

On the same idea of horizontal force applied to the column, Hakuto et al. [2000] performed tests on interior RC connections having rectangular columns and beams. The dimensions of vertical elements were equal to 300 mm x 500 mm, while for beams 300 mm x 460 mm members were built. The different aspect of this program as compared to those in the previous paragraph was represented by no column axial load. This was an explicit choice of authors, focused on analyzing joint performance; the presence of axial load would have made more favorable conditions from that standpoint. The setup adopted in order to achieve this objective is shown in Figure 2.4. Such scheme was also

selected by Raffaele and Wight [1995] for tests on 4 interior RC subassemblages with square columns 360 mm x 360 mm and beams having width ranging between 190 mm and 250 mm, and height of either 380 mm or 560 mm. In this case, even though no vertical actuator was present in the setup, the axial load was applied to the column by means of post-tensioning jacks.

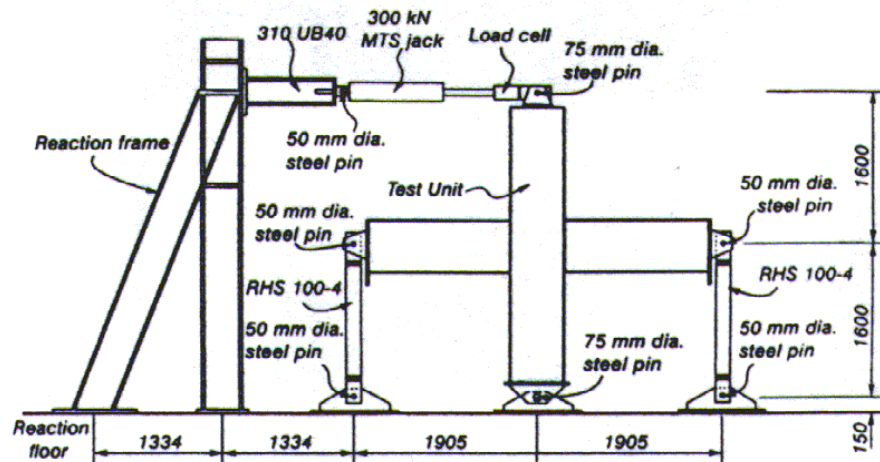
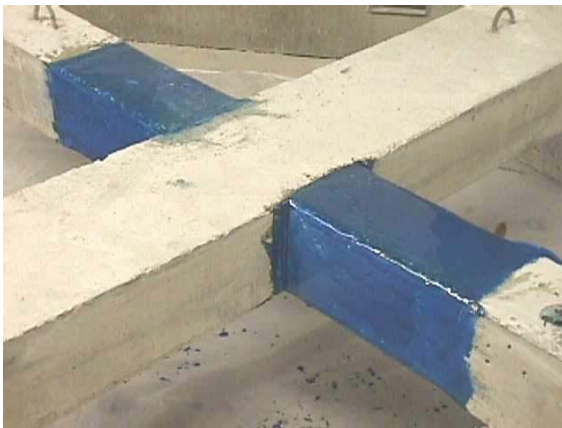


Figure 2. 4 Test setup used by Hakuto et al. (2000)

3. PROPOSED UPGRADE TECHNIQUE FOR GLD SUBASSEMBLAGES

3.1 DESCRIPTION

The proposed technique is based on the combined use of FRP laminates and FRP NSM rods for upgrading RC beam-column connections. The laminates are installed by manual lay-up and impregnated in-situ. Within the present research they were either wrapped around columns (Figure 3.1-a), externally bonded onto the panel (Figure 3.1-b) or U-wrapped around the beams (Figures 3.1-c and 3.1-d). In this last application, fibers were bonded on each lateral face and on the bottom of the member (Figure 3.1-c),



a)



b)



c)



d)

Figure 3. 1 Laminates installed in different regions of the connection

without wrapping the top surface (Figure 3.1-d) because in reality these surfaces are typically unreachable due to the presence of a slab or any other floor system.

FRP NSM rods are installed in epoxy filled grooves. Two conditions are possible: (1) Figure 3.2-a depicts their use as additional non-metallic reinforcement of the column, passing through the joint region; (2) Figure 3.2-b shows the application of NSM FRP rods by externally reinforcing the joint region in the beam direction.



Figure 3. 2 NSM rods in the columns (a) and joint (b)

3. 2 OBJECTIVES

The goal of this research is to investigate the effects of FRP reinforcement on the behavior of beam-column connections, by investigating the failure mechanism and the ductility capacity. The planned experimental program is expected to demonstrate that it is possible to establish a strength hierarchy in the subassembly by means of selective target strengthening. This hierarchy starts from the lowest level (i.e., column failure) given by the virgin specimen. The first level of FRP upgrade moves the failure to the panel, and then, further strengthening boosts it to the next level (i.e., beam failure).

The influence of the axial load applied to the column is also investigated. The experimented results are used to develop design guidelines that, for different situations, would allow the choice of the upgrade level for the subassemblage depending on the desired strength and/or ductility. Ultimately, the engineer could have the tools to modify the performance of an existing structure with an economical and sound technology.

3.3 EXPERIMENTAL PROGRAM

The experimental program consisted of 12 tests on interior RC beam-column connections; two of them were characterized by incomplete recorded information during the test due to data acquisition system problems. However, they are considered in the following sections for the amount of evidence they provided to the program.

The investigated parameters were: the axial load level on the column, P , the type of FRP reinforcement (FRP laminates and/or NSM rods), and the amount of FRP reinforcement applied.

3.3.1 Compressive stress in the superior column. To select the level of constant axial load to apply on the columns during experiments, a literature survey was carried out in order to choose typical values already adopted in similar experiments on interior connections.

Beres et al. [1992b] adopted 9.44 MPa (1.37 ksi) and 2.69 MPa (0.39 ksi) as average column compressive stresses for the 20 full-scale tests they conducted. Tabata et al. [1996] used average axial stresses equal to 20% of the design concrete strength, corresponding to 11.76 MPa (1.70 ksi), 8.24 MPa (1.19) and 7.06 MPa (1.02 ksi). In order to analyze the effect of the axial load on the seismic behavior of interior

connections, Fu et al. [2000] tested 10 connections with different average stresses, ranging between a minimum of 1.4 MPa (0.2 ksi) and a maximum value of 10 MPa (1.45 ksi).

Ghobarah et al. [1997] tested exterior RC connections fixing an axial compression load ratio $P/A_g f'_c$ (where P is the applied axial load on the column, A_g the area of its cross section and f'_c the compressive strength of concrete) equal to 0.08, which yielded an average column stress equal to 1.84 MPa (0.27 ksi). A value of the axial compression load ratio $P/A_g f'_c$ equal to 0.1 was used by Pantelides et al. [2000a] for testing exterior RC connections with an average compressive stress equal to 4.55 MPa (0.66 ksi).

The same ratio $P/A_g f'_c$ was selected equal to 0.2 or 0.1 by Rodriguez et al. [1994] for seismic tests on typical RC building columns, resulting in average column stresses ranging between 5.9 MPa (0.85 ksi) and 1.94 MPa (0.28 ksi). Saadatmanesh et al. [1997] tested 1/5 scale prototype bridge columns applying axial loads inducing average compressive stresses equal to 6.09 MPa (0.88 ksi) and 5.02 MPa (0.73 ksi).

Taking into account the above data, three different axial loads for the superior column were selected corresponding to average stresses equal to 3 MPa (0.43 ksi), 6 MPa (0.87 ksi) and 9 MPa (1.30 ksi). In the following, subassemblages characterized by average compressive stresses of the superior column equal to 3 MPa, 6 MPa and 9 MPa will be denoted, respectively, with L, H and M. Table 3.1 summarizes the number of tested specimens and their corresponding compressive stress.

3.3.2 Design of the RC subassemblage. In choosing the dimensions of the specimen, typical frame and geometrical ratios were taken into account even though some scaling was adopted to maintain the specimen size and weight to a manageable

level. Final dimensions were also defined accounting for laboratory space and testing equipment limitations.

Table 3. 1 Average compressive stress of the superior column

SPECIMEN	Average compressive stress on the superior column	
	(MPa)	(ksi)
L1	3.0	0.43
L2	3.0	0.43
L3	3.0	0.43
L4	3.0	0.43
H1	6.0	0.87
H2	6.0	0.87
H2L	6.0	0.87
H2U	6.0	0.87
H3	6.0	0.87
H4	6.0	0.87
H5	6.0	0.87
M3	9.0	1.30

The objective was to design beam-column connections typical of GLD frames built during the 60's without seismic provisions. For this, specimen design was carried out following the recommendations of the building code ACI 318-63 pre-dating the current one, as it is representative of a larger number of existing buildings.

Review of ACI detailing manuals and codes, and consultation with practicing structural engineers allowed Beres et al. [1996] to come up with the following typical constructive details, which can jeopardize the safety of GLD structures subjected to a seismic event:

- 1) Longitudinal reinforcement in the columns less than or equal to 2%.
- 2) Lapped splices of column reinforcement above the construction joint.
- 3) Lack of confinement to column concrete due to widely spaced ties.
- 4) Little or no transverse reinforcement of the panel.

- 5) Insufficient anchorage of discontinuous positive beam reinforcement into the column.
- 6) Construction joints below and above the connection.
- 7) Weak column-strong beam construction.

Due to the limited number of planned tests, it was decided to reduce the number of variables avoiding lapped splices (item 2) (Figure A.4), discontinuous reinforcement in the beam (item 5) (Figure A.2) and construction joints (item 6).

Considering that ACI 318-63 indicates as minimum longitudinal reinforcement for columns 1% of their gross cross-sectional area and as minimum bar size 16 mm (#5), the column reinforcement was determined in order to respect the minimum code prescription, without overcoming the 2% limit (item 1).

Diameter (minimum 6 mm) and spacing (minimum of $16 d_v$, $48 d_t$, or least column dimension) of column ties were determined according to ACI 318-63 recommendations for 11 specimens; a lack of confinement (item 3) was analyzed with subassemblage HAL5, as depicted in Figure A.7. The specimen design was also oriented, as Figure A.3 shows, to having no transverse reinforcement of the panel (item 4) and weak column-strong beam construction (item 7).

3.3.3 Subassemblage geometry and reinforcement. Based on the above considerations, a square column with the sides equal to 200 mm (8 in.) and a beam with a cross-section 200 mm (8 in.) by 355 mm (14 in.) was selected. In order to obtain the average stresses discussed in section 3.2.1, the lower column of specimen types L, H and M was subjected to an axial load level of 124.5 kN (28 kips), 249 kN (56 kips) and 373.5 kN (84 kips), respectively.

Spacing of the inserts on the laboratory strong floor governed the length of the elements, resulting in a cross-shaped specimen 2.64 m (8.7 ft.) and 3.05 m (10 ft.) long, respectively, in the column and beam directions.

Four D16 (5/8 in.) bars were placed as longitudinal column reinforcement, yielding a ratio between area of steel and area of the gross section area equal to 1.92%. D10 (3/8 in.) stirrups, spaced at 200 mm (8 in.) on center, were used as transverse reinforcement of columns. According to ACI recommendations, for the first stirrup of each column an halved spacing of 100 mm (4 in.) was adopted, as depicted in Figure A.4.

Three D22 (7/8 in.) and two D18 (6/8 in.) bars were placed, respectively, as negative and positive longitudinal reinforcement of the beams; such amount of longitudinal steel corresponds to ratios of tension and compression reinforcement equal to, respectively, $\rho=0.018$ and $\rho'=0.09$. Open D10 (3/8 in.) ties, spaced at 100 (4 in.) on center, were used as transverse reinforcement of beams. For both columns and beams the concrete cover was equal to 38 mm (1.5 in.). Geometric properties of the specimen and steel reinforcement of both column and beam are depicted in Figure 3.3.

3. 4 MATERIALS

The present section deals with properties of used materials. In the following, results of coupon tests on concrete, steel and FRP rods will be outlined; mechanical properties of resins and FRP laminates will be also reported.

3.4.1 Concrete. The design compressive strength of concrete was $f'_c=31$ MPa (4,500 psi). This was the strength requested to the concrete supplier, along with a

maximum gravel size, d_{\max} , equal to 12.7 mm (1/2 in.). Due to limited physical availability of space in the laboratory and specimen dimensions, four different pours were needed. Moreover, after the first pour concrete supplier was unable to satisfy the requirement about the maximum aggregate dimension. This caused that for second, third and fourth pours the delivered concrete was characterized by d_{\max} equal to $\Phi 19$ mm (3/4 in.).

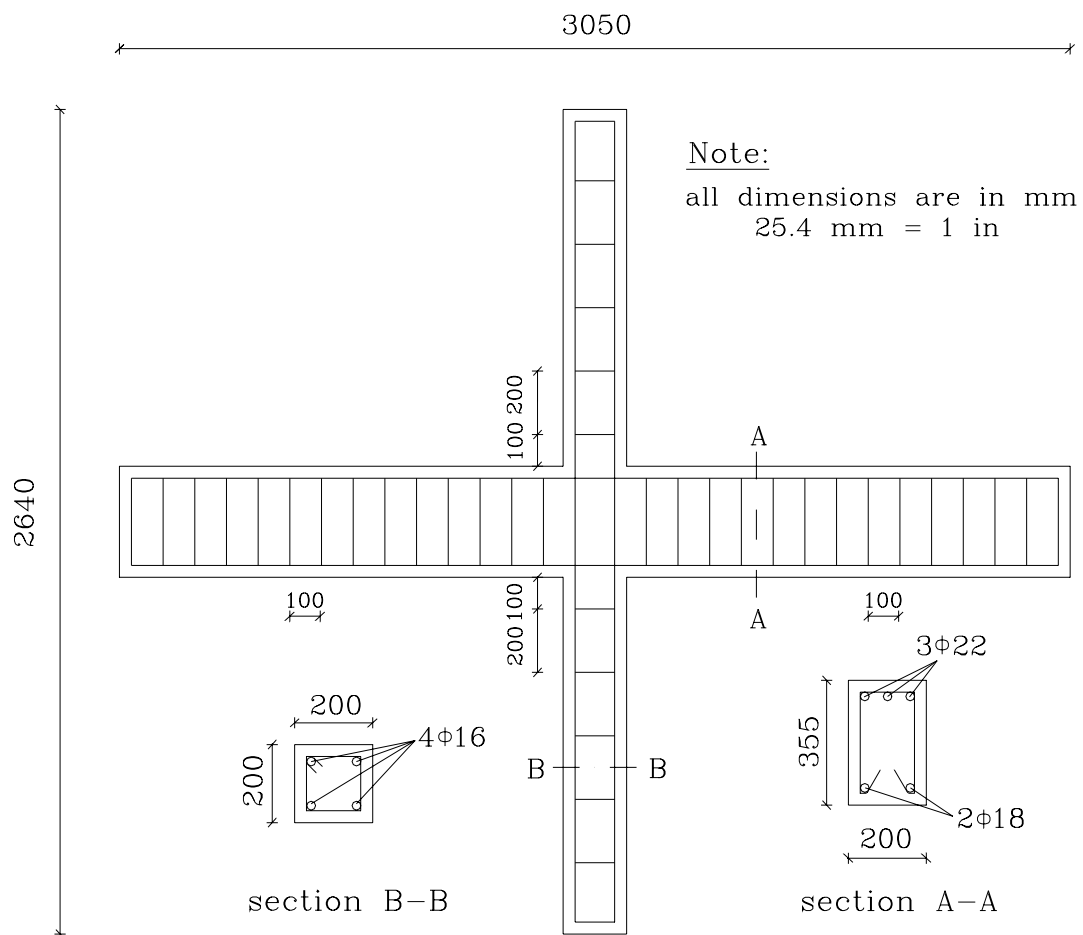


Figure 3. 3 Geometry and reinforcement of the specimen

During each pour, six cylinders with diameter equal to 152 mm (6 in.) and height equal to 508 mm (20 in.) were obtained. Table 3.2 summarizes the actual compressive

strength of concrete obtained by averaging the results of compression tests on the cylinders conducted at the same time of specimen tests.

Table 3. 2 Compressive concrete strength of all specimens

SPECIMEN	Batch	Compressive strength of concrete		Coeff. of var. (%)
		(MPa)	(psi)	
L1	Second	38.9	5633	7.9
L2	Third	39.8	5763	4.3
L3	Second	38.9	5633	7.9
L4	Fourth	36.5	5285	2.6
H1	First	31.7	4590	3.8
H2	Fourth	36.5	5285	2.6
H2L	Second	38.9	5633	7.9
H2U	Fourth	36.5	5285	2.6
H3	First	31.7	4590	3.8
H4	Third	39.8	5763	4.3
H5	Second	38.9	5633	7.9
M3	Third	39.8	5763	4.3

3.4.2 Reinforcing steel. As depicted in Figure 3.3, ASTM A 615 standard steel bars were used for both columns and beams. In particular, $\Phi 16$ bars were placed as longitudinal reinforcement of columns, while $\Phi 18$ and $\Phi 22$ were used in the beams. In both cases, transverse reinforcement consisted of $\Phi 10$ bars.

Tensile tests were performed in accordance with ASTM A370-97 on three coupon specimens for each different diameter of rebar. The yield strength was calculated averaging the results of each set of three samples. Results are presented in Table 3.3.

Table 3. 3 Yield strength of reinforcing steel

Bar diameter (mm)	Bar diameter (in.)	Average yield strength		Coeff. of var. (%)
		(MPa)	(ksi)	
16	5/8	448	65	0.43
18	6/8	559	81	0.52
22	7/8	511	74	0.34

3.4.3 CFRP bars. Two different types of carbon FRP rods were used for strength the connections. The former is a CFRP deformed rod commercially known as C-Bar and it was supplied by Marshall Industries Composites Inc., Ohio. The latter is a smooth CFRP rod, commercially known as Galileo rod; it was supplied by MAC Spa, Treviso, Italy. Both are depicted in Figure 3.4, where it can be noticed the difference between the non perfectly circular cross section of C-Bars compared to that circular of the Galileo rods. For both types of FRP bars, tensile characterization was conducted in the laboratory.

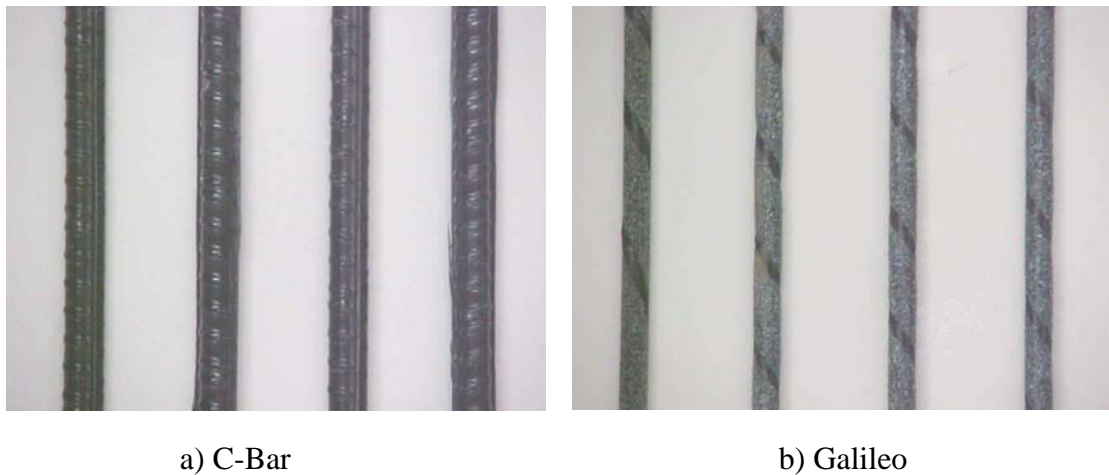


Figure 3. 4 Carbon FRP rods.

For tensile characterization, since the transverse compressive strength of FRP bars is controlled by resin properties and is much lower than their longitudinal strength, which is governed by fibers, a particular anchor device was needed in order to grip the sample and prevent slippage or premature local failure (Micelli and Nanni [2001]). Two steel pipes, one at each end of the bar, were filled with an expansive grout, BRISTAR 100 by Onoda Cement Corporation, Tokyo, Japan mixed according to supplier's suggestions with a water/cement ratio of 0.29 (in weight). After pouring, the specimen was let curing

for three days, time necessary to the grout for developing the necessary. The dimensions of each pipe were: length equal to 457 mm (18 in.), outside diameter 42 mm (1.66 in.), wall thickness 4.85 mm (0.191 in.). The total length of the specimen was 1524 mm (5 ft), including both test and anchoring section.

A Tinius-Olsen Universal Testing Machine was used for conducting such tests. The specimen was set up across the two cross-heads of the machine and aligned with the axis of the machine grips. At one end, the anchor was fixed to the top cross-head; a 20 mm (3/4 in) plate, having a slot and placed between anchor and cross-head, was used to distribute the load. Figure 3.5 depicts this detail.

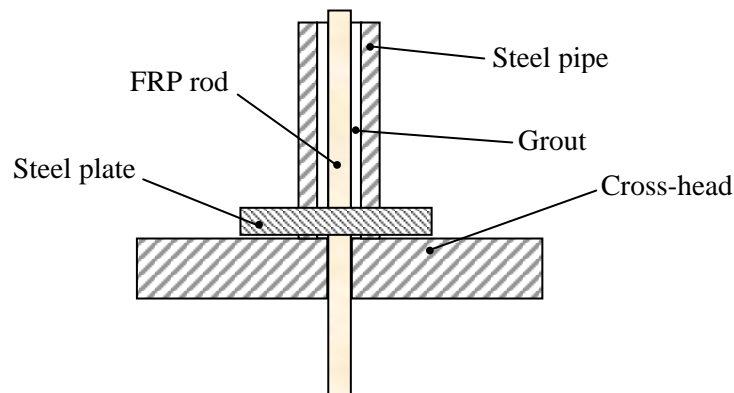


Figure 3. 5 Anchor detail on the top cross head

Another identical plate was used on the bottom cross-head. An extensometer with gage length of 51 mm (2 in) was mounted across mid-length of the bar in the direction of the applied tensile load in order to measure its deformation. Figure 3.6 shows a typical test setup with the rod ready to be loaded.

All tested bars showed a linear elastic behavior up to failure and experienced an acceptable tensile failure; this confirmed that each specimen developed its full tensile

capacity and the anchor allowed to avoid slippage and local failures. Figure 3.7 depicts typical failure mode of tested rods.

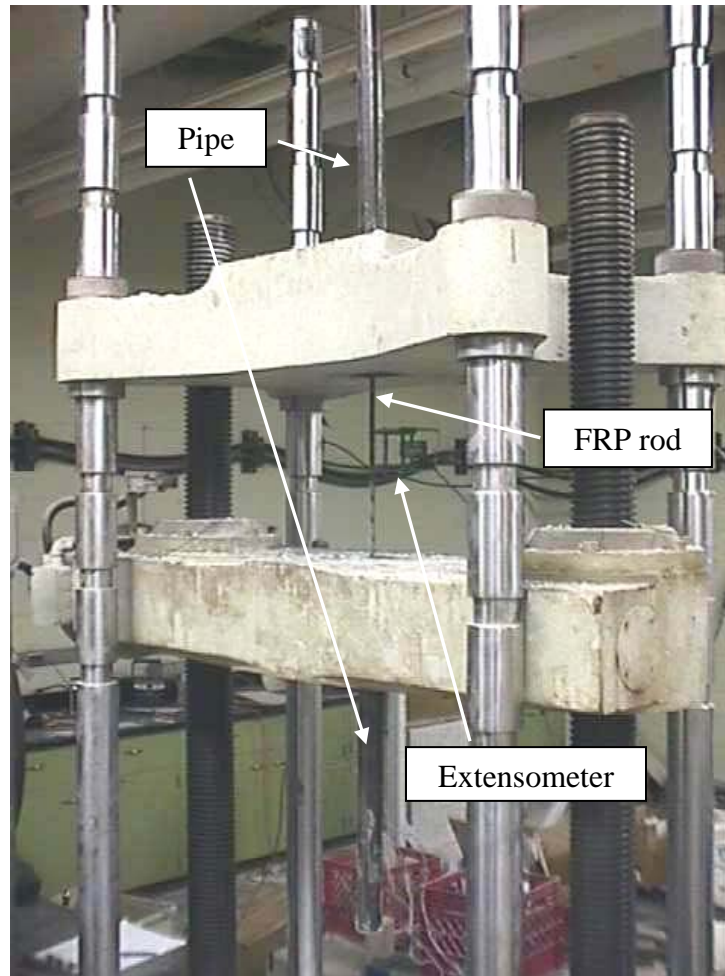


Figure 3. 6 Typical test setup

In order to compute tensile strength, ultimate strain and modulus of elasticity, recorded load and strain were used, along with the nominal cross-sectional area of the rod. Test results are reported in Tables 3.4 and 3.5, respectively for C-Bar and Galileo bars. The modulus of elasticity was determined considering that portion of data between 20% and 60% of the ultimate tensile capacity. Since the extensometer was removed

before failure of the rod, the ultimate strain was obtained by dividing the ultimate stress by the calculated modulus of elasticity.



a) C-Bar

b) Galileo

Figure 3. 7 Carbon FRP rods

Table 3.7 highlights specimens upgraded with C-Bar (i.e., type 1) and Galileo (i.e., type 2) rods, respectively.

Table 3. 4 Mechanical properties of C-Bar rods.

Spec. No.	Nominal diameter		Area (mm ²)	Tensile Strength		Elastic modulus		Ultimate Strain (%)
	(mm)	(in.)		(MPa)	(ksi)	(MPa)	(ksi)	
1	9.5	0.375	70.96	2,127	308	109,406	15,842	1.94
2	9.5	0.375	70.96	2,182	316	120,228	17,409	1.82
3	9.5	0.375	70.96	2,155	312	112,155	16,240	1.92
Average				2,155	312	113,930	16,497	1.89
Standard Deviation				28	4	5,625	814	0.06
Coefficient of Variation (%)				1.3		4.9		3.4

In order to embed the NSM rods in the grooves an epoxy adhesive paste was used. It is commercially known as Concreative 1420 by Master Building Technologies, Cleveland, Ohio, and it is supplied in biaxial cartridges. Its mechanical properties

provided by the manufacturer are: tensile strength (according to ASTM D 638) equal to 13.8 MPa (2,000 psi), elongation at break (according to ASTM D 638) equal to 4%, compressive yield strength (according to ASTM D 695) equal to 55.2 MPa (8,000 psi) and compressive modulus (according to ASTM D 695) equal to 2,762 MPa (400 ksi).

Table 3. 5 Mechanical properties of Galileo rods.

Spec. No.	Nominal diameter		Area (mm ²)	Tensile Strength		Elastic modulus		Ultimate Strain (%)
	(mm)	(in.)		(MPa)	(ksi)	(MPa)	(ksi)	
1	8.0	0.312	50.24	1,906	276	106,954	15,487	1.78
2	8.0	0.312	50.24	1,878	272	110,601	16,015	1.70
3	8.0	0.312	50.24	2,258	327	107,244	15,529	2.11
Average				2,014	292	108,266	15,677	1.86
Standard Deviation				212	31	2,027	293	0.22
Coefficient of Variation (%)				10.5		1.9		11.7

3.4.4 CFRP laminates. Unidirectional carbon fiber unidirectional sheets, supplied by Master Builders Technologies, Cleveland, Ohio, were applied within the present experimental program. They are commercially known as C1-30 sheets and provided in the form of rolls, as depicted in Figure 3.8-a.

Manufacturer provides the following properties for such laminates: ultimate tensile strength in the direction of fibers equal to 3,800 MPa (550 ksi), modulus of elasticity in the direction of fibers equal to 230,000 MPa (33,300 ksi) and thickness equal to 0.165 mm (0.0065 in.). No additional laboratory test was performed for confirming these properties, which have been well determined and widely accepted (Yang et al. [2001]).

Three basic epoxy resins are commonly used during the installation process; they are named primer, putty and saturant. In particular, the impregnation of fibers with the last one allows to form the in-situ saturated laminate; in it, the saturant acts as a matrix with the double function of distributing stresses among fibers and protect them from environmental effects. Figure 3.8-b shows a schematic diagram of the used wet lay up system. All the above resins are bi-component and they were all mixed with a volumetric ratio A to B equal to 3 according to manufacturer's specifications. Table 3.6 summarizes resin's tensile properties.



a)

b)

Figure 3. 8 C1-30 fibers on the left; scheme of wet lay up system on the right

Table 3. 6 Tensile properties of used resins

	Tensile Strength		Tensile Elastic Modulus		Tensile Strain
	(MPa)	(psi)	(MPa)	(ksi)	(%)
Primer	12.4	1,800	725	105	3
Putty	12.4	1,800	1,796	260	1.5
Saturant	54.6	7,900	3,039	440	2.5

3. 5 UPGRADE SCHEMES AND SPECIMEN PREPARATION

Tested subassemblages were characterized by different level of upgrade achieved by applying CFRP laminates and/or NSM rods. In the following, a description for each

different upgrade scheme is provided along with some remarks concerning application issues. A synthetic summary is provided in Table 3.7.

Table 3. 7 Summary of upgrade schemes

Spec.	P (kN)	NSM bars	Column		Joint		
			Laminates Wrapping	NSM bars	Laminates parallel to beam axis	Laminates perpendicular to beam axis	NSM bars parallel to beam axis
L1	124.5	-----	-----	-----	-----	-----	-----
L2	124.5	-----	x	-----	-----	-----	-----
L3	124.5	type 1	x	x	-----	-----	-----
L4	124.5	type 2	x	x	-----	x	x
H1	249	-----	-----	-----	-----	-----	-----
H2	249	-----	x	-----	-----	-----	-----
H2U	249	-----	x	-----	-----	-----	-----
H3	249	type 1	x	x	-----	-----	-----
H4	249	type 2	x	x	-----	x	x
H5	249	type 1	x	x	x	x	-----
M3	373.5	type 2	x	x	-----	-----	-----

3.5.1 Subassemblages L1 and H1. Specimens L1 and H1 were used as control specimens. As discussed in 3.3.1, they were loaded with different axial load levels; however, both were tested without any strengthening. The geometry was depicted in Figure 3.3. Figures A.1-4 show details of the typical control connections prior to pouring of concrete.

Figures A.8-9 depict the specimen during the casting phase and after casting. In particular, Figure A.7 allow to observe four steel hooks inserted on the top of each arm of the cross-shaped member: their only function was to allow to lift and move the specimen in the laboratory.

3.5.2 Subassemblages L2, H2, H2L and H2U. Within the experimental program these are the specimens strengthened with the least amount of composites; as anticipated

in section 3.2, this is the first level of upgrade aimed at moving the failure from the lowest level (i.e., failure of the column) to the next stage (i.e., failure of the panel) of the strength hierarchy. This objective was pursued by wrapping the end of each column for a length of 380 mm. Figure 3.11-a shows a front view of the upgraded connection: the wrapping was carried out by two plies of carbon fibers C1-30 on each column end.

Figures A.2-4 represent a typical detail of such specimens before pouring concrete; as anticipated in section 3.3.2 a confinement defect was also studied by omitting the first two stirrups at the end of one column in specimen H2U. Such detail is represented in Figure A.7. After 28 days of curing, the formwork was stripped and a preliminary preparation of the surfaces was carried out prior to the laminates application.

Since carbon fibers were used for the wrapping, the first step was to round off the corners of each column along the zone to be covered with laminates by means of a small grinder, as depicted in Figure A.10. Figure A.11 represents a particular side of a column after the corner was completely rounded off. The same detail can be observed also in Figure 3.12-a.

The following step consisted of sandblasting and accurately cleaning the area to be wrapped. On the prepared surface, primer was applied in order to fill the concrete pores and guarantee adequate support for the laminates; its application is shown in Figure A.12. Once the primer had partially cured (about one hour), putty was spread onto the surface (Figure A.13) to fill holes and imperfections and provide a smooth substrate for the sheets.

After the putty assumed the required consistency (20 minutes), the surface was covered with saturant; then the fiber sheet was wrapped around the column and it was

impregnated with another layer of saturant. Then, the second sheet was installed and subsequently impregnated with an additional layer of saturant.

Figure 3.12-a represents a schematic section of the wrapped column. In the case of multiple plies, it is common practice to splice the fiber sheets on alternate sides of the section in order to avoid a weak link.

In order to obtain an optimal application, a complete impregnation of fibers was ensured by carefully rolling the sheets to remove any entrapped air (Figure A.14.)

Laminates application on specimens H2 and H2U allowed to experience an interesting phenomenon that can occur when fibers are applied during the cold season. Due to limited space inside the laboratory, two specimens were kept outdoors, covered with plastic sheets and exposed to cold temperatures and air moisture.

When time for the strengthening came, they were moved inside. After about 8 hours, fibers were applied following the above procedure. Even though the immediate installation looked perfectly achieved, after about 48 hours both specimens showed diffuse presence of bubbles of different size, where the laminate was not bonded to the concrete support.

An accurate investigation was then conducted in order to monitor the surface and mark the unbonded zones, as depicted in Figure 3.9. For those zones with area bigger than 645 mm^2 (1 sq in.), defects were injected with primer using a syringe, as Figure 3.10 represents. Primer injection was preferred due to the high viscosity of this resin compared to that of saturant. The behavior of these two specimens observed during testing will be discussed in section 6.2; here it is only anticipated that the adopted remedy allowed them to perform satisfactorily.



Figure 3. 9 Monitored debonding zones on specimens H2 and H2U

3.5.3 Subassemblages L3, H3 and M3. For the specimens L3, H3 and M3, NSM rods were installed on the columns prior to wrapping them with carbon laminates. Application of such FRP bars, continuous through the nodal zone, allows to increase the column flexural capacity, providing additional reinforcement fully anchored and effective in the maximum moment region of the column. Such reinforcement is also beneficial for the panel, even though it is placed in peripheral zones.



Figure 3. 10 Primer injection of bubbles by a syringe

Figure 3.11-b depicts a typical subassemblage. It can be observed that four $\Phi 8$ or $\Phi 10$ NSM rods, each 2130 mm (7 ft.) long, were installed on each side of the column.

After, the member was wrapped with two plies of CFRP laminates. Figures 3.12-b and 3.12-c illustrate, respectively, a section of the column within the wrapped length and its section with only NSM rods. The dimension of the groove for the NSM FRP rod was determined as 14 mm (9/16") based on studies performed by De Lorenzis and Nanni [2001].

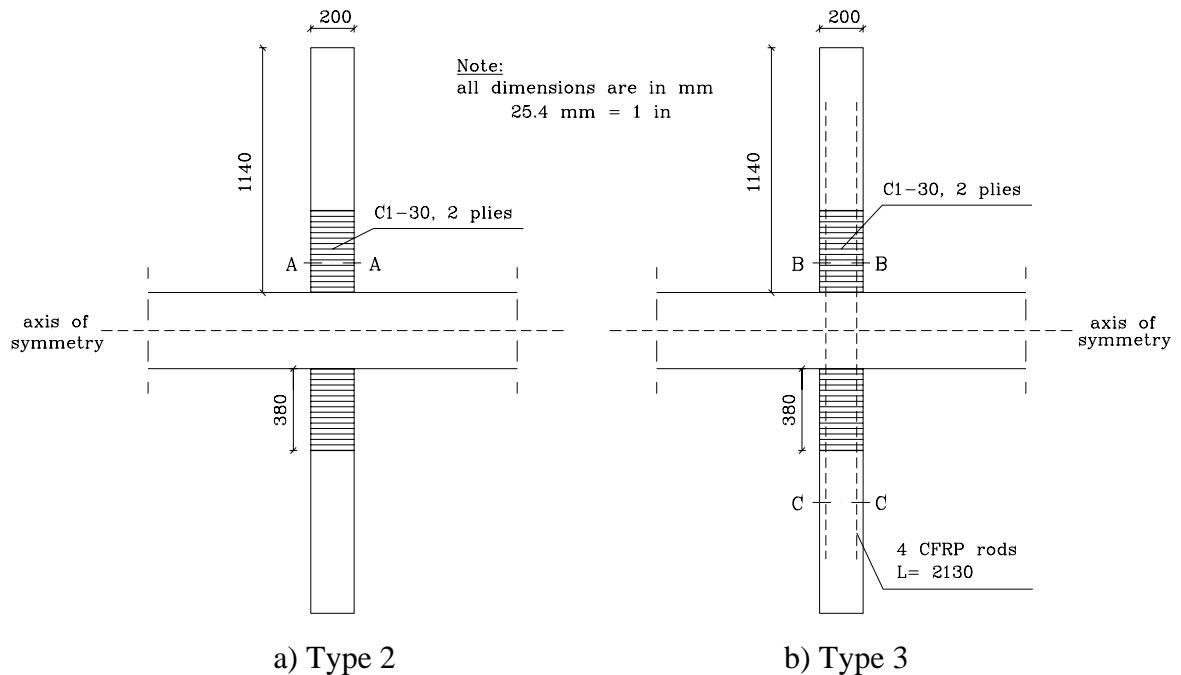


Figure 3. 11 Front view of upgraded subassemblages

In order to achieve a less difficult and more precise installation of the NSM rods, eight wooden strips were nailed to the forms, as depicted in Figure A.5 and Figure A-7. This allowed also to speed up the preparation procedure of the specimens, making it easier to groove the column and drill through the panel. It has been demonstrated in other projects that the grooving and drilling is possible in the field with conventional tools (Alkhrdaji and Nanni [2000]). It is recognized here that specific future research

could be focused on this constructability issue in order to highlight appropriate tools and steps for improving the present techniques.

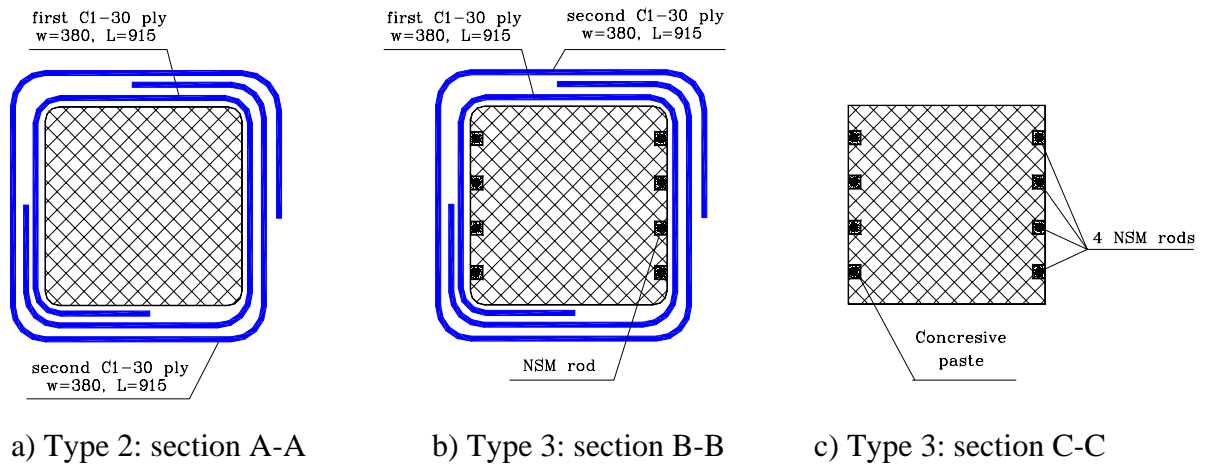


Figure 3. 12 Cross section of column

Since $\Phi 8$ and $\Phi 10$ NSM rods were used, square wooden strips with side equal to 14 mm (9/16 in) were adopted. In order to apply the rods, the first step consisted in removing the strips from the sides and drilling through the panel. The latter operation is depicted in Figure A.15, while Figure A.16 shows the specimen ready to be strengthened. Before applying the first layer of concrete paste, the grooves needed to be carefully cleaned from the dust, as illustrated in Figures A21-22.

Once the grooves had been cleaned, they were partially filled with concrete paste (Figure A.19) for the subsequent installation of the rod, represented in Figure A.20. Another layer of concrete paste was then applied (Figure A.21) and the surface was smoothed as showed in Figure A.22. Figure A.23 shows the connection after the installation was completed.

3.5.4 Subassemblages L4 and H4. Upgrade schemes discussed in sections 3.5.2 and 3.5.3 were mainly based on the strengthening of the columns, either providing them with a greater level of confinement (i.e., only wrapping) or with an increase in both confinement and flexural reinforcement (i.e., wrapping plus NSM rods). In the latter case, some reinforcement was also provided to the panel by the NSM rods passing through it.

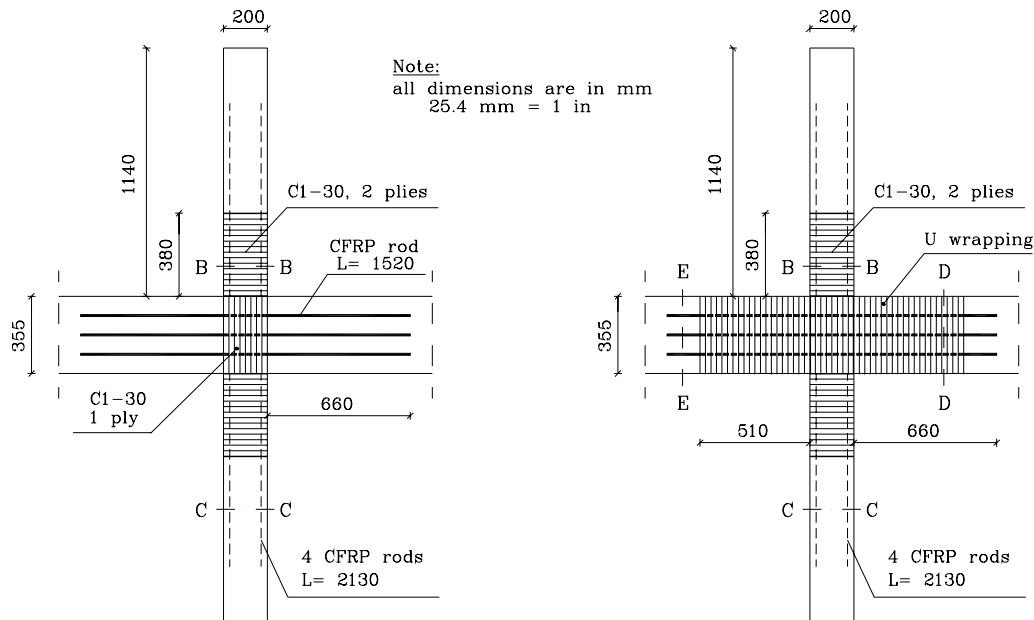
Specimens L4 and H4 were characterized by the same upgrade scheme of those presented in section 3.5.3 (i.e., wrapping plus FRP rods through the panel), but also the panel was strengthened. Amount and installation of wrapping and NSM rods to the columns was already discussed in section 3.5.3. Since the major concern for the panel is constituted by shear stresses, ideally a diagonal reinforcement should be used.

Considerations based on the practical installation of such reinforcement suggested strengthening the nodal zone in both directions parallel and perpendicular to the beam axis. In the direction parallel to the beam axis, NSM rods were used, while in the perpendicular direction carbon laminate was applied, as shown in Figure 3.13-a. Three $\Phi 8$ carbon rods, each 1520 mm (5 ft) long, were installed; the carbon sheet covered only the area of the panel without extending on the columns.

Even though it would be more effective to anchor it underneath the column wrapping, it was stopped at the interface column-panel because in reality the presence of a slab or any other floor system would not allow to extend it on the columns.

In order to anchor the NSM rods, U-wrapping of the beams for a width of 510 mm (20 in) from the beam-panel interface was also realized. Figure 3.13-b depicts a front view of specimen L4 or H4 once the upgrade has been completed. Figures 3.14-a and

3.14-b allow to underline that the U-wrapping regarded the bottom surface of each beam and that round off of the corners was needed for the length were the beam was U-wrapped.



a) NSM rods and sheet on the panel

b) Upgrade completed by beam U-wrapping

Figure 3.13 Upgrade scheme type 4

As illustrated in Figures A.6, A.8 and A.12, wooden strips were used also for easing the installation of the NSM rods on the panel. As already stated in section 3.5.3, for both column and panel the dimensions of the grooves were selected equal to 1.5 times the diameter of the FRP rebar.

In terms of preparation procedure, first NSM rods were installed as depicted in Figures A.24-25. After, the columns were wrapped and the joint was reinforced in the vertical direction with carbon fibers, as shown in Figure A.26. Finally, the U-wrap on both sides of the beam was realized. A view of the specimen once composites have been completely installed is represented in Figure A.27.

3.5.5 Subassemblage H5. The upgrade level for specimen H5 is equivalent to that presented in section 3.5.4. The difference was in using only fibers for strengthening the panel, while connections presented in section 3.5.4 were characterized by NSM rods in the horizontal direction. Despite this difference in the type of adopted composite material, the objective is again to validate an upgrade scheme where the panel is strengthened along with columns.

Column strengthening with NSM rods and wrapping was detailed in section 3.5.3. Figure 3.15-a shows the first step of the panel upgrade. A carbon fiber laminate was applied on the nodal zone area in the direction parallel to the column axis. In the horizontal direction another carbon sheet was installed, extending for 380 mm (15 in) on each side of the beam. As Figure 3.15-b allows to observe, the upgrade scheme was completed by U-wrapping the beam in order to anchor the fibers running in the horizontal direction; this is also depicted in Figure 3.14-c.

The sequence in composites application was based first on the installation of NSM rods in the columns through the nodal zone. After, primer was applied on the prepared surfaces, as depicted in Figure A.28; once the primer was cured, the substrate for the laminates was smoothed by putty application, as it can be observed in Figure A.29. Carbon fibers were then installed as described in section 3.5.2; as already underlined in section 3.5.5, the U-wrapping of the beam regarded its bottom surface. Such detail is represented in Figures A.30-31.

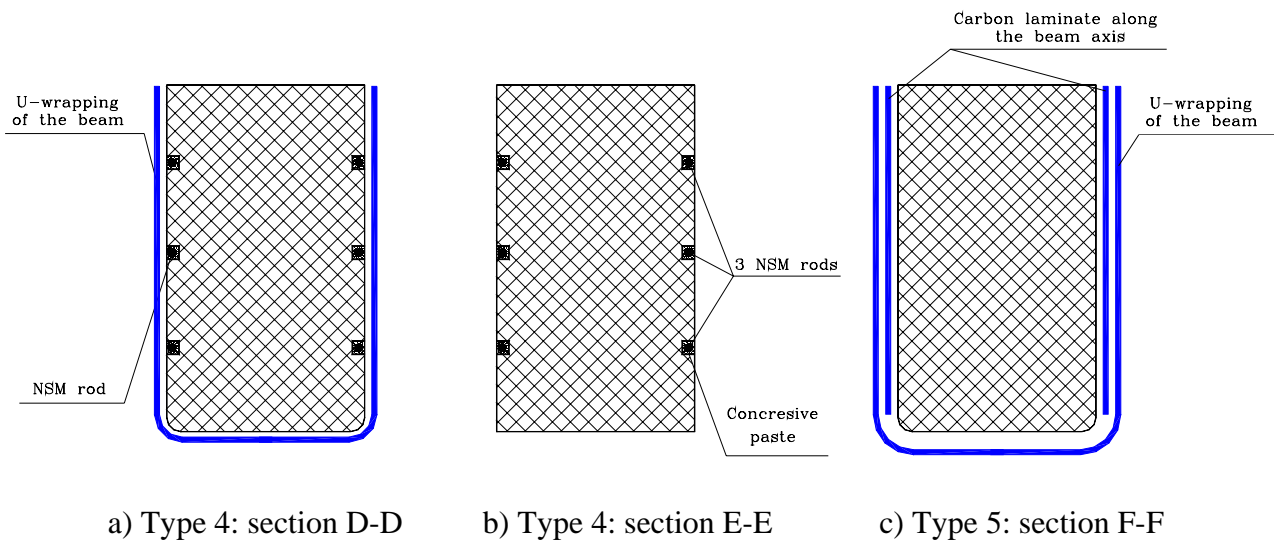


Figure 3.14 Cross section of beam

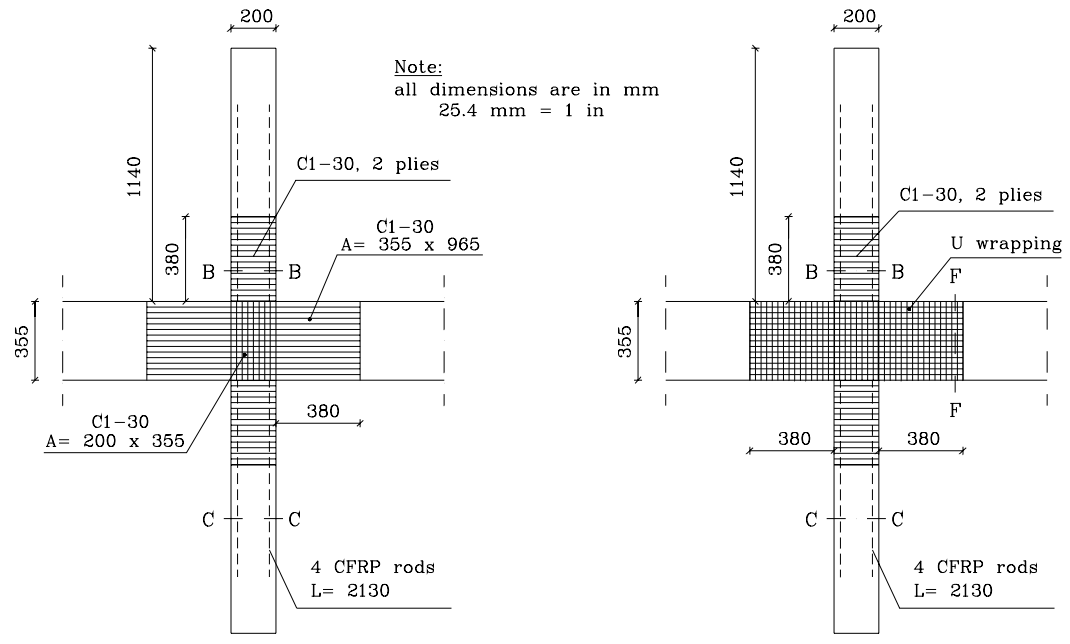


Figure 3.15 Upgrade scheme type 5

4. TESTING CONFIGURATION AND RESULTS

4.1 TESTING CONFIGURATION

The present section deals with testing configuration, detailing the laboratory test setup and the loading pattern, and discussing type and location of the instrumentation used during a typical test.

4.1.1 Loading arrangement. The set-up of each specimen on the laboratory floor is shown in Figure 4.1. At one of the column ends a constant axial load P is applied by means of a hydraulic jack (i.e., 1 in Figure 4.1) independently operated. At the other end of the column, a load cell is placed to record the applied load P . The restraints at the extremes of the columns simulate hinges that allow rotation by means of a pair of steel bars on both sides of the element, as depicted in Figure B1. Two additional shear loads are applied on the extremes of each beam. Even in this case, the jacks (i.e., 2 and 3 in Figure 4.1) are independently operated. A load cell on each cylinder contacting the beam records the applied force. A greased plywood sheet between the specimen and the floor limits the friction and allows for the free movement of the beams and column.

Once the specimen is in place (as depicted in Figures B.2-3), the loading process includes the following steps:

- *Axial column load application*: this is the preliminary step, during which gradually the prefixed load P is applied to the column. During the application of the axial load, the beam ends are free to move in order to allow the small displacements in their transverse direction.

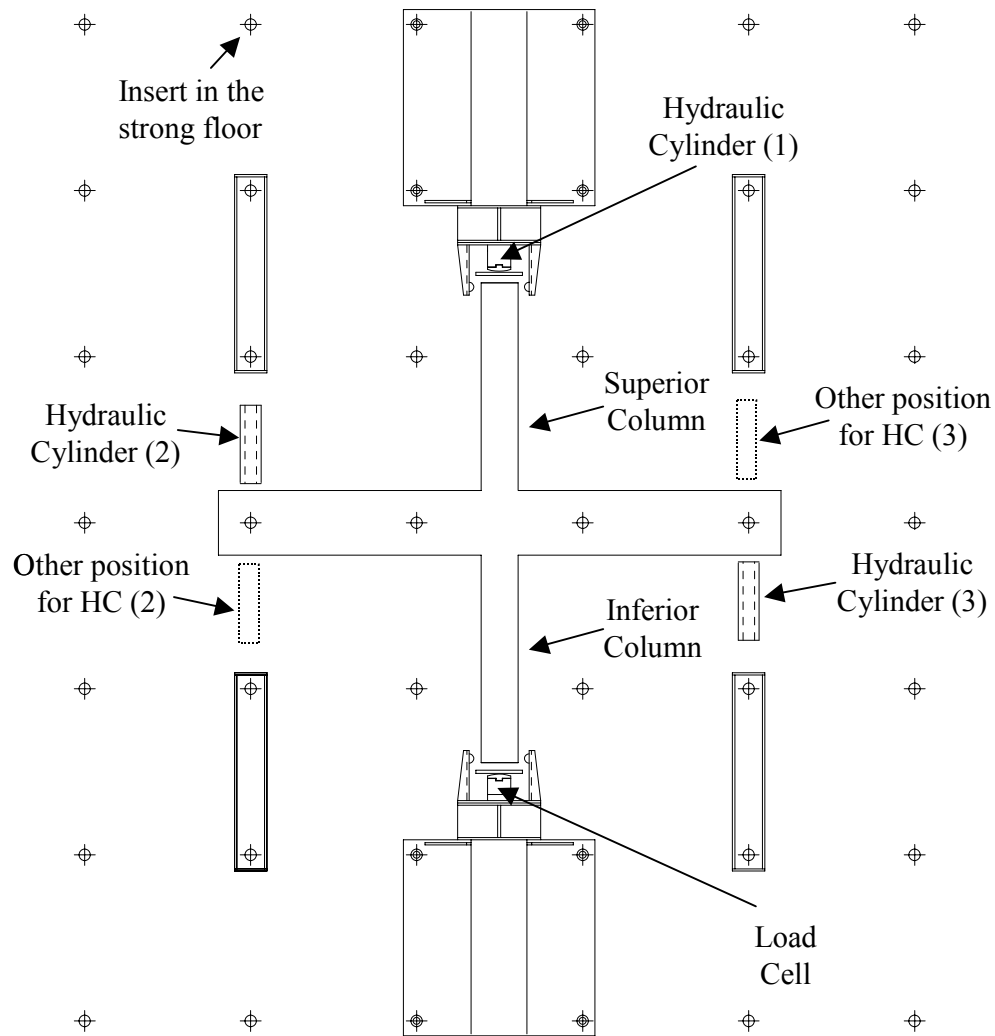


Figure 4. 1 Test setup

- Gravity beam loads application: after the axial load has reached the fixed value and is kept constant, the beam load setup is arranged. Two equal shear forces are then applied to the beam ends in order to simulate the effect of gravity loads. The amount of the total load was calculated to reproduce on the beams the serviceability situation. In particular, the adopted value $V = 40 \text{ kN}$ (9 kips) generates a maximum flexural moment equal to half of the design moment obtained according to ACI provisions. The beam-column connection configuration in the laboratory during this phase is shown in the Figures B2-3.

- *Reversed load cycles*: with this step the earthquake simulation starts. As soon as the beam shear is unequal at each side of the connection, a flexural moment and shear forces are generated in the column to maintain equilibrium. The increment/decrement $\Delta V = 4.45$ kN (1 kip) was established so that at least six reversed load cycles were needed before reaching the design moment strength in the unstrengthened column calculated according to ACI provisions. The algebraic sum of beams shears and compressive column axial force was kept constant during the test.

Figure 4.2 provides a schematic representation of Figures B.2-3; it shows the shears application performed by maintaining the jacks from the same side of the beams and increasing/decreasing their forces. For every shear force increment/decrement, three repetitions are performed (Beres et al. [1992a], Beres et al. [1992b], Beres et al. [1996], Pantelides et al. [2000a], Pantelides et al. [2000b]).

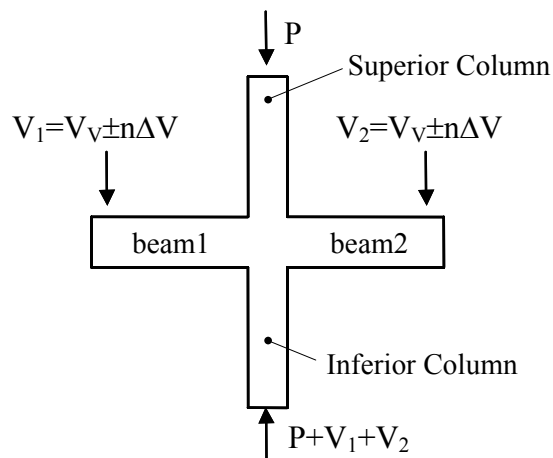


Figure 4. 2 Scheme of loads application before inversion of beam shear

Once zero shear force is reached at one of the beam ends (i.e., nine load cycles), the load configuration is changed switching the cylinders on the beam ends as shown in Figure 4.3.

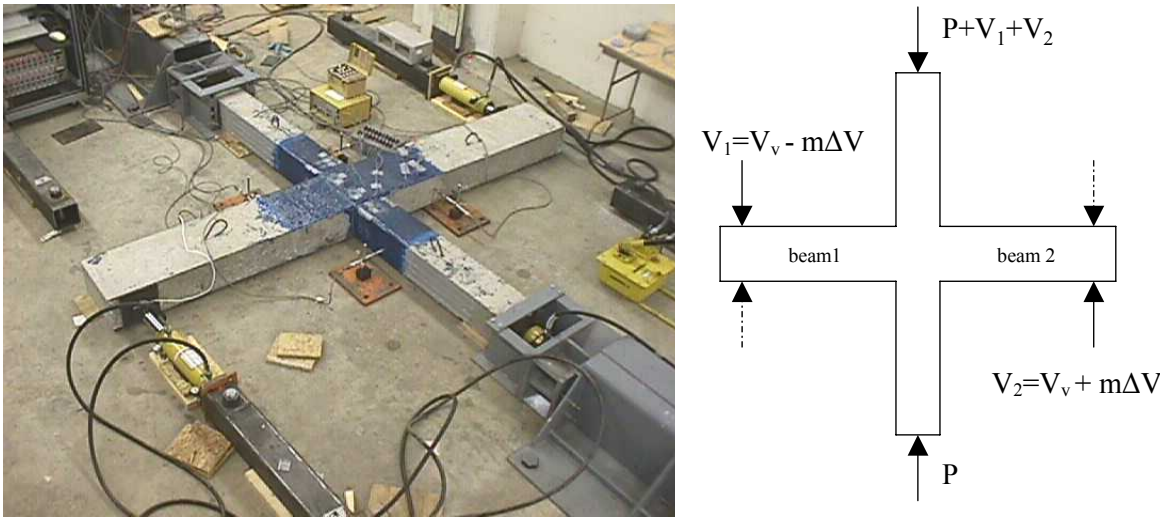


Figure 4. 3 Loads application after inversion of beam shear

Park [1994] underlined how the lateral load could be applied to the connection as shown in Figure 4.4-a (i.e., column ends displaced); that arrangement is the one that provides the best simulation of the horizontal displacements the subassembly actually experiences. However, the arrangement (i.e., beam ends displaced) adopted within the present research (Figure 4.4-b) also represents a valid alternative, provided that eventual P-Δ effects on columns are separately considered.

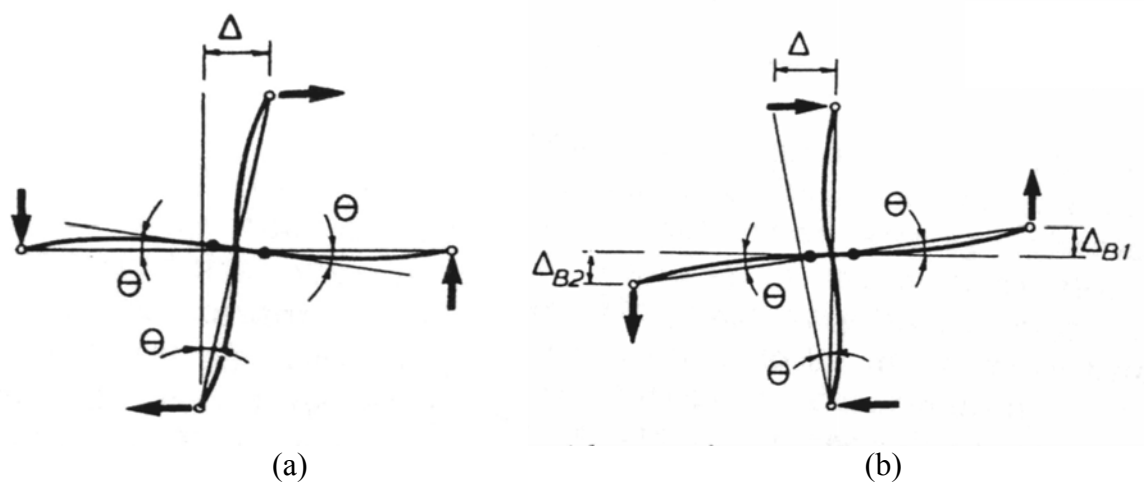


Figure 4. 4 Alternatives for seismic load application (Park, 1994)

The three steps described above are shown in Figure 4.5, which represents the temporal load application recorded during a test. V_V is the resultant gravity beam load; V_1 and V_2 represent the current beam shear at any cycle.

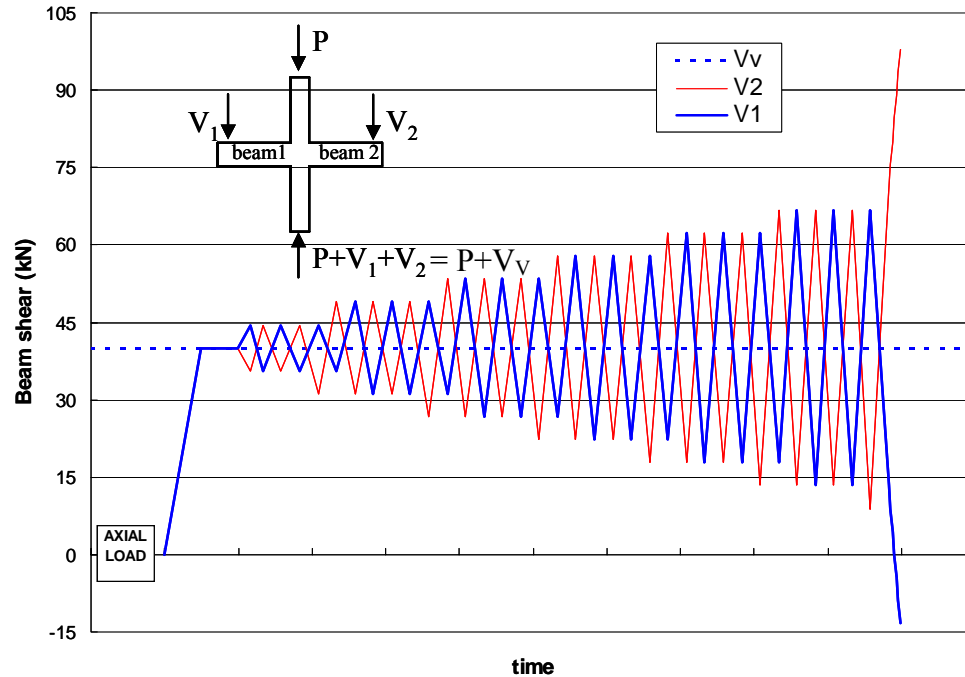
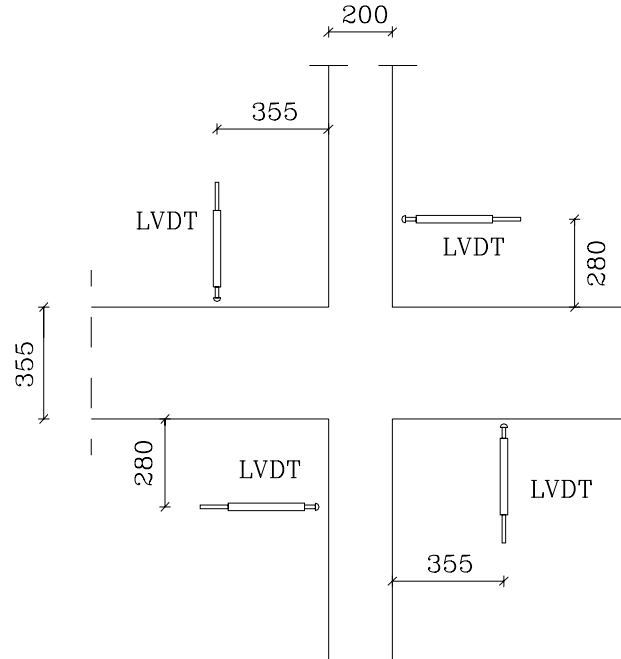


Figure 4. 5 Load history

4.1.2 Instrumentation. As stated in section 4.1.1, three load cells were used: one recorded the axial load in the columns, while the other two registered the shear load on each beam. Member displacements were measured by means of four linear variable displacement transducers (LVDT), two on the beams and two on the columns. They allowed to record relative displacements of cross sections adjacent to the panel over a distance of 355 mm (14 in) in the beams and 280 mm (11 in) in the columns, as Figure 4.6 and Figure B.4 illustrate.



Note: all dimensions are in mm (25.4 mm = 1 in)

Figure 4. 6 LVDT locations

For all the specimens, eight strain-gages were placed on the internal metallic reinforcement. Four of them were located on the longitudinal steel rebars of the beam in order to derive the experimental curvature of the cross sections close to the nodal zone, two on the longitudinal steel rebars of the column to check their strain at ultimate and two on the column steel tie closest to the panel.

Twelve more strain gages were utilized for specimen types 2, 3, 4 and 5. They were applied to the FRP laminate in the direction of the fibers (i.e., hoop direction) on two lines parallel to the axis of the beam at 50 mm (2 in) and 100 mm (4 in) from the ends of the column (Figure 4.7).

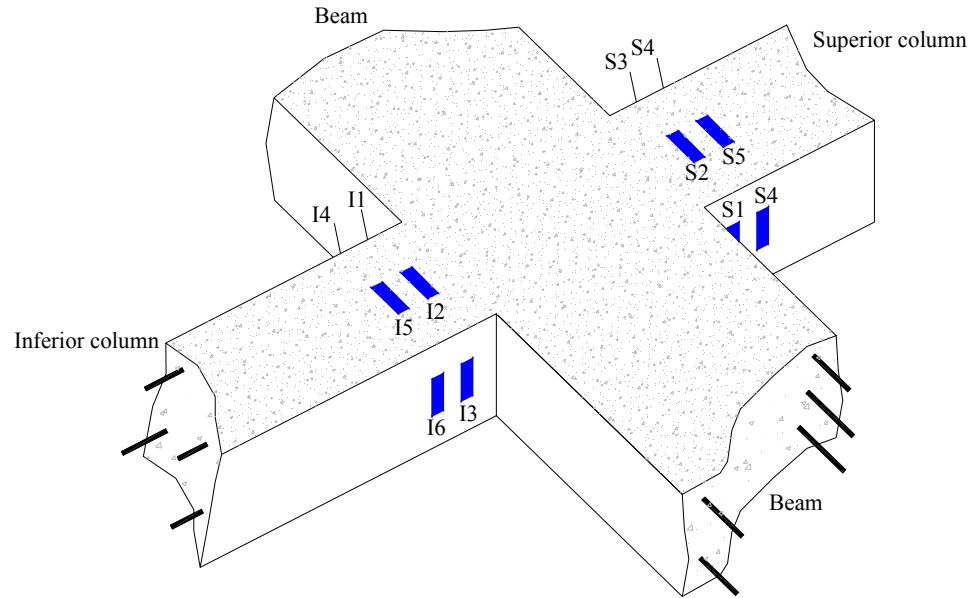


Figure 4.7 Strain gages on the column wrapping

4. 2 TEST RESULTS

This section presents the test results individually for each subassemblage.

4.2.1 Subassemblage L1. Connection L1 was the control specimen for series L (axial load equal to 124.5 kN (28 kips) on the superior column). Keeping that constant load level on the columns, the specimen was loaded as discussed in section 4.1.1.

Between first and second cycles after application of gravity loads, flexural cracks started to open on the top surface of the beams and they propagated toward the bottom surface as the applied shear increased (Figures B.5 and B.6). Then, as the loading proceeded through the pre-determined cycles, the crack pattern evolved in the following sequence: initiation of diagonal shear cracks on the nodal zone (Figure B.7), flexural cracks on the columns (Figure B.8), series of shear cracks parallel to panel diagonals (Figure B.9).

During the eighth cycle column failure occurred (Figures B.10, B.11 and B.12). As expected, the damage was more pronounced on the lower column, subjected to higher axial load. At ultimate, the shear in the columns, calculated by equilibrium, was equal to 41.18 kN (9.08 kips), while the average column lateral displacement (obtained averaging values recorded by the two LVDTs) was equal to 7.66 mm (0.3 in). Figure C.1 illustrates the variation of the column shear with its average lateral displacement.

Displacements measured by LVDTs on the beams allowed to determine the story drift angle, whose value at ultimate was equal to 3.11%. It was calculated as the amount of rotation that must be applied to the specimen in order to restore the position that the ends of its beams had under gravity loads (Beres et al. [1996]). Figure C.2 depicts the column shear versus the story drift angle along the cyclic loading.

4.2.2 Subassemblage H1. Specimen H1 represents the control specimen for series H (axial load equal to 249 kN (56 kips) on the superior column). The crack pattern was similar to that described in section 4.2.1 for connection L1. First, flexural cracks were observed on the beam (Figure B.13); they propagated from its top surface to the bottom one, while the beam shear increased. Then, diagonal cracks started to initiate in the nodal zone (Figure B.14), followed by opening of flexural cracks in the columns (Figure B.15). Panel cracks increased in number before column failure was reached (Figures B.16, B.17 and B.18). Again the damage entity was higher in the lower column. At ultimate, the column shear was equal to 38.45 kN (8.47 kips), corresponding to an average lateral displacement equal to 4.63 mm (0.18 in) and a story drift angle equal to 2.82%. Figures C.3 and C.4 represent the column shear versus the average lateral

displacement and the story drift angle, respectively. Table 4.1 summarizes the results for type 1 subassemblages, recalling also the compressive strength of their concrete as discussed in section 3.4.1.

Table 4. 1 Experimental outcomes for specimens L1 and H1

Sp.	Axial Load		Ultimate Column Shear		Avg. ultimate Lat. Displ.		Story Drift Angle %	f'_c	
	(kN)	(kips)	(kN)	(kips)	(mm)	(in)		(MPa)	(psi)
L1	124.5	28	41.18	9.08	7.66	0.30	3.11	38.9	5633
H1	249	56	38.45	8.47	4.63	0.18	2.82	31.7	4590

4.2.3 Subassemblage L2. This specimen belongs to series L (axial load equal to 124.5 kN (28 kips) on the superior column) and was strengthened by wrapping the columns. As the load was applied, flexural cracks appeared in the beams as already expressed above. Then, diagonal crack initiated and progressed in the nodal zone (Figures B.19 and B.20) until tension failure occurred in the columns (Figures B.21, B.22 and B.23).

The ultimate column shear was equal to 44.21 kN (9.75 kips) corresponding to an average lateral displacement equal to 4.79 mm (0.19 in) and to story drift angle equal to 2.76% (Table 4.4). The variation of the column shear with the lateral displacement and the story drift are illustrated in Figure C.5 and Figure C.6, respectively.

Strain gages placed on the laminates (Figure 4.7) provided information about FRP strains as the load was applied. On the inferior column of specimen L2, strain gage I6 did not work, while on the superior strain gages S1 and S4 were lost. At failure of the specimen, strain gages I3 (i.e., inferior column), S3 and S6 (i.e., superior) were on the compressed face of columns; they recorded strains equal to 0.00079, 0.00187 and 0.00048, respectively. Strain gages I1 and I4, which were located on the tension side at

failure of the connection, provided maximum strains equal to 0.00141 and 0.00083, respectively, for moment values equal to 42.51 kNm and 41.03 kNm. Variations of column moment versus laminate strain are depicted in Figures C.7-10.

This is a typical feature that the reader will notice as strain data are reported. For all specimens, strain measured by gages on the compression side will be provided. Maximum strains of those located at failure on the tension face will be also given; information about the ratio between the maximum strain at each location and the maximum value recorded on the same line, and the ratio between the corresponding moments will be also reported. It is important to recall that, since the moment diagram has a linear variation along the member, strain gages I1, I3, S1 and S3 will have the same moment, higher than that acting at location of I4, I6, S4 and S6.

Table 4.2 summarizes the strains recorded on the columns of connection L2. S^{Max} is the maximum strain value measured at each location. $S^{\text{Max}}/S^{\text{Ult}}$ represents the ratio between the maximum strain at that particular location (S^{Max}) over the maximum strain recorded on the same line at ultimate (S^{Ult}), while $M^{\text{Max}}/M^{\text{Ult}}$ is the ratio between corresponding moments. Both ratios are obviously equal to 1 for those gages that at ultimate were on the compression face and then measured maximum strain values.

Table 4. 2 Strain measurements for specimen L2

Strain Gage	S^{Max}	$S^{\text{Max}}/S^{\text{Ult}}$	$M^{\text{Max}}/M^{\text{Ult}}$
I1	0.00141	1.78	0.91
I3	0.00079	1	1
I4	0.00083	-----	-----
S3	0.00187	1	1
S6	0.00048	1	1

4.2.4 Subassemblages H2, H2L, and H2U. These three connections were subjected to the same axial load level (249 kN (56 kips) on the superior column); their strengthening was based on wrapping the columns with carbon fibers, as presented in section 3.5.2.

In particular, H2 and H2L were identical except for the compressive concrete strength; the reason to have two of them was due to a database problem that caused an incomplete registration of the data for H2L. H2U had a pre-induced confinement problem on one side of the column.

For all of them, initiation of cracks was in the beams and it propagated in the panel with appearance of diagonal cracks that increased while the loading proceeded through the pre-determined cycles (Figures B.24-29). Such similar crack pattern evolved in two different failure modes.

In the case of connections H2 and H2U, the ultimate condition was characterized by shear crisis of the panel (Figures B.30-33) combined with tension failure of the column (Figures B.34 and B.35), resulting in a mixed panel-column failure (Figure B.36). Initiation of carbon fibers breaking evidenced also high strains (Tables 4.5-6) in the compression regions of columns (Figure B.37). For subassemblage H2U, measurements of average crack width at failure were carried out before and after load removal. As depicted in Figure 4.8, portions of two major cracks marked and measurements were conducted. Points S and I correspond to the ends of both cracks at interface of the panel with the superior and inferior column, respectively. The linearized cracks are defined by points S-IB-IA-I and S-IIB-IIA-I; portions between the indicated vertexes are characterized by quite constant crack width. Results are summarized in Table 4.3.

Locally a maximum crack width under load of 1 mm (0.04 in) was recorded along portion IA-IB; cracks at column ends (Figure B.35) were found to have a width equal to about 6 mm (1/4 in) with no major size reduction after load removal.

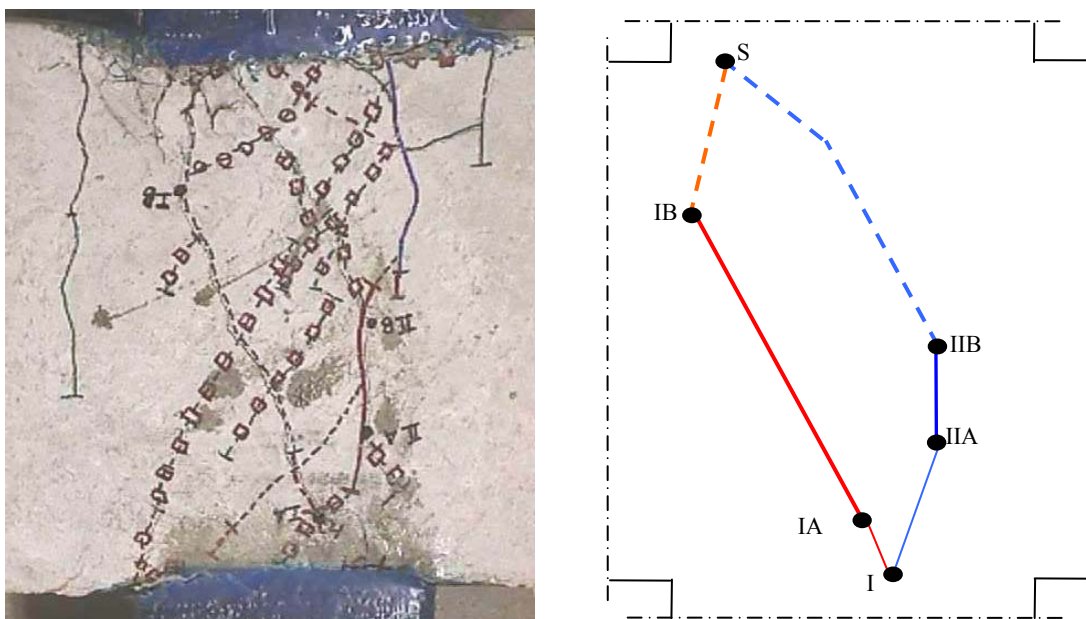


Figure 4. 8 Cracks at failure in the panel of subassemblage H2U

Table 4. 3 Average crack width: specimen H2U

Crack Portion	Avg. Crack Width under Load		Avg. Crack Width under no Load	
	(mm)	(in)	(mm)	(in)
I - IIA	0.15	0.006	0.10	0.004
IIA - IIB	0.40	0.016	0.25	0.010
IIB - S	0.55	0.022	0.30	0.012
I - IA	0.25	0.010	0.15	0.006
IA - IB	0.80	0.031	0.35	0.014
IB - S	0.25	0.010	0.15	0.006

Shear crisis of the panel was predominant in the failure of connection H2L, even though a certain level of damage was observed in the tensile regions of column ends (Figure B.38). As underlined for subassemblages H2 and H2U, high compressive strain at column ends were evidenced by the breaking of fibers close to the maximum moment section (Figure B.39).

For simplicity, the experimental results for connections H2 and H2U, along with those above mentioned for subassembly L2, are summarized in Table 4.4 in terms of ultimate column shear, corresponding average lateral displacement and story drift angle; for each specimen, the actual compressive concrete strength is recalled as discussed in section 3.4.1. For the mentioned data acquisition problems no reliable data was available for specimen H2L. The variation of column shear with lateral displacement and story drift angle is illustrated in Figure C.11 for specimen H2, in Figures C.16-7 for specimen H2U.

Table 4. 4 Experimental outcomes for specimens L2, H2 and H2U

Sp.	Axial Load		Ultimate Column Shear		Av. Ult. Lat. Displ.		Story Drift Angle %	f'_c	
	(kN)	(kips)	(kN)	(kips)	(mm)	(in)		(MPa)	(psi)
L2	124.5	28	44.21	9.75	4.79	0.19	2.76	39.8	5763
H2	249	56	49.70	11.17	-	-	3.50	36.5	5285
H2U	249	56	51.19	11.50	5.63	0.22	3.53	36.5	5285

In terms of laminate strains, for both connections H2 and H2U all placed strain gages recorded up to failure of the subassembly. The results are summarized in Tables 4.5-6, while Figures C.12-15 and Figures C.18-21 show the variation of column moment versus laminate strain at each location.

Table 4. 5 Strain measurements for subassembly H2

Strain Gage	S^{Max}	$S^{\text{Max}}/S^{\text{Ult}}$	$M^{\text{Max}}/M^{\text{Ult}}$
I1	0.0012	1	1
I3	0.00116	0.96	0.82
I4	0.00093	1	1
I6	0.00092	0.99	0.86
S1	0.00149	1	1
S3	0.00099	0.67	0.85
S4	0.00089	1	1
S6	0.00040	0.45	0.88

Table 4. 6 Strain measurements for subassemblage H2U

Strain Gage	S^{Max}	S^{Max}/S^{Ult}	M^{Max}/M^{Ult}
I1	0.00082	0.51	0.82
I3	0.00160	1	1
I4	0.00098	0.79	0.84
I6	0.00124	1	1
S1	0.00047	0.17	0.82
S3	0.00269	1	1
S4	0.00067	0.53	0.88
S6	0.00126	1	1

4.2.5 Subassemblage L3. As presented in section 3.5, connections type 3 were characterized by strengthening of columns by using FRP NSM rods and sheets. The axial load on the superior column of subassemblage L3 was equal to 124.5 kN (28 kips).

As the cyclic load was applied, crack pattern evolved as described in previous sections. First, flexural cracks appeared and propagated from the top to the bottom surface of the beam; then, shear cracks started to open in the panel (Figures B.40 and B.41). The crisis of the specimen was due to shear failure of the panel, as shown in Figures B.42 and B.43.

The column shear at ultimate calculated from equilibrium resulted equal to 57.24 kN (12.62 kips) with an average lateral displacement of 5.8 mm (0.23 in) and a story drift angle equal to 3.3% (Table 4.9). Figures C.22 and C.23 depict the column shear versus the lateral displacement and the story drift angle, respectively.

With the exception of strain gage S4, all strain gages installed on the laminate worked properly up to failure of the subassemblage, recording values as showed in Table 4.7. The variation of the column moment with laminate strain is indeed depicted in Figures C.24-27.

Table 4. 7 Strain measurements for subassemblage L3

Strain Gage	S^{Max}	$S^{\text{Max}}/S^{\text{Ult}}$	$M^{\text{Max}}/M^{\text{Ult}}$
I1	0.00070	0.54	0.71
I3	0.00129	1	1
I4	0.00051	0.71	0.76
I6	0.00071	1	1
S1	0.00032	0.21	0.77
S3	0.00149	1	1
S6	0.00062	1	1

4.2.6 Subassemblage H3. Specimen H3 was different from specimen L3 discussed in section 4.2.5 for the axial load level applied on the superior column (249 kN (56 kips)). However, its crack pattern and failure mode were observed to be very similar to those described for connection L3 (Figures B.44 and B.45). The shear failure of the panel happened when the column shear was equal to 62.35 kN (13.75 kips), corresponding to an ultimate average lateral displacement equal to 3.65 mm (0.14 in) and an ultimate story drift angle equal to 2.42% (Table 4.9). The cyclic variation of column shear with lateral displacement and story drift angle are shown in Figures C.28 and C.29, respectively.

Laminate strains were not recorded in this case due to data acquisition problems.

4.2.7 Subassemblage M3. Even though it was subjected to an axial load (373.5 kN (84 kips) higher than specimens L3 and H3, connection M3 showed the same development of the crack pattern and the same failure. In this case, the shear failure of the panel (Figures B.46 and B.47) occurred when column shear was equal to 56.17 kN (12.38 kips) and caused an ultimate average lateral column displacement of 4.88 mm (0.19 in) and an ultimate story drift angle equal to 3.27% (Table 4.9). Figures C.30 and C.31 illustrate how the column shear varies with the lateral column displacement and the

story drift angle, respectively. Table 4.9 summarizes the test results for all connections type 3.

Laminate strains recorded by all placed strain gages up to failure of connection M3 are summarized in Table 4.8, while Figures C.32-35 show how column moment changes depending on laminate strain at each location.

Table 4. 8 Strain measurements for subassemblage M3

Strain Gage	S^{Max}	$S^{\text{Max}}/S^{\text{Ult}}$	$M^{\text{Max}}/M^{\text{Ult}}$
I1	0.00068	0.55	0.77
I3	0.00124	1	1
I4	0.00078	0.80	0.79
I6	0.00097	1	1
S1	0.00040	0.30	0.77
S3	0.00129	1	1
S4	0.00027	0.43	0.77
S6	0.00063	1	1

4.2.8 Subassemblage L4. As described in section 3.5, connections type 4 are characterized by application of FRP materials on both column and panel. Specimen L4 belongs to that category and it was tested under an axial load of 124.5 kN (28 kips). Composites used for upgrading the connection did not allow to observe the crack pattern during the test, except for the usual flexural cracks opening on the top surface of the beam.

The failure initiated along the interfacial planes between panel and column. It could be referred as interface failure in order to underline that it was due to separation of the panel from the column, in its tension region. Figures B.48-51 allow to observe such crisis of the sub-assemblage. It occurred at an ultimate column shear equal to 56.60 kN (12.48 kips), determining an average lateral column displacement equal to 8.27 mm (0.33

in) and a story drift angle equal to 5.38% (Table 4.11). Figures C.36 and C.37 show how the column shear changes during the load application with the lateral displacement and the story drift angle.

Table 4. 9 Experimental results for subassemblages L3, H3 and M3

Sp.	Axial Load		Ultimate Column Shear		Av. Ult. Lat. Displ.		Story Drift Angle %	f'_c	
	(kN)	(kips)	(kN)	(kips)	(mm)	(in)		(MPa)	(psi)
L3	124.5	28	57.24	12.62	5.80	0.23	3.30	38.9	5633
H3	249	56	62.35	13.75	3.65	0.14	2.42	31.7	4590
M3	373.5	84	56.17	12.38	4.88	0.19	3.27	39.8	5763

Strain measurements provided by all strain gages up to failure of subassemblage L4 are reported in Table 4.10, while trends of column moments versus laminate strains are shown in Figures C.38-41.

Table 4. 10 Strain measurements for subassemblage L4

Strain Gage	S^{Max}	$S^{\text{Max}}/S^{\text{Ult}}$	$M^{\text{Max}}/M^{\text{Ult}}$
I1	0.00075	0.25	0.78
I3	0.00298	1	1
I4	0.00023	0.16	0.77
I6	0.00158	1	1
S1	0.00025	0.14	0.76
S3	0.00187	1	1
S4	0.00023	0.26	0.70
S6	0.00089	1	1

4.2.9 Subassemblage H4. Specimen H4 was characterized by an axial load on the superior column equal to 249 kN (58 kips), but it showed a failure mode very similar to that already described in section VI.2.8 for Specimen L4. Figures B52-55 show this likeness.

The column shear at ultimate was equal to 70.42 kN (15.83 kips), with correspondent average lateral column displacement equal to 6.35 mm (0.25 in) and story drift angle equal to 4.27% (Table 4.11). The entire plot of the column shear versus the lateral displacement and the story angle are reported in Figures C.42 and C.43, respectively. Table 4.11 summarizes the experimental outcomes for type 4 connections.

Results in terms of strain measured on the columns by all strain gages are provided in Table 4.12, while variations of column moment versus laminate strain can be observed in Figures C. 44-47.

Table 4. 11 Experimental results for subassemblages L4 and H4

Sp.	Axial Load		Ultimate Column Shear		Av. Ult. Lat. Displ.		Story Drift Angle %	f'_c	
	(kN)	(kips)	(kN)	(kips)	(mm)	(in)		(MPa)	(psi)
L4	124.5	28	56.60	12.48	8.27	0.33	5.38	36.5	5285
H4	249	56	70.42	15.83	6.35	0.25	4.27	39.8	5763

Table 4. 12 Strain measurements for subassemblage H4

Strain Gage	S^{Max}	$S^{\text{Max}}/S^{\text{Ult}}$	$M^{\text{Max}}/M^{\text{Ult}}$
I1	0.00042	0.26	0.65
I3	0.00162	1	1
I4	0.00045	0.38	0.65
I6	0.00116	1	1
S1	0.00046	0.22	0.64
S3	0.00211	1	1
S4	0.00033	0.27	0.65
S6	0.00122	1	1

4.2.10 Subassemblage H5. No data are available for this connection due to a problem concerning one of the used load cells. However, test of connection H5 confirmed the same failure mode already discussed in sections 4.2.8 and 4.2.9, as illustrated in Figures B.56-58.

5. ANALYSIS AND DISCUSSION OF TEST RESULTS

Experimental outcomes have been already presented in Chapter 4. Herein, failure modes are analyzed and compared to understand whether or not the upgrade level could attain a desirable failure mechanism. Experimental results are compared in terms of strength and story drift angle. Joint stresses are also computed both at its first cracking and at failure of the connection: such analysis aims at understanding joint failure mechanisms and defining stress limitations in order to prevent it. The effectiveness of the FRP wrapping of columns is then evaluated by comparing strain gages measurements. Overall remarks are finally proposed taking into account the influence of different components and parameters on the seismic performance of the subassemblage.

5.1 FAILURE MODES

Both control connections (i.e., L1 and H1) showed column failure due to concrete crushing (Figures B10-11 and B.16-17). The experimental evidence confirmed that the design objective was reached: as pointed out in section 3.3.2, regardless of the axial load ratio, the goal was to start with control subassemblages simulating typical situations of real GLD frames. In terms of failure mode, this means to begin from the lower bound of the hierarchy of strength (i.e., column failure).

The wrapping of columns moved the failure from the compression to the tension side (Figures B.21-23) when the axial load ratio was equal to 0.1 (i.e., L2). The column wrapping increased the level of confinement and prevented concrete crushing; however, the crisis of columns was not avoided due to deficiency on the tension side.

For axial load ratio equal to 0.2 (i.e., H2 and H2U), the column wrapping allowed a combined column-joint failure (Figures B.30-36). In this case, the higher column compressive strain due to gravity load played a beneficial effect on tensile deficiency.

The installation of NSM bars along with wrapping (i.e., L3, H3 and M3) allowed for moving the failure from the column to the joint (i.e., shear failure) regardless the axial load ratio (Figures B.42-47). Experiments confirmed that the addition of NSM bars is crucial in order to step up to the intermediate level of the strength hierarchy (i.e., shear failure of the joint). Calvi et al. [2001] underlined that, in the case of interior connections, moving the crisis from the column to the joint can improve the global behavior of the frame, reducing the displacement demand on the column. However, the shear crisis of the joint is brittle and its influence on the global performance needs to be assessed in order to understand its positive or negative contribution in terms of energy dissipation of the entire frame.

The strengthening of the joint region (i.e., L4, H4 and H5) induced the failure to occur at column-joint interface (Figures B.48-58). This type of failure is function of the configuration of the FRP reinforcement: as discussed in section 3.5.4, in the direction perpendicular to the beam axis the laminate was terminated at column-joint interface in order to account for the presence of the floor system. For this reason, the interface was unable to withstand high stress and experienced local failure.

5. 2 STRENGTH AND STORY DRIFT ANGLE

The design of seismic upgrade should always look at both strength and ductility; a trade off between these two parameters should be achieved in order to optimize the improvement of structural performance and provide a significant contribution to the

global behavior of the frame. In this section, a comparison for each series of tested subassemblages (i.e., L and H) is conducted first; similar connections (i.e., same upgrade schemes) are then analysed in order to evaluate the influence of the axial load ratio. General remarks are provided considering the influence of different parameters.

5.2.1 Comparison for each series. The series of connections with low axial load ratio (i.e., 0.1) is based on specimens L1, L2, L3 and L4. In terms of strength, the wrapping of columns (i.e., L2) allowed for an increase of 7.4 %, while the addition of NSM rods (i.e., L3) boosted it of about 39%. The installation of FRP on the joint (i.e., L4) did not alter the gain in strength compared to L3 also due to an initial lower compressive strength (i.e., about 6.4 % less). In terms of ductility, the first level of upgrade (i.e., L2) determined a reduction of the story drift angle of about 11.3 %; this upgrade improved strength, but also increased stiffness, influencing the global deformation capacity of the entire subassemblage. Adding NSM rebars (i.e., L3) provided a gain in ductility of about 6.1 %, while the highest level of upgrade (i.e., L4) allowed for a ductility increase equal to about 73 %. The strengthening of the joint avoided its shear failure, which is brittle, and then determined a substantial gain in ductility. These results are summarized in Table 5.1 and depicted in Figure C.48 in terms of envelope curves.

Table 5. 1 Comparison between series L specimens

Sp.	Ultimate Column Shear		Strength Increase (%)	Story Drift Angle %	Ductility Increase (%)	f'_c	
	(kN)	(kips)				(MPa)	(psi)
L1	41.18	9.08	-----	3.11	-----	38.9	5633
L2	44.21	9.75	7.4	2.76	-11.3	39.8	5763
L3	57.24	12.62	38.9	3.30	6.1	38.9	5633
L4	56.60	12.48	37.4	5.38	72.9	36.5	5285

Series H is characterized by axial load ratio equal to 0.2. As mentioned in section 3.3.2, an additional specimen was built (i.e., H2U) in order to evaluate if wrapping could correct a lack of confinement due to a construction or design error. As showed in Table 5.2, the FRP wrapping of columns allowed subassemblage H2U to achieve strength and ductility performances very close to a similar connection having no confinement defect (i.e., H2). In both cases, the strength of the control specimen was increased of about 30%, while the addition of NSM rods in the column (i.e., H3) boosted that value of about 62%. Upgrading the joint region (i.e., H4) determined that the control strength was improved up to about 83%. In terms of ductility, for this axial load ratio the wrapping of columns improved the deformation capacity of the subassemblage of about 25%. The presence of NSM rods increased both strength and stiffness of columns, decreasing the story drift of about 14%. With the upgrade of the joint, the story drift was increased of about 51%.

As Table 5.2 allows to observe, specimens of series H also have some differences in concrete strength; the analysis of the experimental results needs to take this into account. Figure C.49 depicts a comparison between series H connections in terms of envelope curves reporting column shear versus story drift angle. Both Figures C.48 and C.49 allow for a qualitative comparison between different specimens in terms of dissipated energy, which is somehow related to the area under each envelope curve. Regardless of ultimate drift values summarized in Tables 5.1-2, the energy dissipation capacity appears to increase as more FRP is installed on the specimen; preliminary outcomes from work presently in progress on energy calculations confirmed such visual observation. This is a very meaningful outcome of the experimental program, which

confirms that the use of the proposed technique could allow for improving the energy dissipation capacity of the structure.

5.2.2 Comparison based on f'_c and P. As Tables 4.1, 4.4, 4.9 and 4.11 report, a comparison between connections with the same upgrade scheme could not neglect the differences concerning f'_c along with axial load ratio. Envelope curves are compared for similar specimens in Figures C.50-53.

Table 5. 2 Comparison between series H specimens

Sp.	Ultimate Column Shear		Strength Increase (%)	Story Drift Angle %	Ductility Increase (%)	f'_c	
	(kN)	(kips)				(MPa)	(psi)
H1	38.45	8.47	-----	2.82	-----	31.7	4590
H2	49.70	11.17	29.3	3.50	24.1	36.5	5285
H2U	51.19	11.50	33.1	3.53	25.2	36.5	5285
H3	62.35	13.75	62.2	2.42	-14.2	31.7	4590
H4	70.42	15.83	83.1	4.27	51.4	39.8	5763

For control connections, the lower axial load ratio (i.e., L1) allowed for a story drift angle about 10 % (Table 4. 1) higher than for ratio of 0.2 (i.e., H1). The strength of L1 also was higher of about 7 %. The column wrapping inverted this hierarchy, determining for specimens H2 and H2U strength and story drift angle higher than for L2 of about 13 % and 25%, respectively (Table 4. 4). Further application of NSM bars (i.e., L3, H3 and M3) provided almost same performances for axial load ratio of 0.1 and 0.3 (i.e., L3 and M3), while specimen H3 achieved about 9 % more in strength and about 26 % less in ductility. It is important to underline again that specimen H3 had f'_c about 19 % lower than the other two (Table 4.9). When the joint was also strengthened (i.e., L4 and H4), the connection with lower axial load ratio (i.e., L4) achieved a ductility about 26

% higher than that of H4; however, its strength was lower than that reached by H4 of about 19 % (Table 4.11).

5. 3 ANALYSIS OF JOINT STRESSES

The analysis of stresses within the joint region was conducted according to the approach suggested by Paulay and Priestley [1992]. If, as Figure 5.1 shows, the following entities are defined: V_{jh} as the horizontal joint shear force, V_{jv} as the vertical joint shear force, V_{col} as the average of column shears above and below the joint, T and T' as the tensile stress resultants of beams, C_c and C_c' as the compression stress resultants of beams, and C_s and C_s' as the compression stress resultants in the steel of beams, V_{jh} can be expressed as:

$$V_{jh} = T + C'_c + C'_s - V_{col} = T' + C_c + C_s - V_{col} \quad (1)$$

and, if the approximation $T' = C'_c + C'_s$ (i.e., no axial force is applied on the beam, then the algebraic sum of tension plus compression must be zero) is acceptable, (1) can be written as:

$$V_{jh} = T + T' - V_{col} \quad (2)$$

Based on the horizontal joint shear force V_{jh} , Paulay and Priestley [6] defined the nominal joint shear stress as:

$$v_j = V_{jh}/A_{col} \quad (3)$$

where A_{col} is the gross area of the column cross section. It is important to recall that the nominal shear stress, v_j , has no physical meaning; it is a useful index in order to

understand and eventually limit the level of shear acting on the joint. Paulay and Priestley [1992] suggested that, for one-way frames, v_j is limited at $0.25f'_c$ in order to avoid brittle failure of the joint due to diagonal compression.

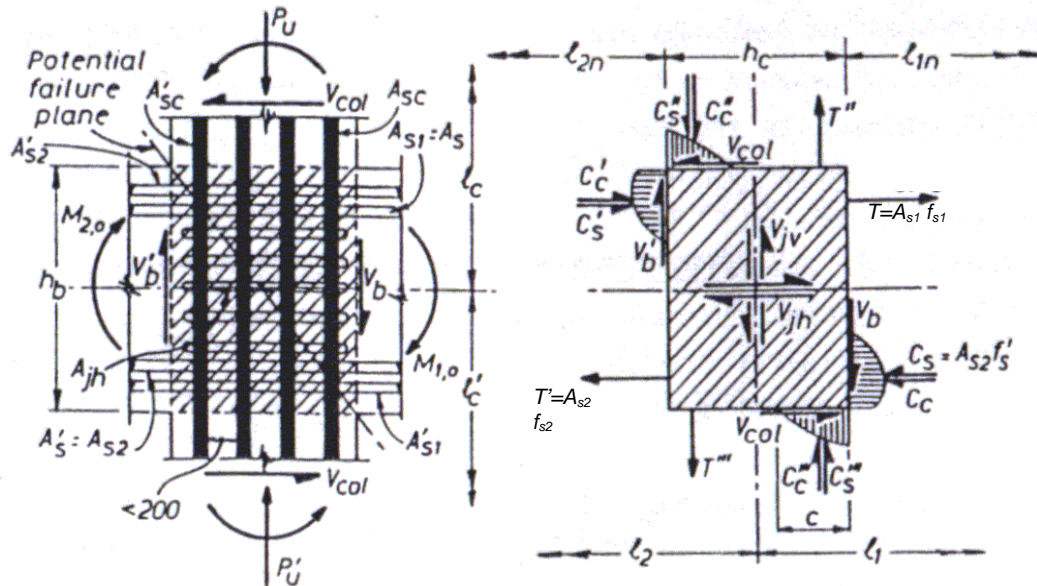


Figure 5. 1 Equilibrium of interior joint (Paulay and Priestley, 1992)

Based on this approach, for specimens having no FRP reinforcement in the joint, calculations of the nominal shear stress were conducted at both first cracking of the joint and failure of the subassembly. Studying also first cracking of the joint and comparing it to ultimate conditions both in terms of strength and story drift angle represents an important step since seismic guidelines (such as ATC 40) consider that as a first level of significant structural degradation. Toward the development of design criteria for the seismic upgrade of these frames, this stage could be used as a limit state and limitations of stresses and/or story drift could be suggested based on its occurrence.

First cracking of joints reinforced with FRP (i.e., L4 and H4) was not estimated as the visual method used for detecting cracking initiation was not possible in these cases.

For such specimens, calculations only at failure of the subassembly were performed. V_{col} was calculated based on equilibrium considerations, while both steel forces were computed considering the strains generated by shear forces on each beam. Results are summarized in Table 5.3. The nominal shear stresses at both first cracking and failure are reported, and the corresponding column shear forces T_{crj}^C and T_{ultsub}^C are showed. The column shear, T_{ultPP}^C , corresponds to a nominal joint shear stress equal to $0.25f'_c$ as suggested by Paulay and Priestley [1992].

For control subassemblages L1 and H1, the nominal shear stress at ultimate was the 76 % and 83 %, respectively, of the Paulay and Priestley limit. This is consistent with the observed failure mode, which did not involve the joint. For type 2 specimens, the ratio between experimental and limit values increased: at failure of connection L2, the ultimate v_j was about 83 % of the limit, while for H2 and H2U it was about 94 % and 97 % of the suggested threshold, respectively.

Table 5. 3 Nominal shear stresses and column shear at cracking of the joint and ultimate of the subassemblage

Sp.	EXPERIMENTAL				THEORETICAL	
	v_j at first cracking of the joint (MPa)	T_{crj}^C (kN)	v_j at failure of the subassemblage (MPa)	T_{ultsub}^C (kN)	$0.25 f'_c$ (MPa)	T_{ultPP}^C (kN)
L1	4.83	15.8	7.48	41.18	9.73	55.8
L2	4.83	15.8	8.2	44.21	9.95	56.7
L3	5.90	26.3	9.85	57.24	9.73	55.8
H1	4.83	15.8	6.57	38.45	7.93	45.9
H2	5.36	21.0	8.56	49.7	9.13	52.7
H2U	5.36	21.0	8.93	51.19	9.13	52.7
H3	5.36	21.0	10.6	62.35	7.93	45.9
M3	7.59	31.5	9.65	56.17	9.95	56.7
L4	-----	-----	10.2	56.60	9.13	52.7
H4	-----	-----	12.6	70.42	9.95	56.7

The smaller increase for series L (i.e., 83 % versus 76 %) can be explained considering that the wrapping of column moved just the failure from the compression to its tension side. For series H, higher values (i.e., 94 % and 97 % versus 83 %) are justified by the fact that specimens H2 and H2U showed a combined column-joint failure. For type 3 specimens, the ultimate nominal shear stress approached (i.e., L3 and M3) and overcame (i.e., H3) the limit value.

The nominal shear stress is just an index that can be used in the design; since the crisis of the joint is due to the crushing of the diagonal strut (Figure 5.2), it appears more appropriate to give a direct limitation to the principal compression stress; this would allow to take into account also the axial load levels on both column and beam.



Figure 5. 2 Crushing of the diagonal strut at failure of specimen L3

Similarly, the value of the principal tension stress could be adopted as a reference for first cracking of the joint. Priestley et al. [1996] showed that, adopting the Mohr's circle analysis, the principal stresses in the joint region can be derived as follows:

$$p_c, p_t = \frac{f_v + f_h}{2} \pm \sqrt{\left(\frac{f_v - f_h}{2}\right)^2 + v_j^2} \quad (4)$$

where p_c and p_t are the principal compression and tension stresses, while f_v and f_h the average axial stresses in vertical and horizontal directions. In this particular case, f_h is equal to zero since no axial load is applied to beams. Discussing about interior joints of bridges, Priestley et al. [1996] suggested that the principal tension stress is limited at $0.29f_c^{0.5}$ in order to avoid the cracking initiation of the joint and the principal compression stress, p_c , is limited at $0.3 f_c$ in order to prevent the compression crisis of the diagonal strut; they underlined that, for column axial load ratio equal to 0.1 and no axial load on beams (i.e., series L within the experimental program), the latter condition corresponds to limiting the nominal shear stress at $0.25 f_c$, as indicated by Paulay and Priestley [1992]. However, the analysis of several tests on interior joints induced Priestley [1997] to suggest as upper limit for the principal compression stress, p_c , the value of $0.5 f_c$.

For type 1, 2 and 3 specimens, principal stresses were computed at both first cracking of the joint and at failure of the subassemblage. Results of these calculations are reported in Table 5.4. Principal stresses are computed and values of column shears corresponding to $p_t=0.29f_c^{0.5}$ (i.e., $T_{cr0.29}^C$), $p_c=0.3f_c$ (i.e., $T_{ult0.3}^C$) and $p_c=0.5f_c$ (i.e., $T_{ult0.5}^C$) are summarized. As Table 5.4 shows, limitations of the principal tension stress at

first cracking of the joint are very conservative as compared to the experimental evidence. Limiting the principal compression stress at 30% of f'_c appears to provide a reliable criterion; the performed tests confirmed that it is conservative in all cases when the crisis regarded the joint (i.e., L3, H3 and M3).

In order to find a more reliable criterion for first cracking of the joint the approach proposed by Kupfer and Gerstle [1973] was followed. They studied the behavior of concrete under biaxial states of stress and summarized the results of their analysis by providing interaction curves. The part of interest within this context concerns the interaction diagram for biaxial state compression-tension, which is representative of stresses induced in the joint as the seismic load is applied. Indicating with σ_1 and σ_2 the principal compression and tension stress, respectively, the interaction curve is expressed by the equation:

$$\frac{\sigma_2}{f'_c} = 1 + 0.8 \frac{\sigma_1}{f'_c} \quad (5)$$

In Figure 5.3, principal stresses at first cracking of type 1 and 2 joints (Table 4) are plotted in the plane σ_1/f'_c and σ_2/f'_c ; they are aligned along the Kupfer and Gerstle curve. For type 3 specimens, work is in progress in order to evaluate the contribution of NSM rods to the principal tension stress. Its outcomes will provide another curve for FRP reinforced joints.

The analysis of stresses within the joint underlined the following aspects:

- at first cracking of the joint (detected by visual observation) the principal tension stress was much higher than the limit of $0.29f'_c{}^{0.5}$ suggested by Priestley et al. [1996].

The experimental evidence provided values of the principal tension stress at cracking

initiation of the joint ranging between 0.44 (i.e., specimen H1) and 0.69 (i.e., specimen L3) of $f'_c{}^{0.5}$;

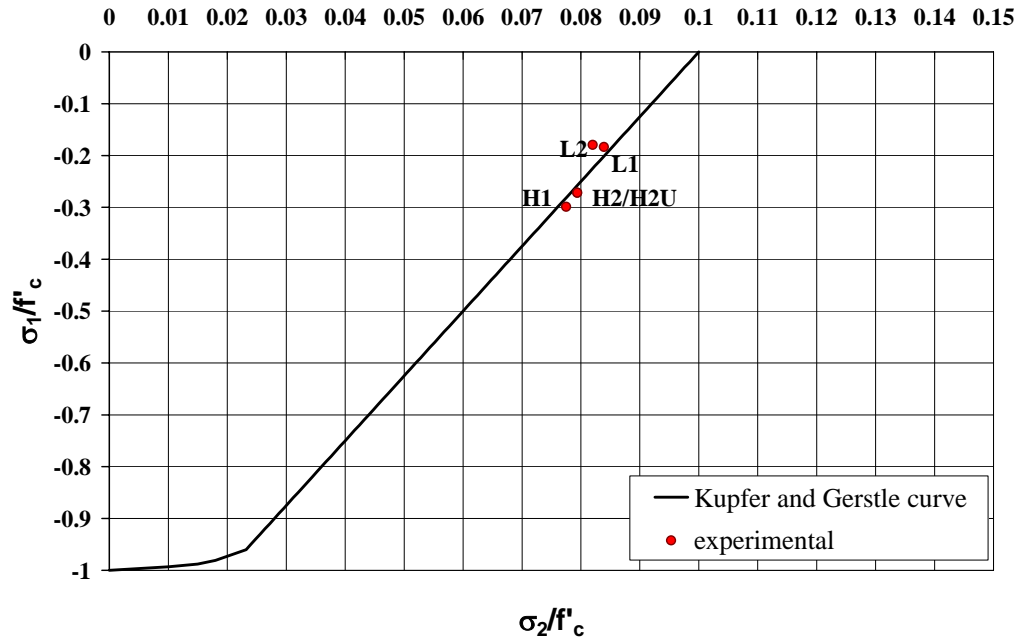


Figure 5.3 Kupfer and Gerstle curve : theoretical vs. experimental

- the Kupfer and Gerstle approach appears to provide more reliable predictions of the column shear corresponding to the first cracking of the joint. The extension of the theory to the case of FRP reinforced joint will allow for computations on a wider number of cases;
- a comparison with experimental outcomes highlights that the limit of $0.3f'_c$ for the principal compression stress at failure of the joint could be a reasonable design criterion, even though it is conservative for high axial load ratios (i.e. type H and M specimens). As Table 4 shows, such limit is conservative in all three cases (i.e., L3, H3 and M3) where failure of the joint was observed; only for specimens L1 and L2 (i.e., column failure), the column shear at failure of the connection corresponded to

- lower values of p_c . On the other side, for low concrete strength (i.e., H1 and H3) or very high axial load, such threshold appears too much conservative;
- the limit of principal compression stress equal to $0.5f_c$ was never reached within the experimental program. For what observed during tests, it appears to provide not conservative predictions;
 - the stress analysis allows for explaining the fact that, for all type 3 connections (i.e., L3, H3 and M3), the failure of the subassemblage due to joint crisis occurred at almost same values the column shear (see section 5.2). Such aspect was also underlined by Murakami et al. [2000] as one of the relevant outcomes provided by a database on many tests on interior RC connections performed in different laboratories since 70's. They found that joint strength was influenced by concrete strength, while a minor effect was played by the axial load ratio. The analysis herein developed shows that the crisis of the joint is due to a particular combination of principal compression and tension stresses for which the joint approaches critical conditions. Such limit states could be expressed in terms of nominal shear stress or as direct limitations on principal stresses; a prediction on joint behavior cannot be done considering only axial load ratio or concrete strength that both influence to the attainment of the above limit states.

5. 4 LAMINATE STRAINS

The effectiveness of column wrapping has been already discussed in previous sections for its influence on failure modes and structural performance (i.e., strength and ductility) of the subassemblage. As reported in Chapter 4, measurements from strain gages placed on the FRP wrapping were also recorded; the analysis of provided strain

values gives an direct measure of how much confinement demand was required for each specimen.

Table 5. 4 Principal stresses and column shear at cracking of the joint and ultimate of the subassembly

Sp.	EXPERIMENTAL						THEORETICAL		
	At first cracking of the joint			At failure of the subassembly			for $p_t=0.29f'_c{}^{0.5}$	for $p_c=0.3f'_c$	for $p_c=0.5f'_c$
	T_{crj}^C (kN)	p_c (MPa)	p_t (MPa)	T_{ultsub}^C (kN)	p_c (MPa)	p_t (MPa)	$T_{cr0.29}^C$ (kN)	$T_{ult0.3}^C$ (kN)	$T_{ult0.5}^C$ (kN)
L1	15.8	7.13	-3.26	41.18	9.66	-5.78	0.6	56.7	103.1
L2	15.8	7.13	-3.26	44.21	10.36	-6.49	0.8	57.8	105.4
L3	26.3	8.14	-4.27	57.24	11.98	-8.10	0.6	56.7	103.1
H1	15.8	9.48	-2.46	38.45	10.96	-3.94	6.0	16.2	69.5
H2	21.0	9.92	-2.90	49.70	12.76	-5.74	7.6	33.5	84.3
H2U	21.0	9.92	-2.90	51.19	13.10	-6.08	7.6	33.5	84.3
H3	21.0	9.92	-2.90	62.35	14.66	-7.64	6.0	16.2	69.5
M3	31.5	13.11	-3.11	56.17	15.87	-5.87	14.9	16.4	82.3

For strain gages I1 and I3 (see Figure 4.7), wrapping strains at failure of the connection were always above 0.0012, with a peak of 0.0030 in the case of specimen L4 (see Table 4.10). Strain gages symmetrically located with respect to the beam axis, S1 and S3, gave strains of the wrapping at ultimate of the subassembly above 0.0013, with a peak of 0.0027 recorded on connection H2U (see Table 4.6). Such high strain occurred on the column where steel ties were deliberately left out (section 3.3.2), as Figure 5.4 shows.

The discussion of section 5.2.2 underlined that such lack in steel ties was fully compensated by FRP wrapping so that connection H2U performed almost in the same way as specimen H2, having no defect. However, the laminate strain (on the first line of

the superior column) at ultimate for H2U was equal to 0.27 % compared to the value of 0.15 % measured on the same column of subassemblage H2.



Figure 5. 4 Confinement defect on the superior column of connection H2U

In terms of strain recorded on lines at higher distance from the column maximum moment cross section, gages I4 and I6 (see Figure 4.7) gave values at ultimate above 0.07 %, with peaks of about 0.12 % measured on specimens H2U and L4 (see Tables 4.6 and 4.10). Gages S4 and S6 provided ultimate strains of the FRP wrapping always above 0.06 %; two peak values of about 0.12 % were observed for specimens H2U and H4 (see Tables 4.6 and 4.12).

Discussed strains of the laminates confirm the effectiveness of the FRP wrapping already observed in terms of structural performance. They also point out the very rapid reduction of confinement demand moving from first (i.e., I1, I3, S1 and S3) to second (i.e., I4, I6, S4 and S6) lines. In the average, the observed FRP strain reduction was equal to about 50 %, while the flexural moment decreased of 5 % (recall that the distance of first and second line from column hinge was 1000 mm and 950 mm, respectively).

5. 5 INFLUENCE OF MEMBERS UPGRADE ON THE PERFORMANCE OF THE SUBASSEMBLAGE

The previous analysis of test results underlined that, depending on the axial load ratio and f'_c , the upgrade of a component (i.e., column or joint) has different effects on strength and ductility of the subassembly. Experimental outcomes could be analyzed in terms of column shear versus story drift angle. This was done at both first cracking of the joint and failure of the subassembly. For each level of upgrade (i.e., 1, 2, 3 and 4), areas having experimental points as vertexes are depicted in Figure 5. 5. No area represents cracking initiation for type 4 specimens since this stage could not be detected due to external FRP reinforcement applied on the joint.

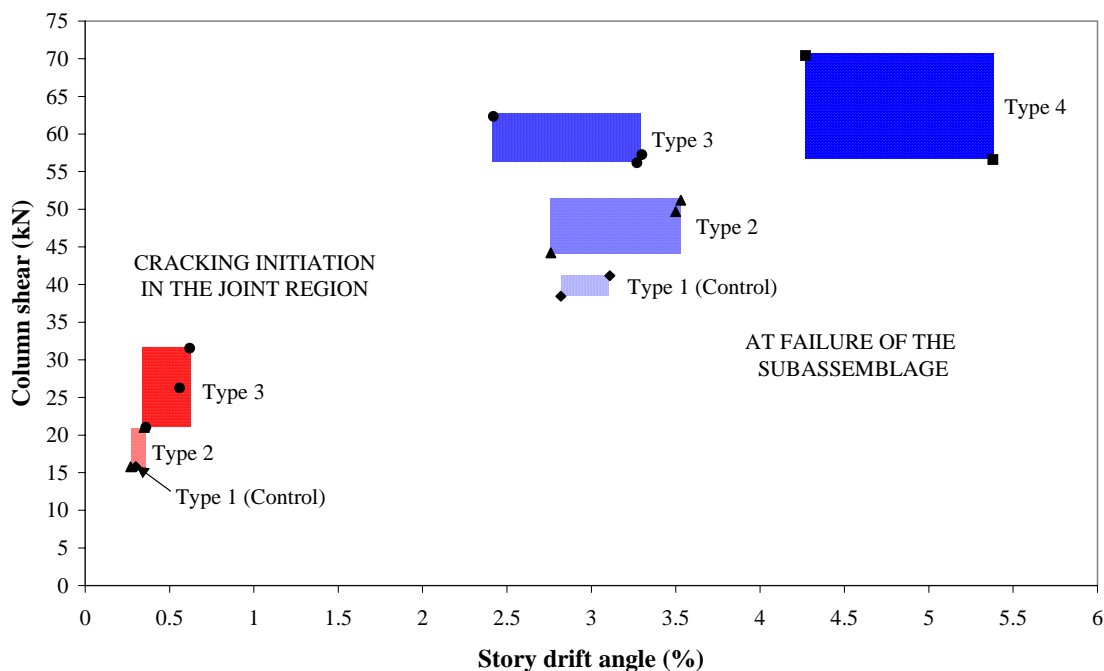


Figure 5. 5 Column shear vs. story drift angle at cracking of the joint (left hand side) and at failure of the subassembly (right hand side)

At cracking initiation of the joint, both control connections reached the same story drift for the same cracking shear in the column (i.e., point indicated by the arrow). The

wrapping of columns did not imply a significant change both in terms of cracking force and ductility, while the combination of FRP laminates and bars allowed a gain of about 60 % in both column shear and story drift at cracking of the joint.

In terms of ultimate performances of the subassemblage, the upgrade level 2 determined a gain in strength ranging between 10% and 26%, while scheme 3 generated an increase between 43% and 55%. Both of them did not allow for a significant improvement in terms of ductility, which could be even reduced by the wrapping of columns with low axial load ratio or by a combined application of FRP laminates and bars to columns with low concrete strength. In these cases, the presence of FRP increased the sectional ductility of the column, but reduced its deformability as member and also provided a stiffening effect on the entire subassemblage. The strengthening of the joint caused a considerable improvement of the seismic performances of the connection, with a gain between 44% and 75% in strength and between 50% and 75% in story drift angle.

These considerations on test results suggest the following remarks:

- along with the amount and location of FRP, axial load ratio and material properties could play an important role on the global performances of upgraded subassemblages;
- strengthening the column (i.e., level 2 and 3) could improve the behavior of the subassemblage, but, due to the brittle failure of the joint, it did not provide too much in terms of ductility. The upgrade of the nodal zone increased the deformability of the joint and also provided a significant contribution to the ductility of the system;
- the configuration of FRP reinforcement on the joint took into account actual field conditions (i.e., presence of slab), but limited the effectiveness of its upgrade. The

- termination of the laminate in the direction perpendicular to the beam axis determined a shear failure at the column-joint interface. This highlights how constructability issues can dramatically affect the strengthening in terms of achievable improvement of structural performance;
- a reliable assessment of the actual conditions of the original structure represents a crucial step toward a successful upgrade. Information about acting loads, material properties and actual hierarchy of strength are preliminary to the strengthening design. Once the actual hierarchy of strength (i.e., where we are) is known, the proposed technique could allow for a selective upgrade (i.e., what we like to reach from a global stand-point) by targeting location and amount of composites.

6. CONCLUSIONS

The experimental program showed that the proposed technique could represent a very effective solution for the seismic upgrade of GLD RC frames. As mentioned in previous sections, tested subassemblages are representative of the behavior of frames which they belong to. Column failure was observed in the case of bare specimens; it also occurred on the wrapped column of connection with low axial load ratio. The application of FRP NSM bars allowed to move the failure on the joint. When further FRP external reinforcement was installed in order to strengthen it, failure at column-joint interface was caused by local stress concentration.

Experimental Outcomes: Tests on different upgrade schemes showed that the strength is always increased as more external FRP reinforcement is added to the subassemblage. The proposed technique allowed to increase the strength of the bare subassemblage up to 83 % (series H), while for series L the maximum increase was equal to 39 %. A different trend was noticed on ductility, expressed in terms of story drift angle. Depending on f'_c and P, each upgrade scheme played a different influence on the ductility of the system. Such aspect has been discussed in section 5.3. The outcomes of the conducted tests could be summarized as:

- the proposed upgrade technique could enable to modify the hierarchy of strength of the subassemblage by targeting amount and location of the FRP reinforcement;
- depending f'_c and P, the influence of different upgrade schemes on the global performance of the subassemblage can change: while the strength increases always as more FRP reinforcement is applied, this is not true for the ductility of the system. A

- preliminary assessment of the actual strength hierarchy of the bare connection and its material properties is needed in order to select the most effective upgrade and optimize its contribution to the global response of the structure;
- conducted tests showed that NSM bars, combined with FRP wrapping, are necessary in order to avoid column failure in GLD structures. Moving the failure to the joint, they provide a significant strength gain, even though the ductility could decrease as joint failure is brittle;
 - the real optimum of structural performance can be reached only by strengthening the joint. In general, this does not add too much in terms of strength, but it allows for more deformability, resulting in higher ultimate story drift angle;
 - the failure at column-joint interface represented an upper bound within this experimental program. More research is needed on this issue in order to exploit improved solutions enabling to withstand high stress concentrations;
 - the structural validation of the proposed technique needs to be completed with a detailed analysis on the constructability of the system. A reliable and sound procedure for drilling through the joint in order to install NSM rods should be defined.

Stress analysis of the joint: The stress analysis of the joint showed that the Kupfer and Gerstle [1973] approach can be used in order to predict cracking initiation of the joint. Its extension in order to account for the contribution of NSM bars to principal tension stress will be analyzed in order to develop a complete and reliable tool for the prediction of first cracking of the joint. Limitations proposed in literature on principal compression stresses have been examined in order to define criteria for the prediction of joint failure.

Experimental-theoretical comparisons showed that the limit of $0.3 f'_c$ gives reliable estimates of joint strength. However, more data would be necessary in order to assess the general validity of such limitation.



Figure A. 1 Typical formworks: on the left H3, on the right H1



Figure A. 2 Typical beam reinforcement



Figure A. 3 Typical metallic reinforcement of the nodal zone



Figure A. 4 Typical stirrup spacing of the column



Figure A. 5 Wooden predisposition for NSMR: L3, L4, H3, H4, H5, M3



Figure A. 6 View of the beam prior to concrete casting: L4



Figure A. 7 Induced confinement defect in the column: H2U



Figure A. 8 Concrete vibration: H1



Figure A. 9 After casting: on the left H1, on the right H4



Figure A. 10 Rounding of the corners prior to laminates application



Figure A. 11 Rounded corner



Figure A. 12 Primer application



Figure A. 13 Filling of holes and imperfections by putty



Figure A. 14 Impregnation of fibers by saturant



Figure A. 15 Drilling through the panel prior to installation of NSM rods



Figure A. 16 Joint prepared for the installation of NSM rods



Figure A. 17 Blowing of the grooves



Figure A. 18 Hand cleaning of the grooves



Figure A. 19 Pouring of the first layer of concrete paste into the grooves



Figure A. 20 Installation of NSM FRP rod

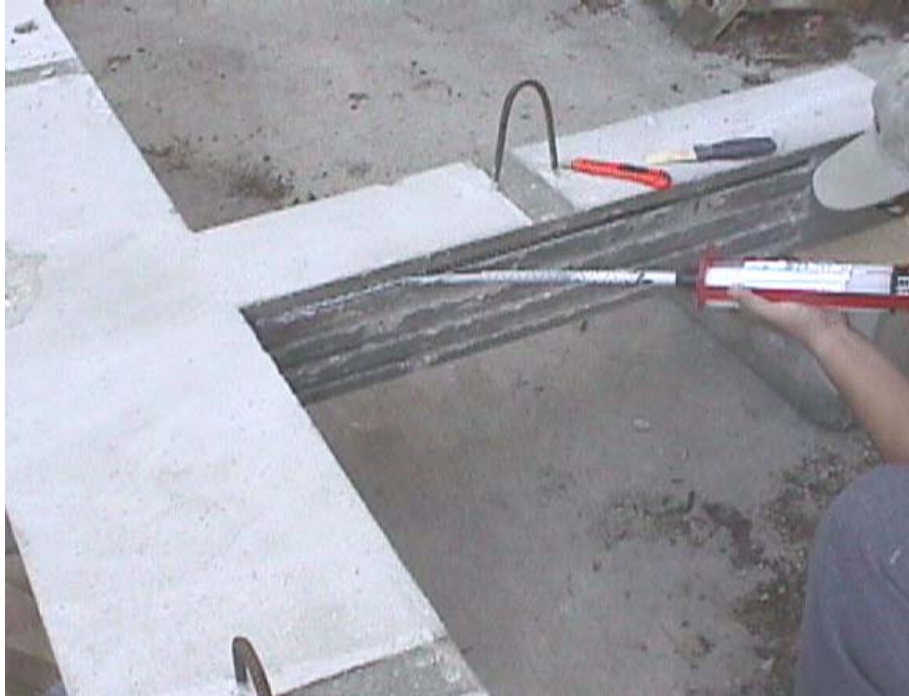


Figure A. 21 Filling of the grooves after rod installation



Figure A. 22 Finishing of the surface after installation of NSM rods



Figure A. 23 Joint after installation of NSM rods has been completed



Figure A. 24 NSM FRP rods as horizontal reinforcement of the panel



Figure A. 25 NSM rods installed into the columns and the panel



Figure A. 26 Application of carbon laminate as vertical reinforcement of the panel



Figure A. 27 Completed upgrade of joints L4 and H4



Figure A. 28 Curing of the primer prior to putty application



Figure A. 29 Curing of putty prior application of saturant



Figure A. 30 U-wrapping of beam around its bottom surface: joint H5



Figure A. 31 View of the top surface of the beam: joint H5

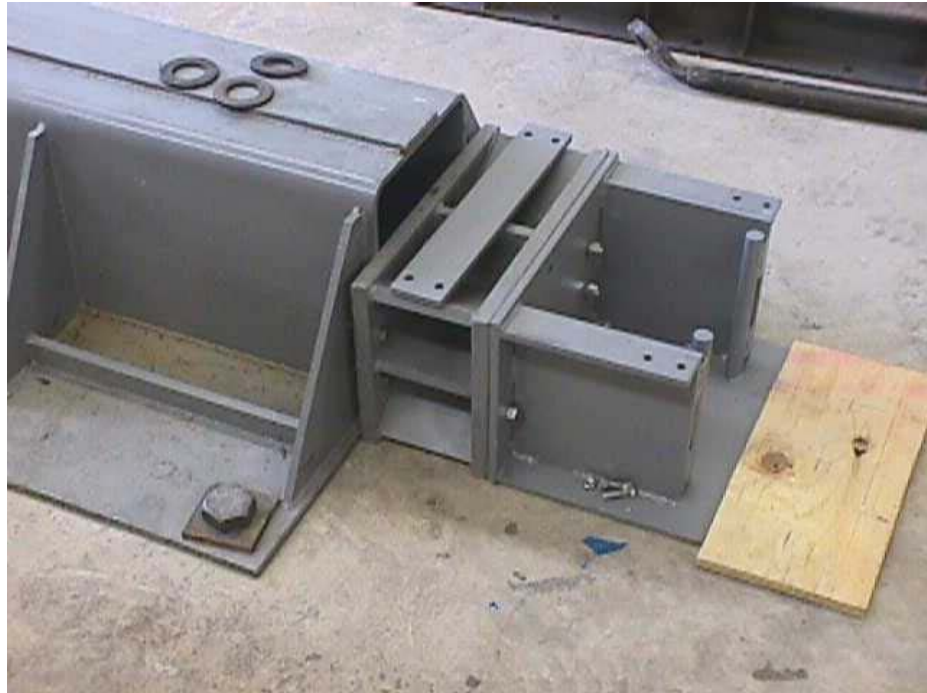


Figure B. 1 Restraint at the column end



Figure B. 2 Test setup view from the inferior column



Figure B. 3 Test setup view from the superior column



Figure B. 4 LVDT transducers on both columns and beams



Figure B. 5 Initiation of flexural cracks in the beam: joint L1



Figure B. 6 Propagation of flexural cracks in the beam: joint L1



Figure B. 7 Initiation of shear cracks in the panel: joint L1

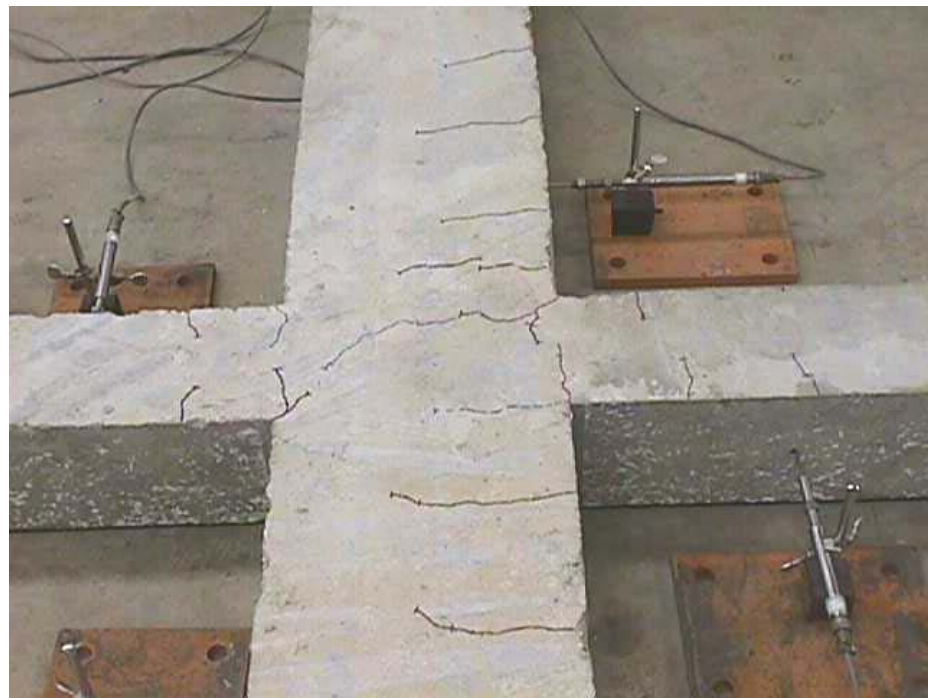


Figure B. 8 Initiation of flexural cracks in the columns: joint L1



Figure B. 9 Propagation of shear cracks in the panel: joint L1



Figure B. 10 Column failure: joint L1



Figure B. 11 Lateral view of failed column: joint L1



Figure B. 12 Crack pattern at failure: joint L1



Figure B. 13 Flexural cracks in the beams: joint H1



Figure B. 14 Initiation of shear cracks in the panel: joint H1



Figure B. 15 Opening of flexural cracks in the columns: joint H1



Figure B. 16 Lateral view of failed column: joint H1



Figure B. 17 Failure of the columns: joint H1

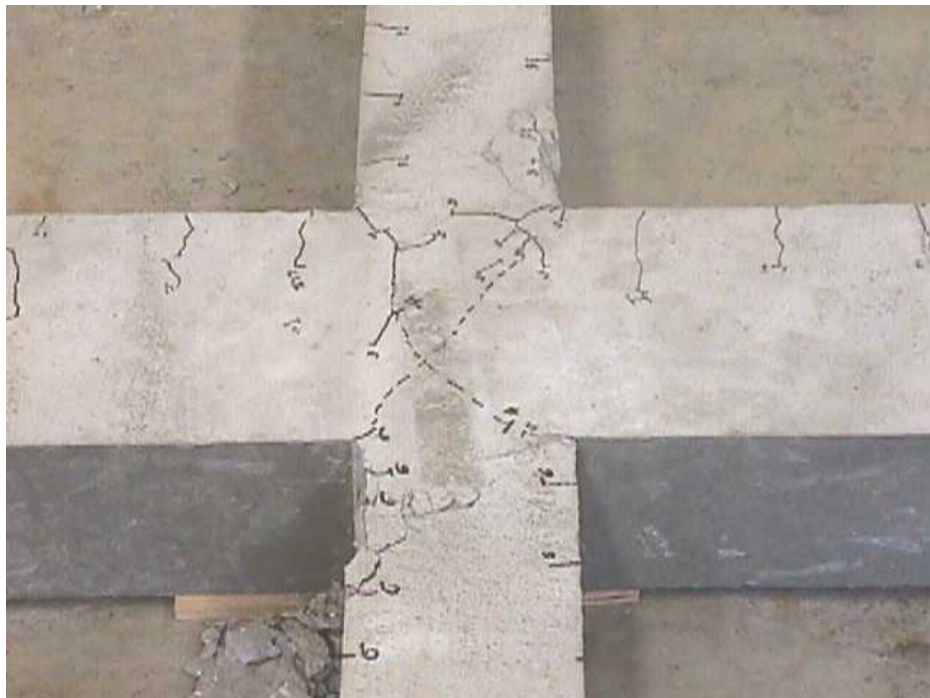


Figure B. 18 Crack pattern at failure: joint H1

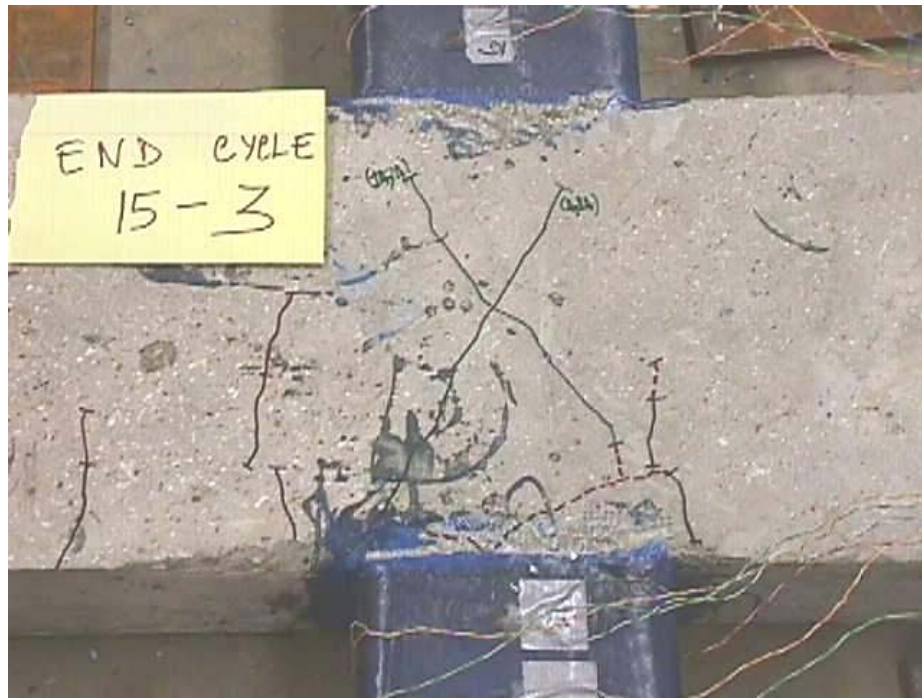


Figure B. 19 Initiation of shear cracks in the panel: joint L2



Figure B. 20 Propagation of shear cracks in the panel: joint L2

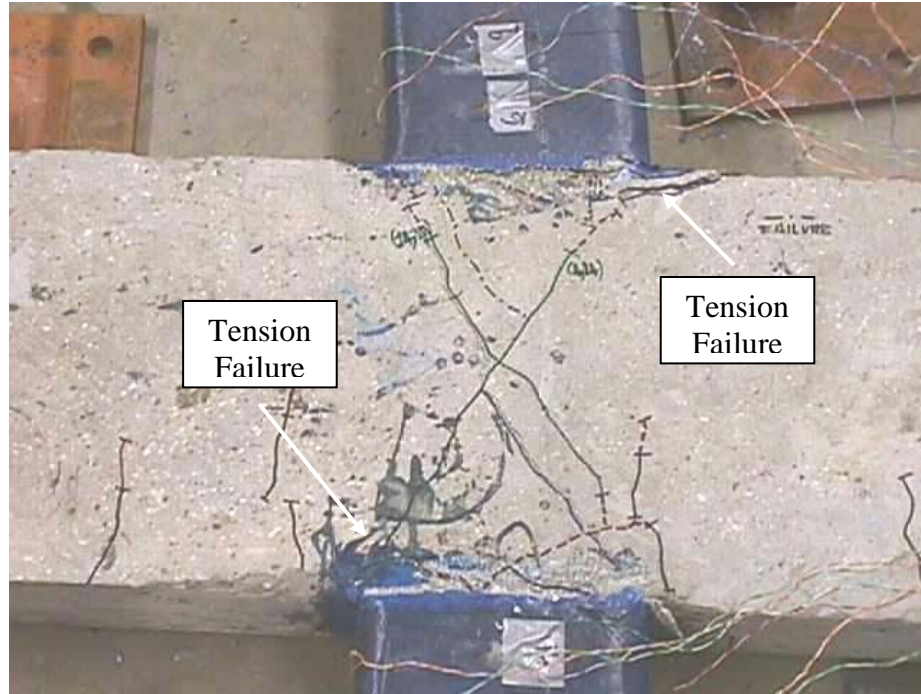


Figure B. 21 Tension failure of the columns: joint L2

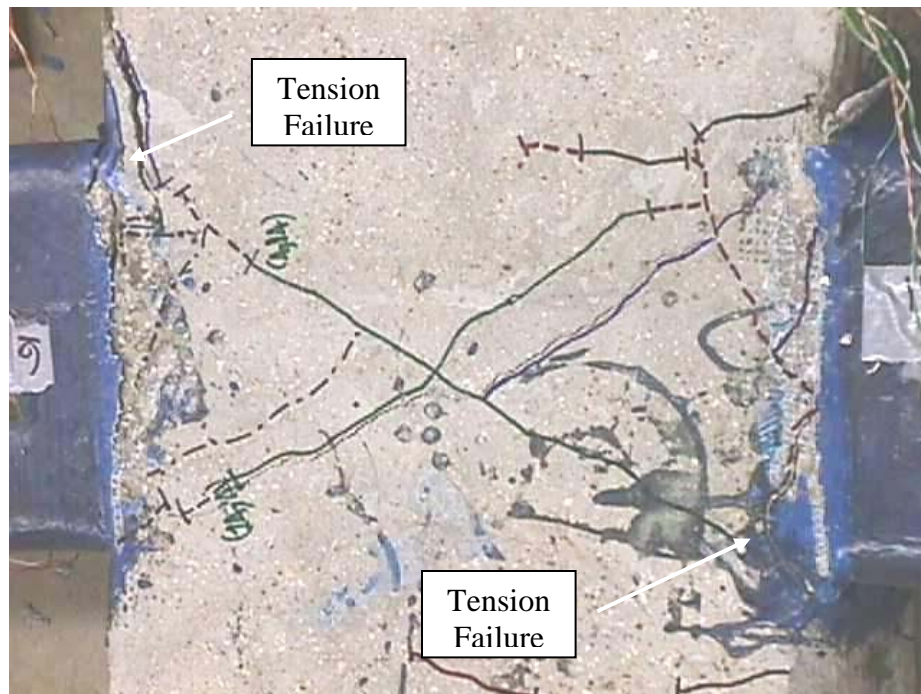


Figure B. 22 Top view of the failure regions: joint L2

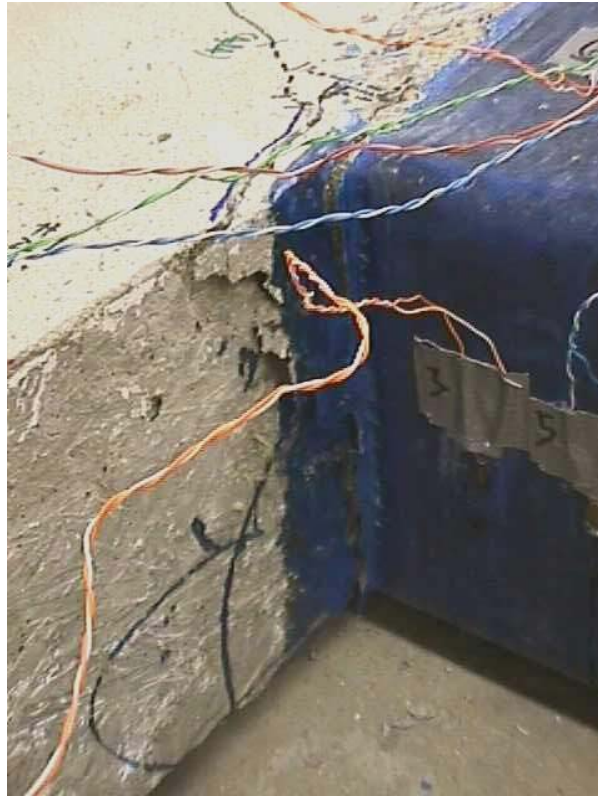


Figure B. 23 Lateral view of failed column: joint L2

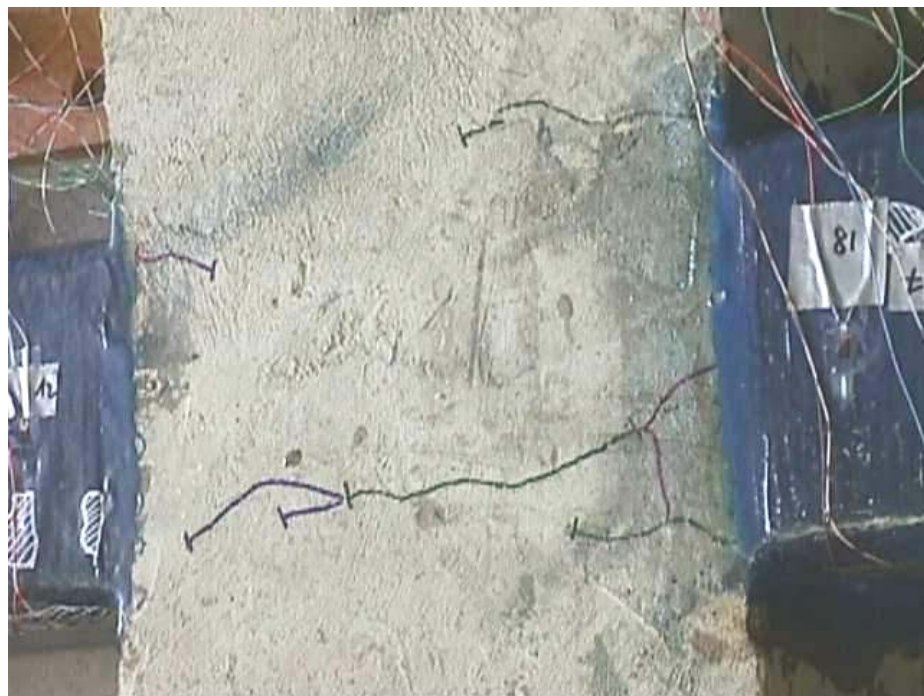


Figure B. 24 Initiation of diagonal cracks in the panel: joint H2



Figure B. 25 Propagation of diagonal cracks in the nodal zone: joint H2



Figure B. 26 Initiation of shear cracks in the panel: joint H2L



Figure B. 27 Propagation of shear cracks in the panel: joint H2L



Figure B. 28 Initiation of diagonal cracks in the nodal zone: joint H2U

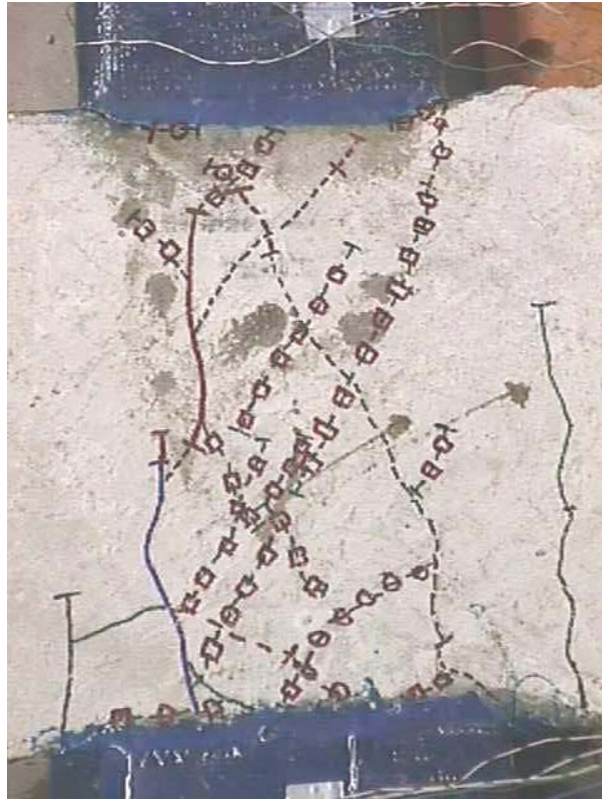


Figure B. 29 Shear cracks in the panel: joint H2U



Figure B. 30 Panel damage: joint H2



Figure B. 31 Panel damage: joint H2



Figure B. 32 View from the bottom of panel damage: joint H2



Figure B. 33 Panel damage: joint H2U



Figure B. 34 Tension failure of column: joint H2



Figure B. 35 Tension failure of column: joint H2U



Figure B. 36 Combined panel-column failure: joint H2



Figure B. 37 Initiation of fibers breaking in column compression region: joint H2



Figure B. 38 Shear failure of the panel: joint H2L



Figure B. 39 Carbon fibers breaking in compression region of column: joint H2L

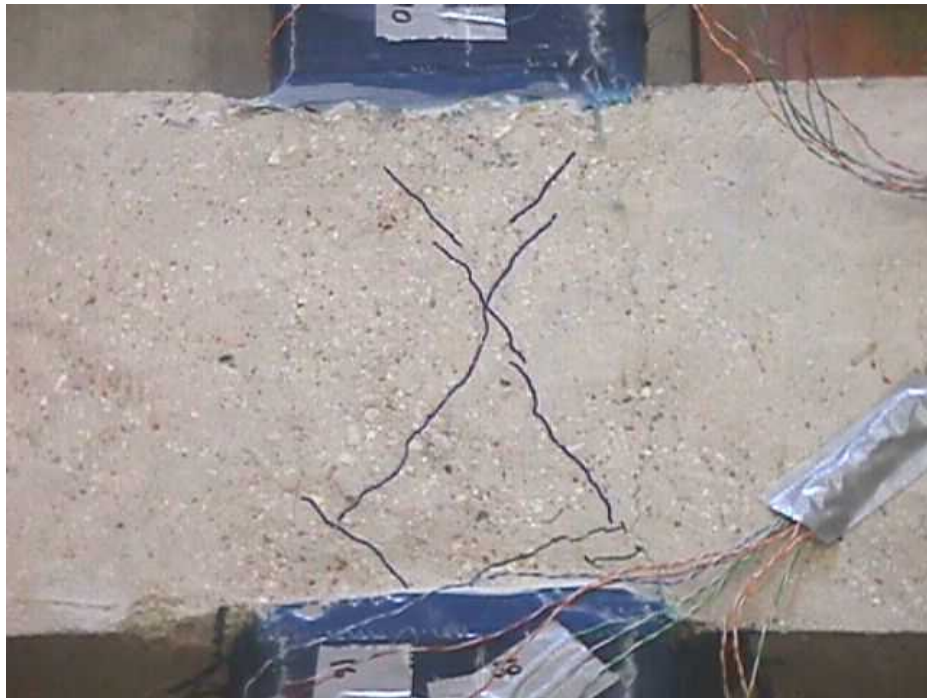


Figure B. 40 Initiation of diagonal cracks in the panel: joint L3

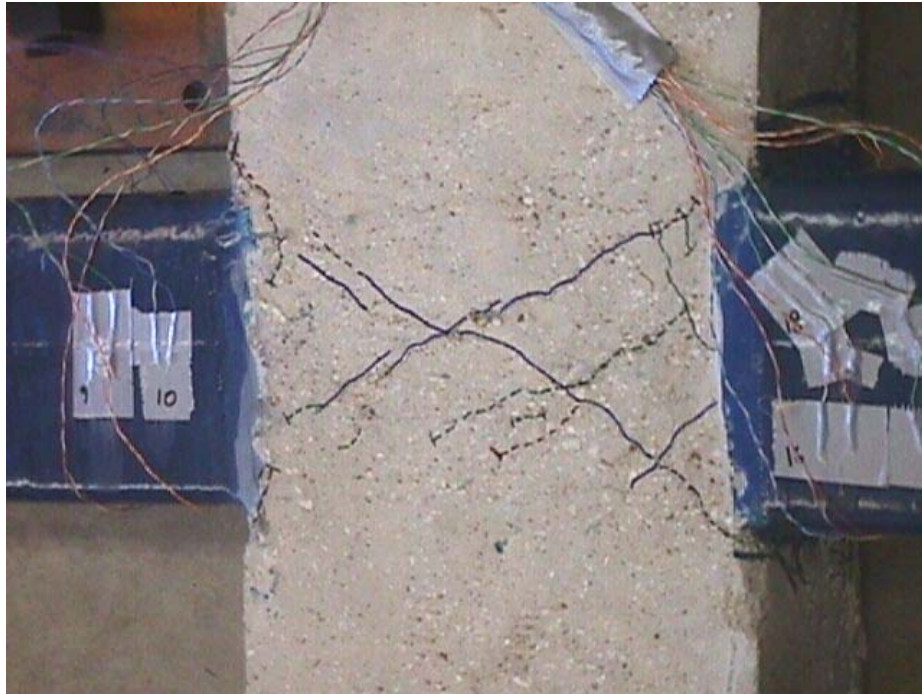


Figure B. 41 Propagation of shear cracks in the panel: joint L3

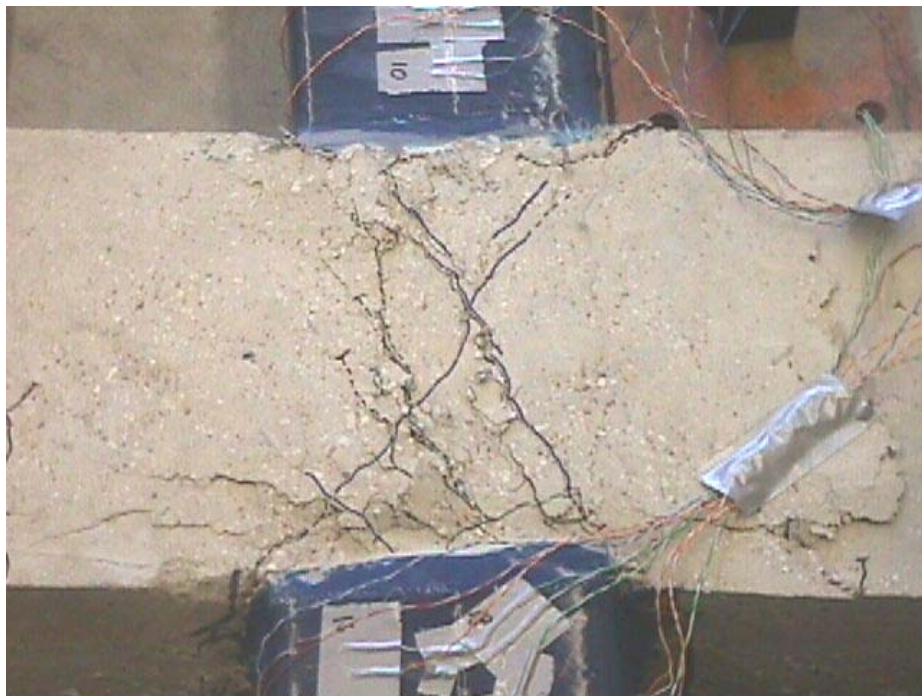


Figure B. 42 Top view of shear failure of the panel: joint L3



Figure B. 43 Shear failure of the panel: joint L3



Figure B. 44 Shear failure of the panel: joint H3



Figure B. 45 Damage due to panel shear failure: joint H3



Figure B. 46 Panel shear failure: joint M3

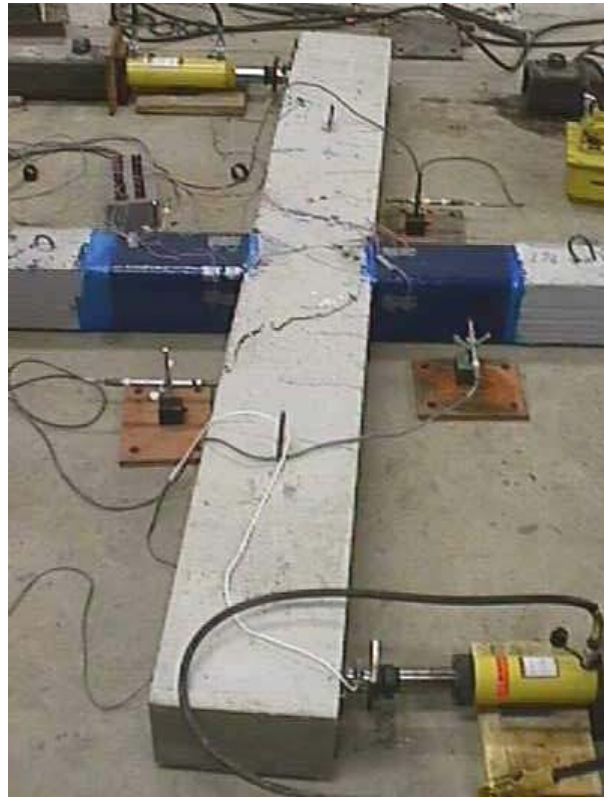


Figure B. 47 Top view of joint M3 at failure

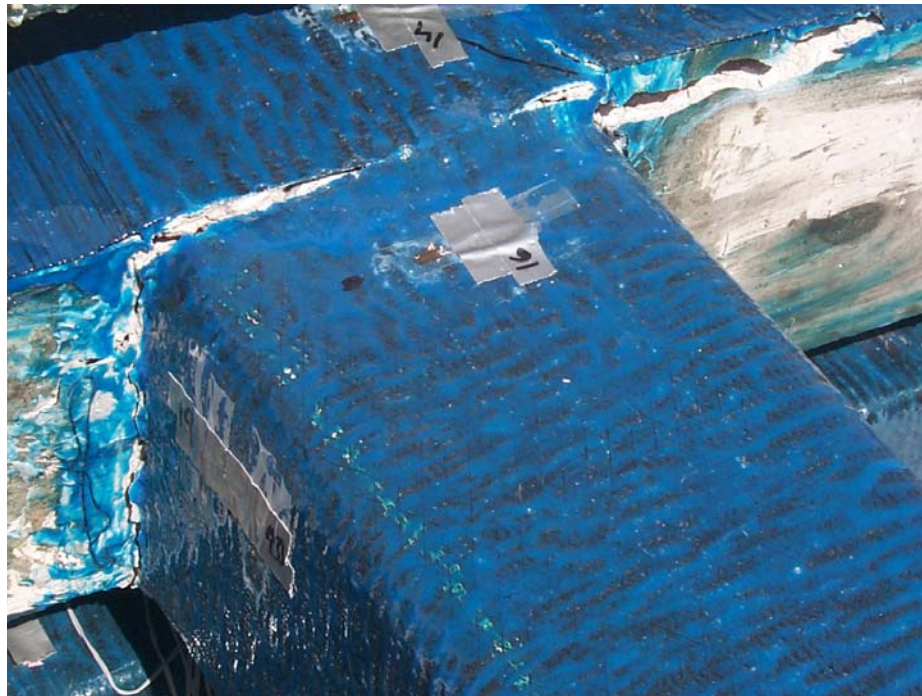


Figure B. 48 Separation at panel-superior column: joint L4



Figure B. 49 Lateral view of the superior column at failure: joint L4



Figure B. 50 Separation at panel-inferior column: joint L4



Figure B. 51 Top view of joint L4 at failure

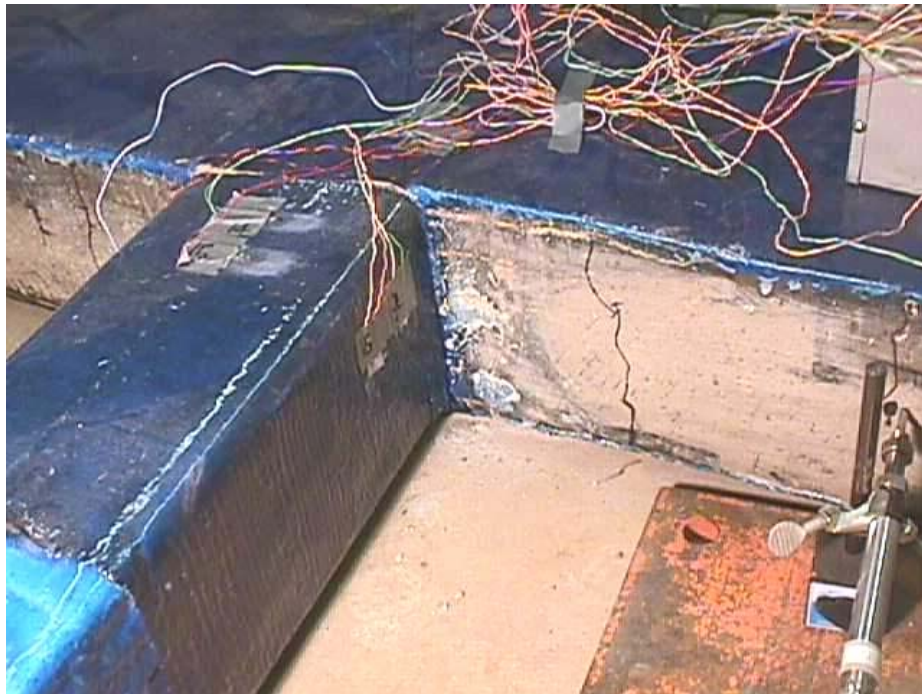


Figure B. 52 View from the superior column at failure: joint H4

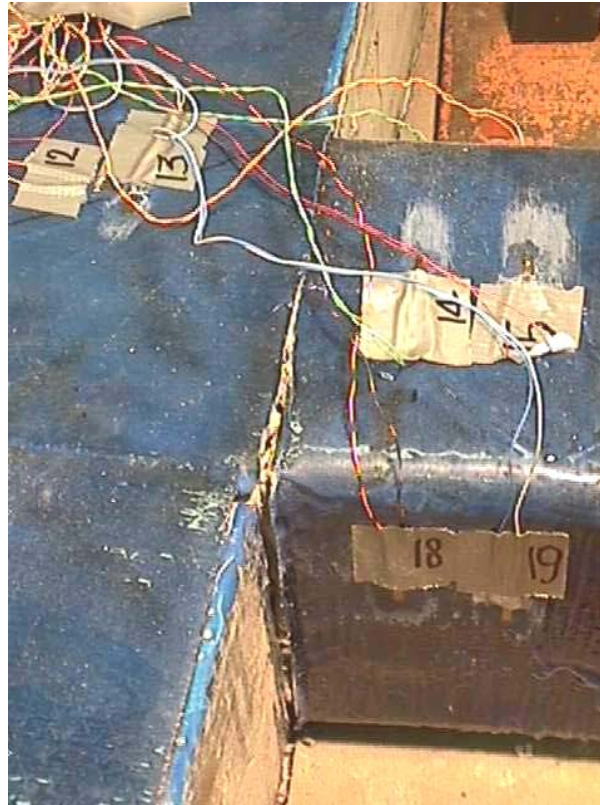


Figure B. 53 Separation at panel-superior column: joint H4



Figure B. 54 View from the inferior column at failure: joint H4

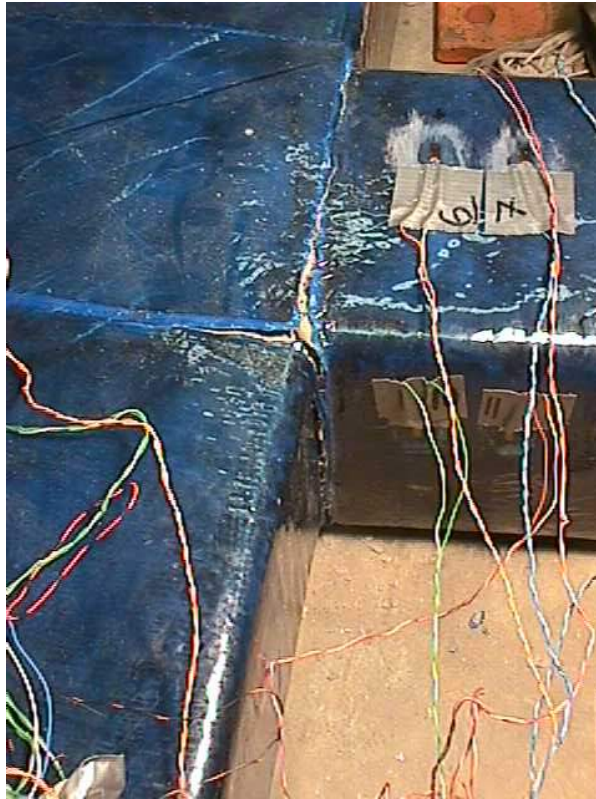


Figure B. 55 Separation at panel-inferior column: joint H4



Figure B. 56 View from the superior column at failure: joint H5



Figure B. 57 Separation at interface panel-superior column: joint H5



Figure B. 58 Joint H5 at failure

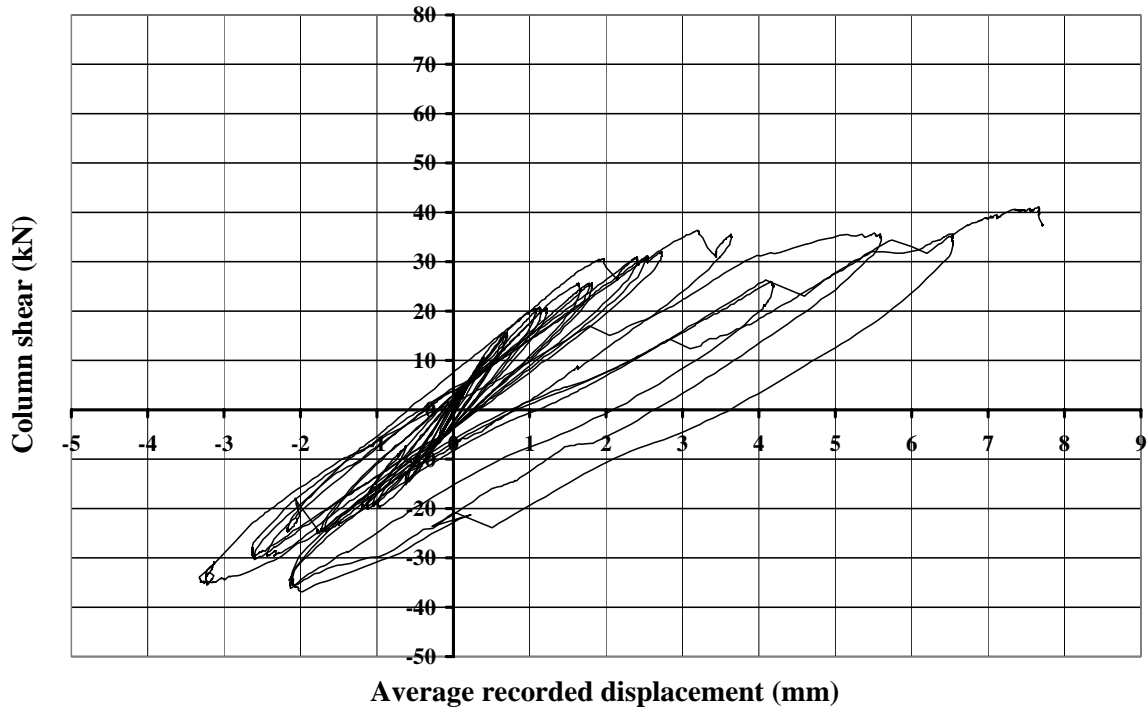


Figure C.1 Column shear-displacement: L1

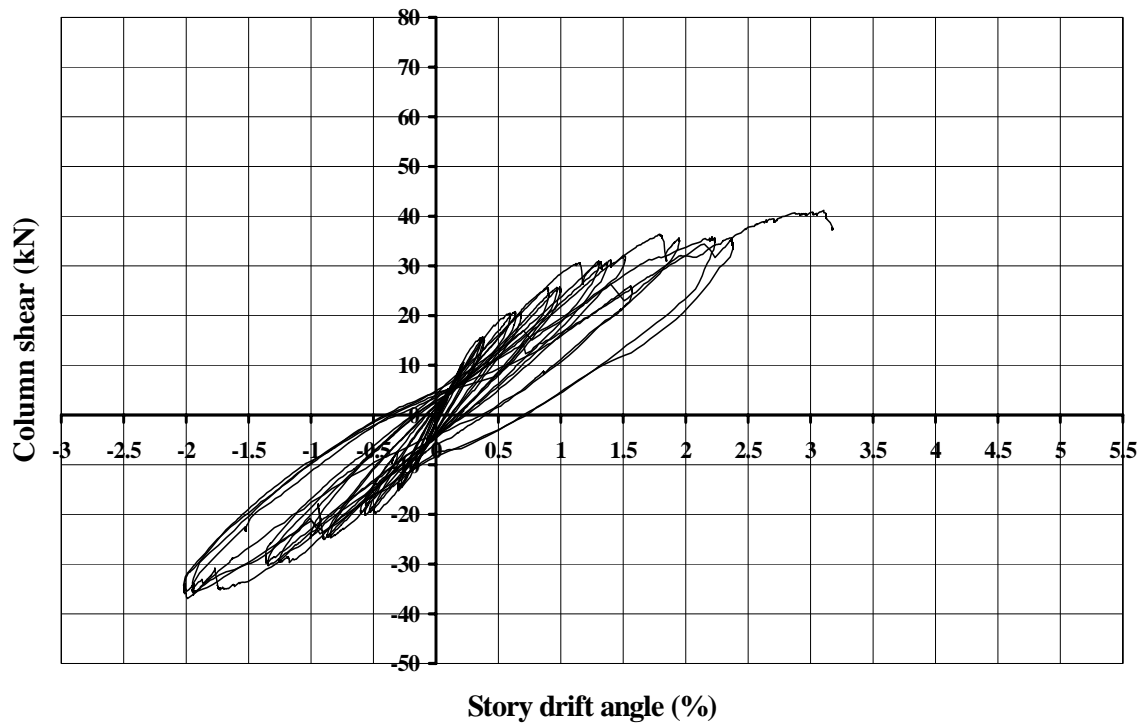


Figure C.2 Column shear-story drift: L1

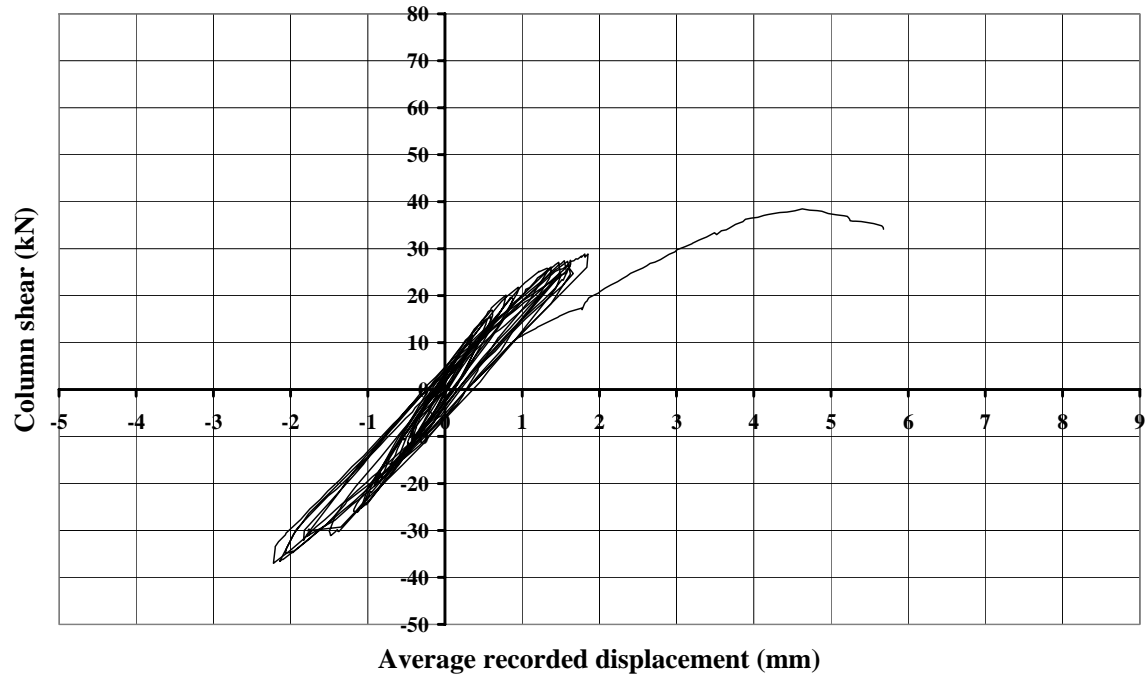


Figure C.3 Column shear-displacement: H1

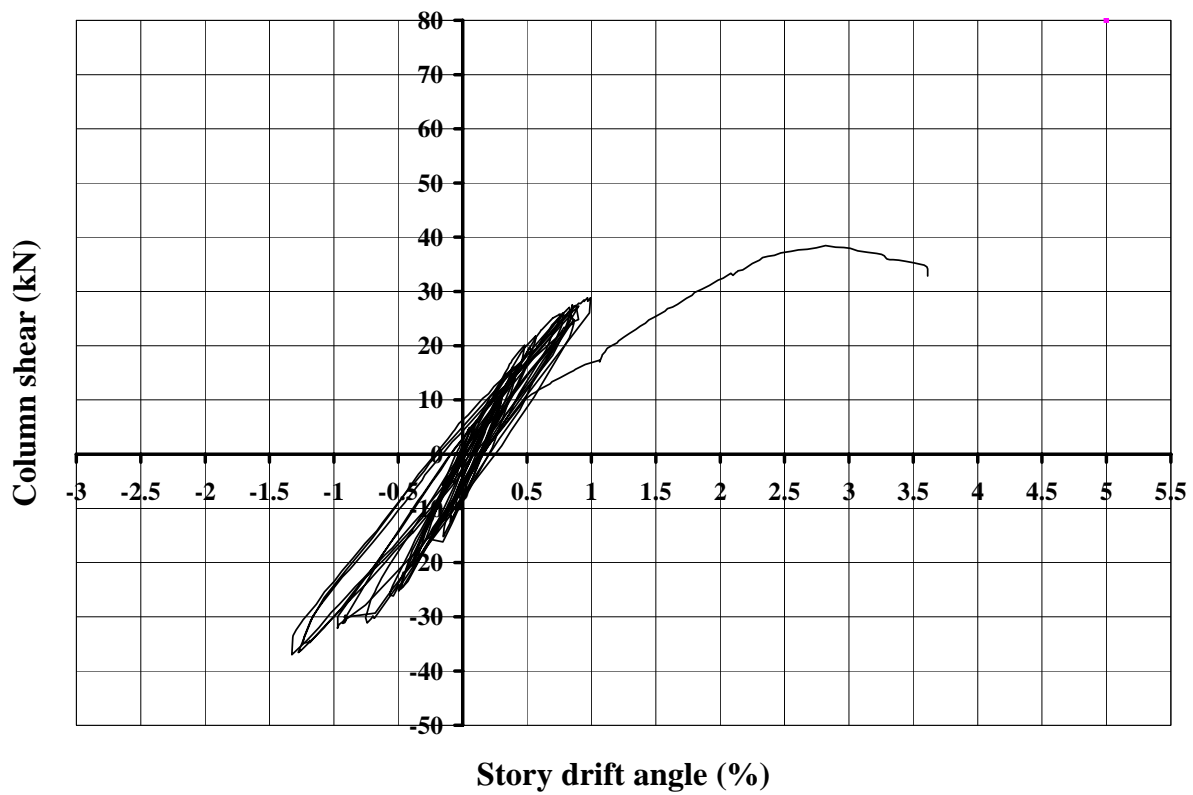


Figure C.4 Column shear-story drift: H1

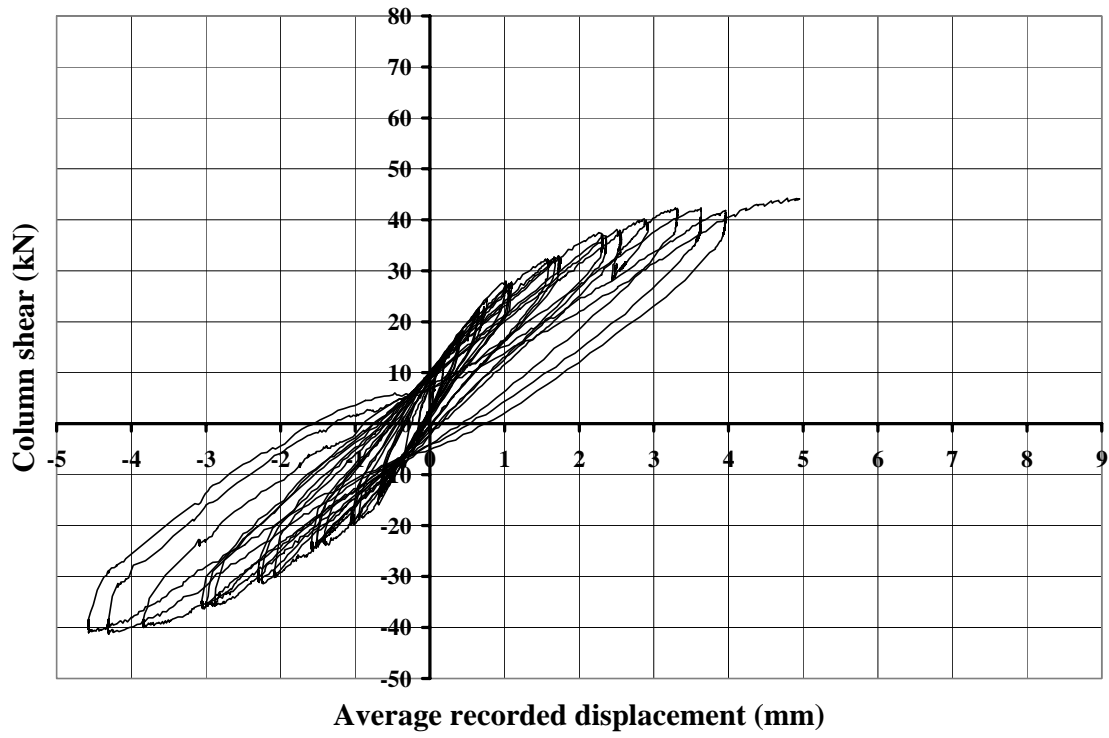


Figure C.5 Column shear-displacement: L2

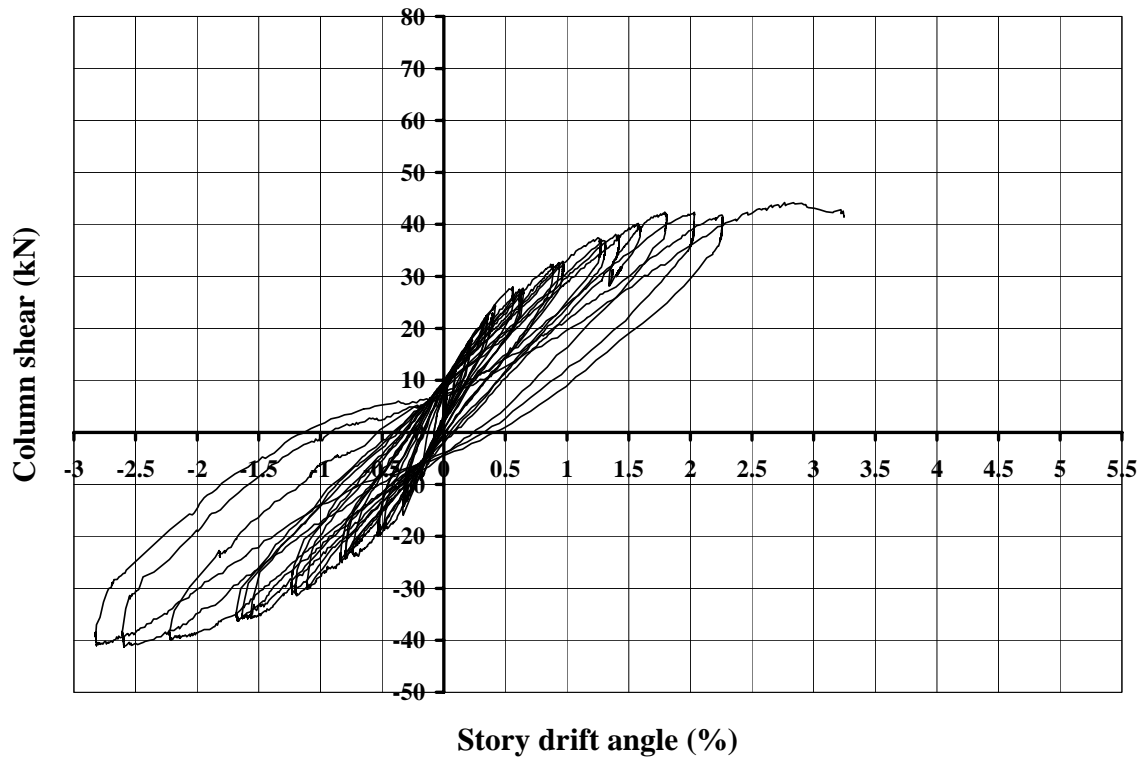


Figure C.6 Column shear-story drift: L2

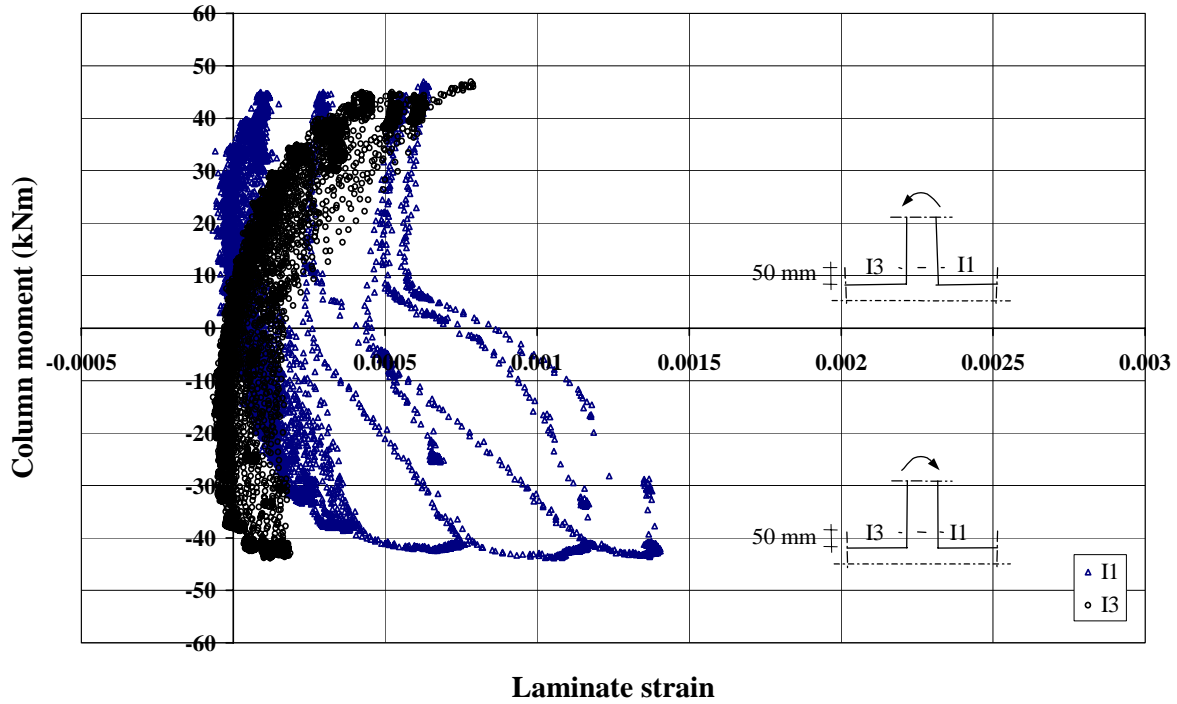


Figure C.7 Inferior column moment-laminate strain: L2

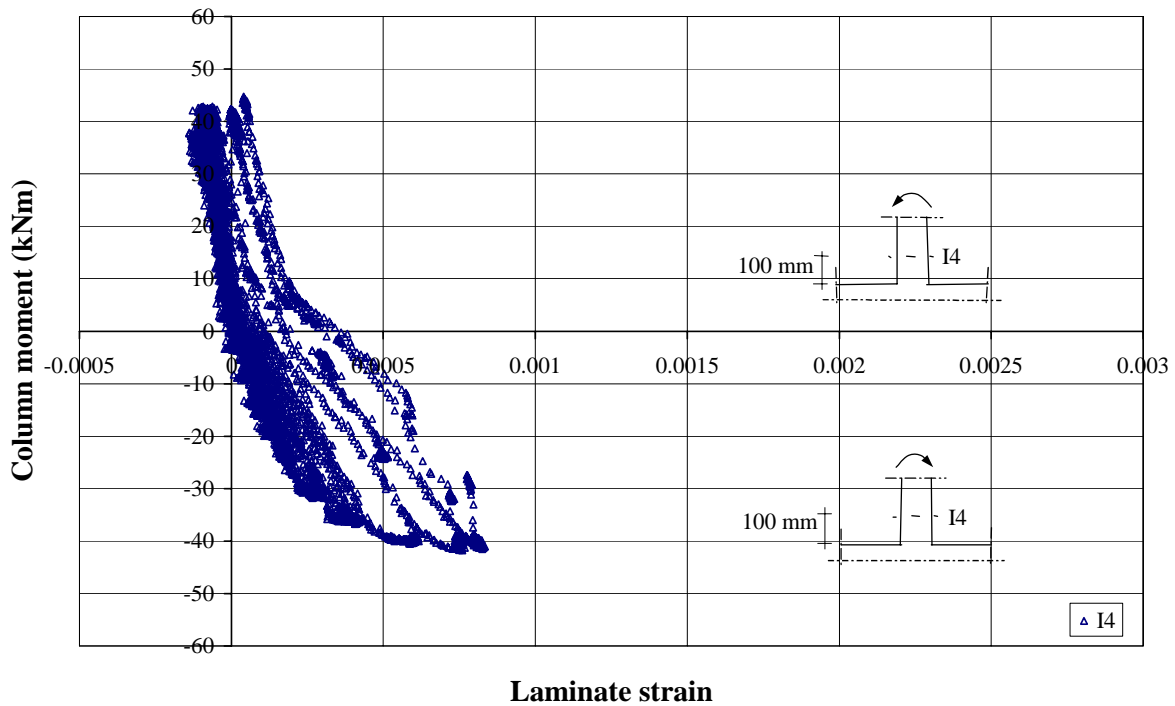


Figure C.8 Inferior column moment-laminate strain: L2

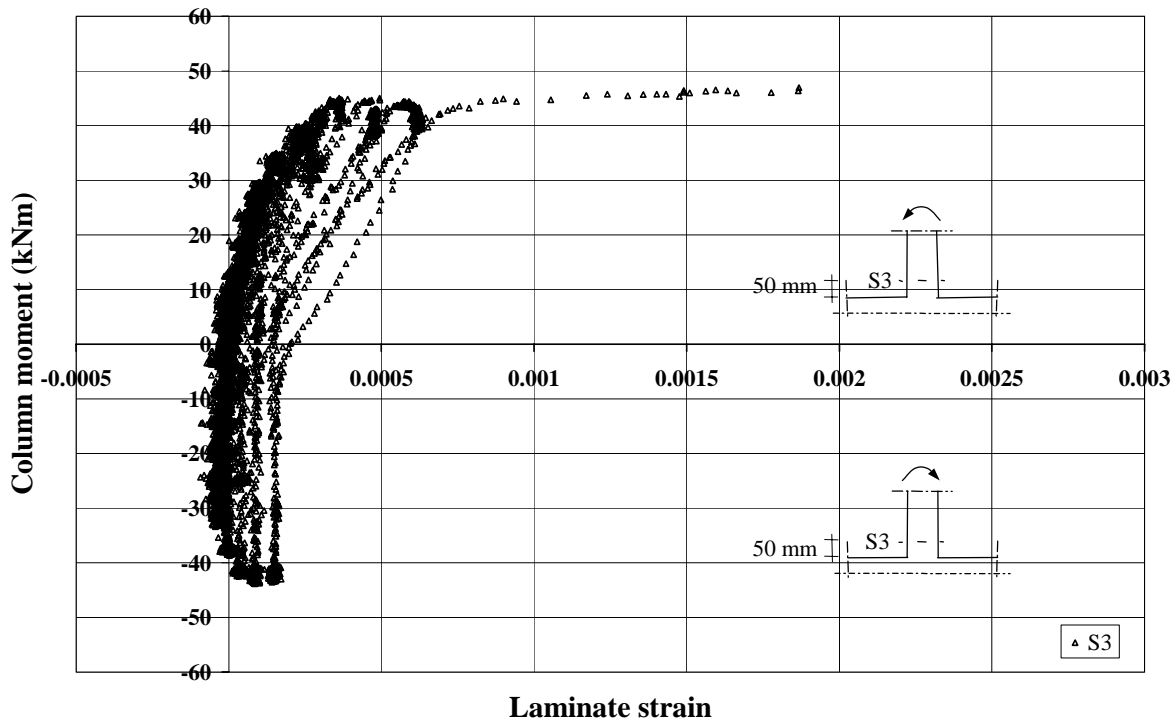


Figure C.9 Superior column moment-laminite strain: L2

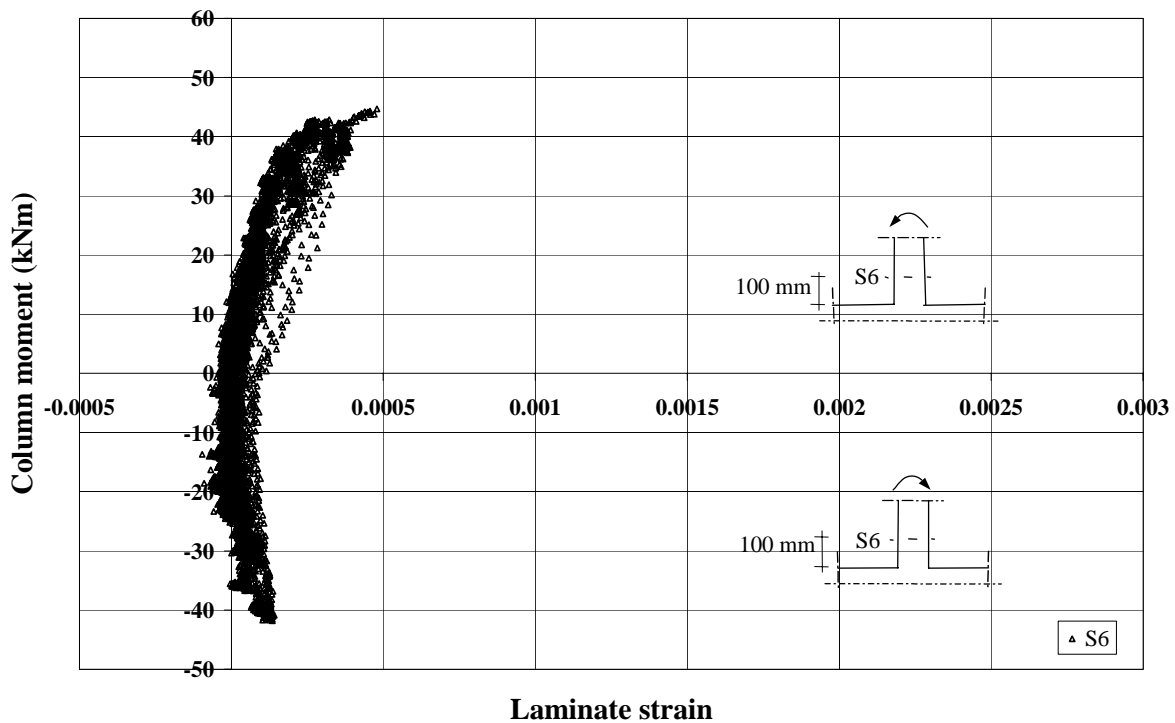


Figure C.10 Superior column moment-laminite strain: L2

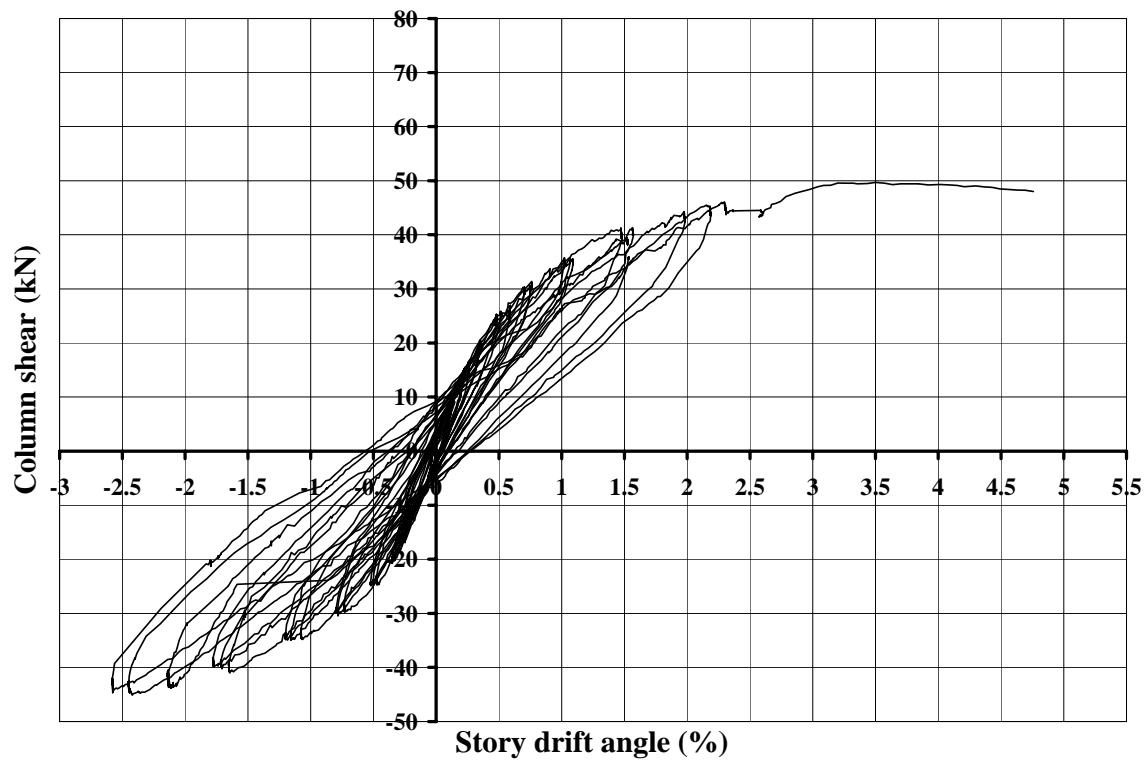


Figure C.11 Column shear-story drift: H2

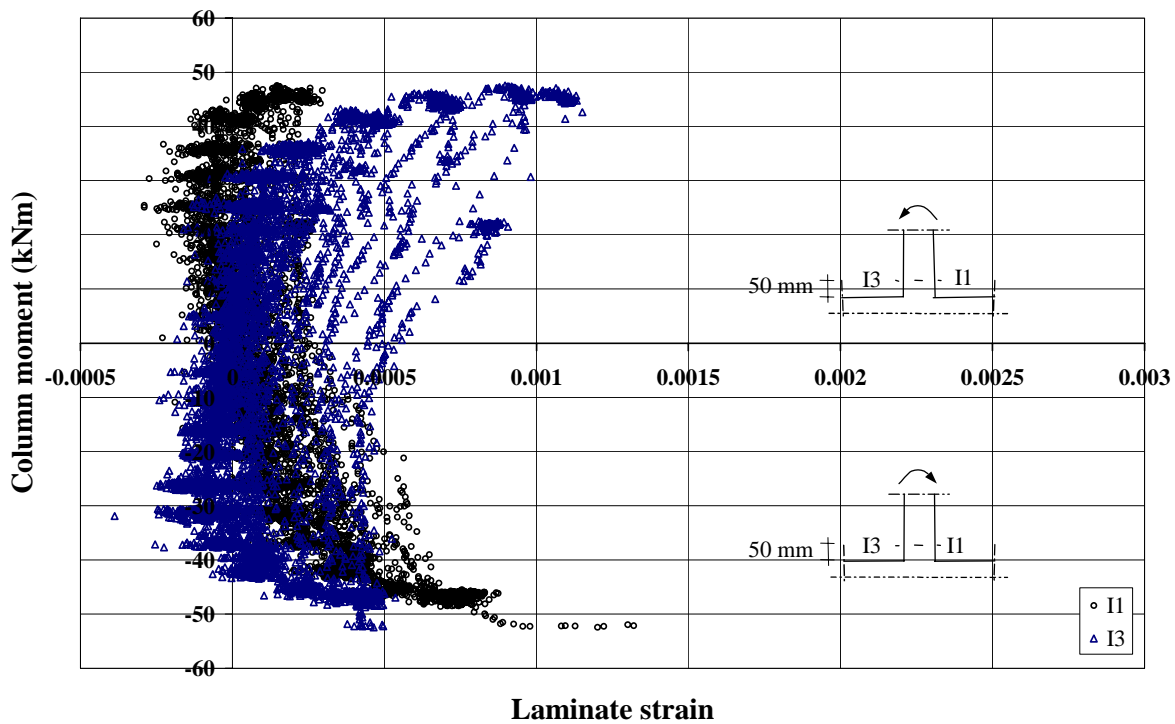


Figure C.12 Inferior column moment-laminate strain: H2

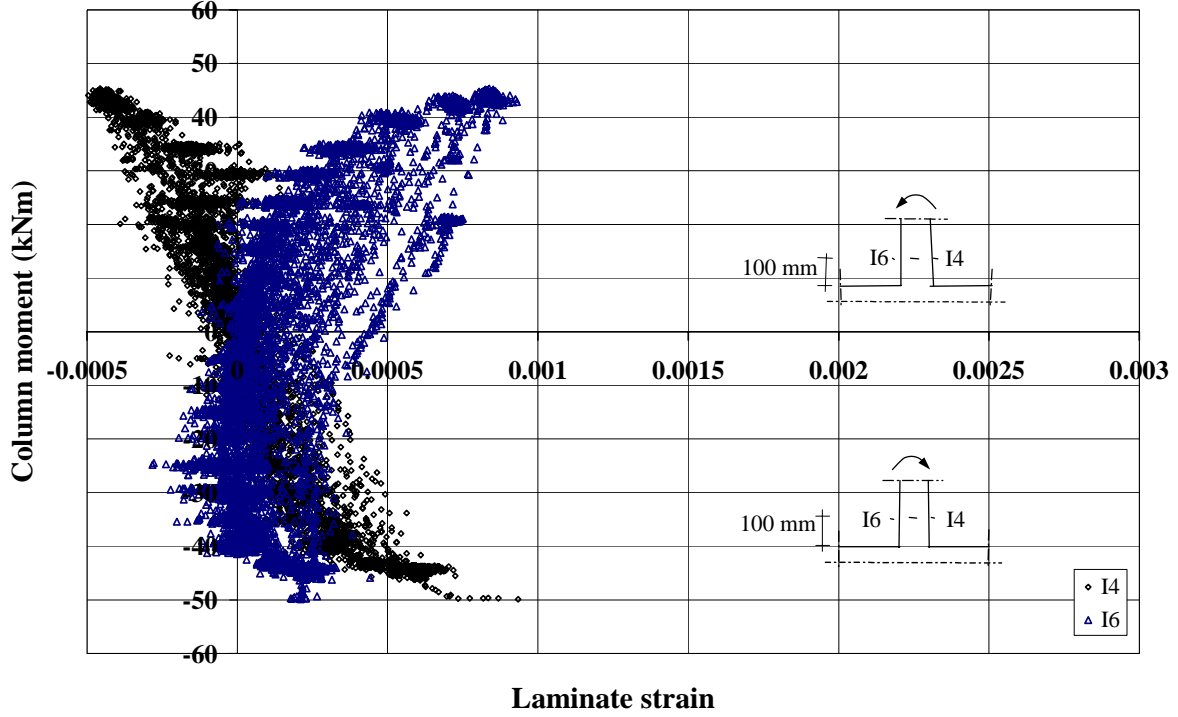


Figure C.13 Inferior column moment-laminate strain: H2

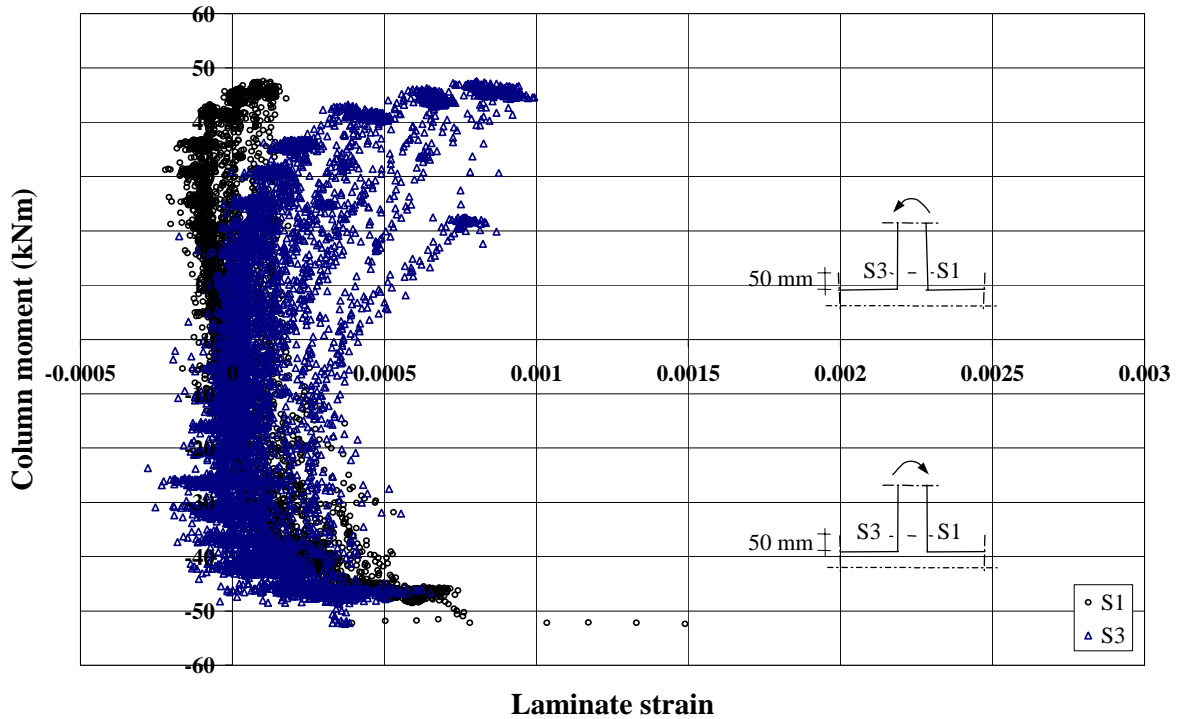


Figure C.14 Superior column moment-laminate strain: H2

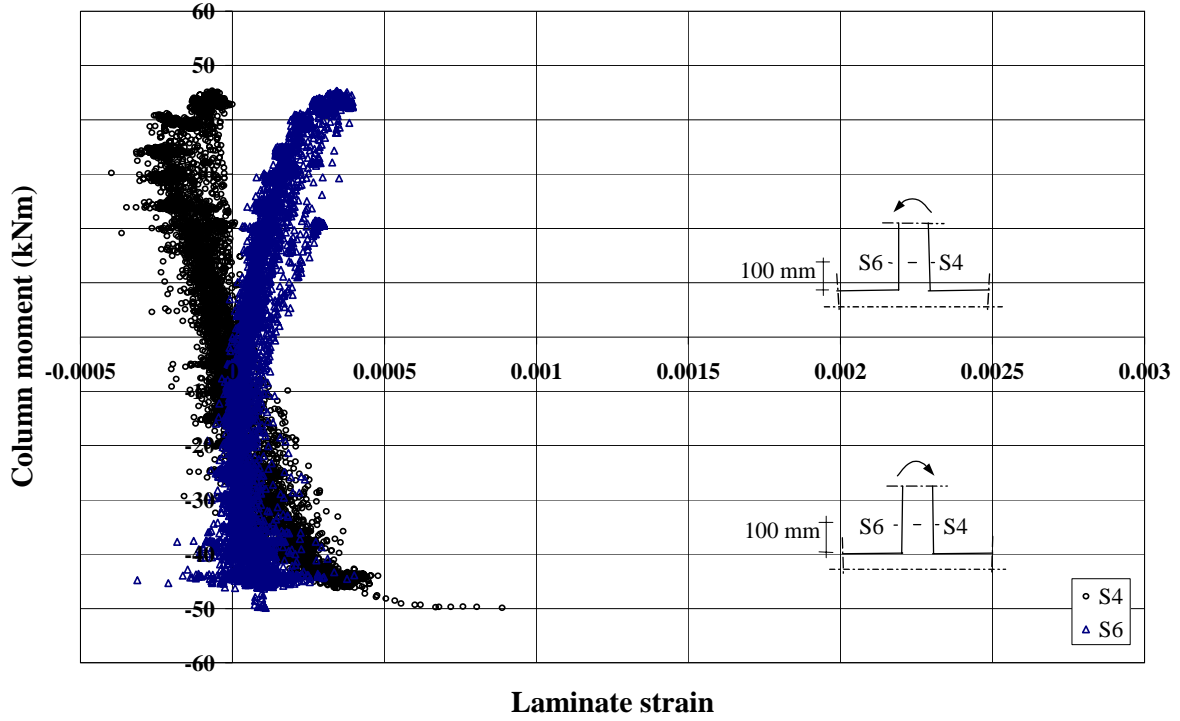


Figure C.15 Superior column moment-laminate strain: H2

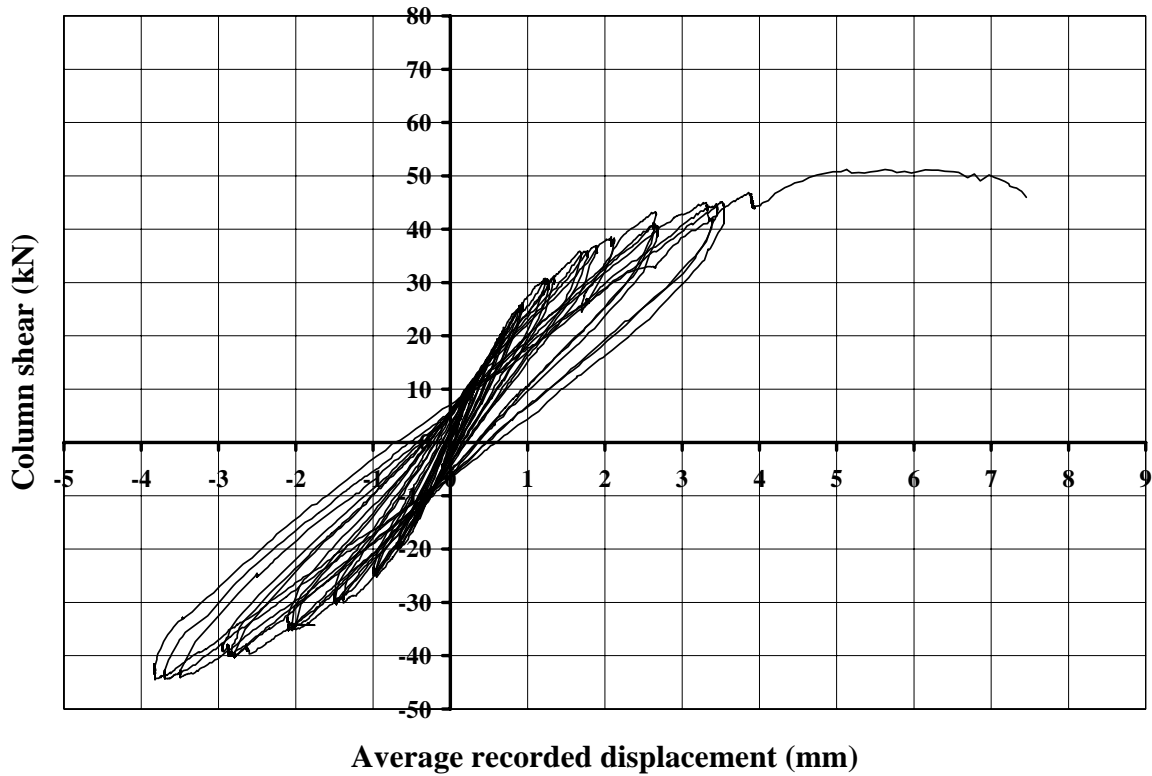


Figure C.16 Column shear-displacement: H2U

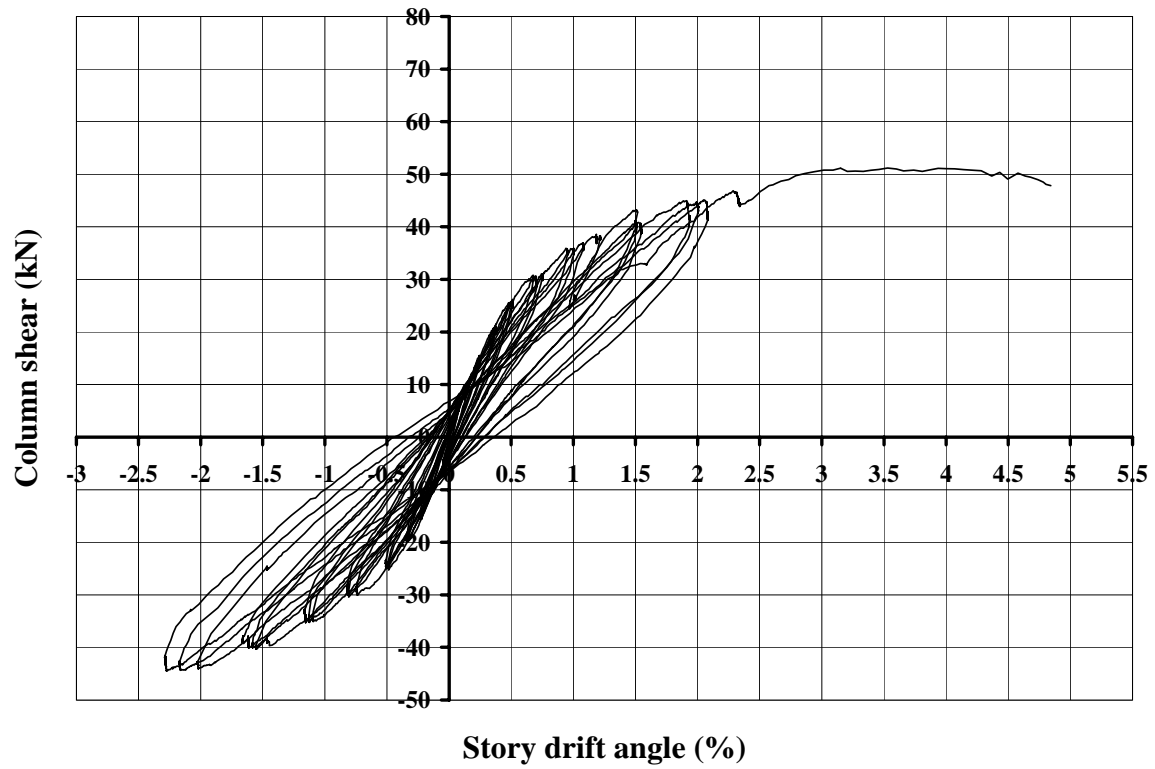


Figure C.17 Column shear-story drift: H2U

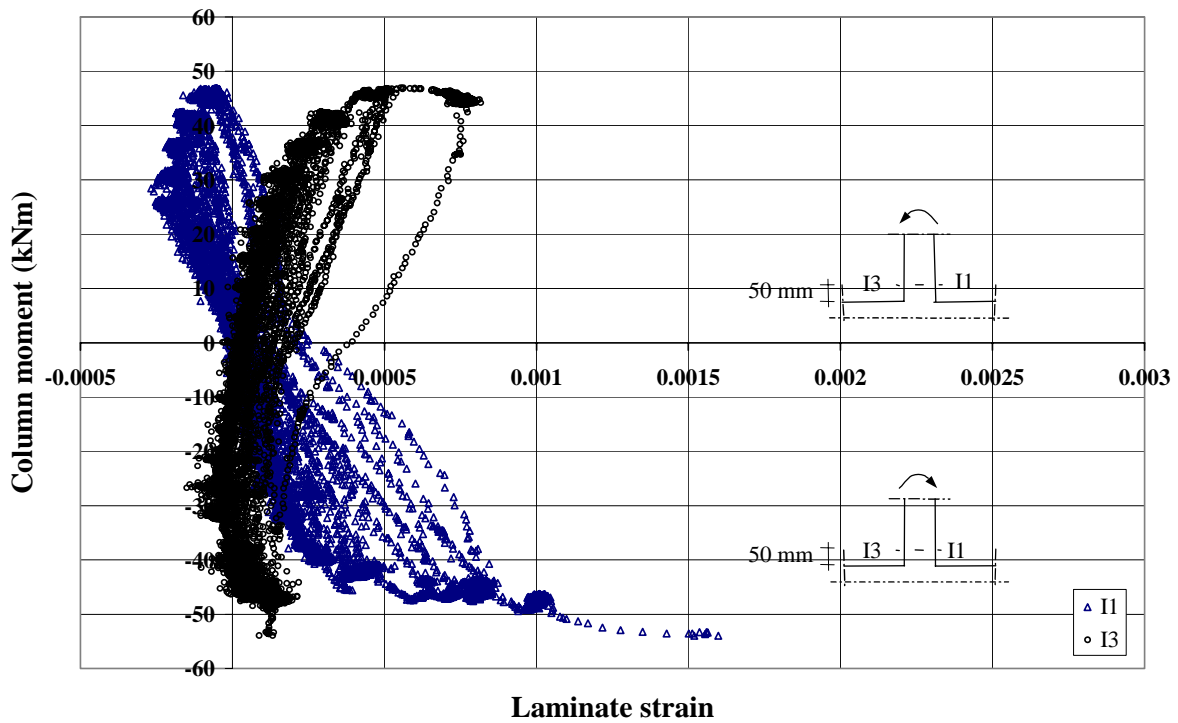


Figure C.18 Inferior column moment-laminate strain: H2U

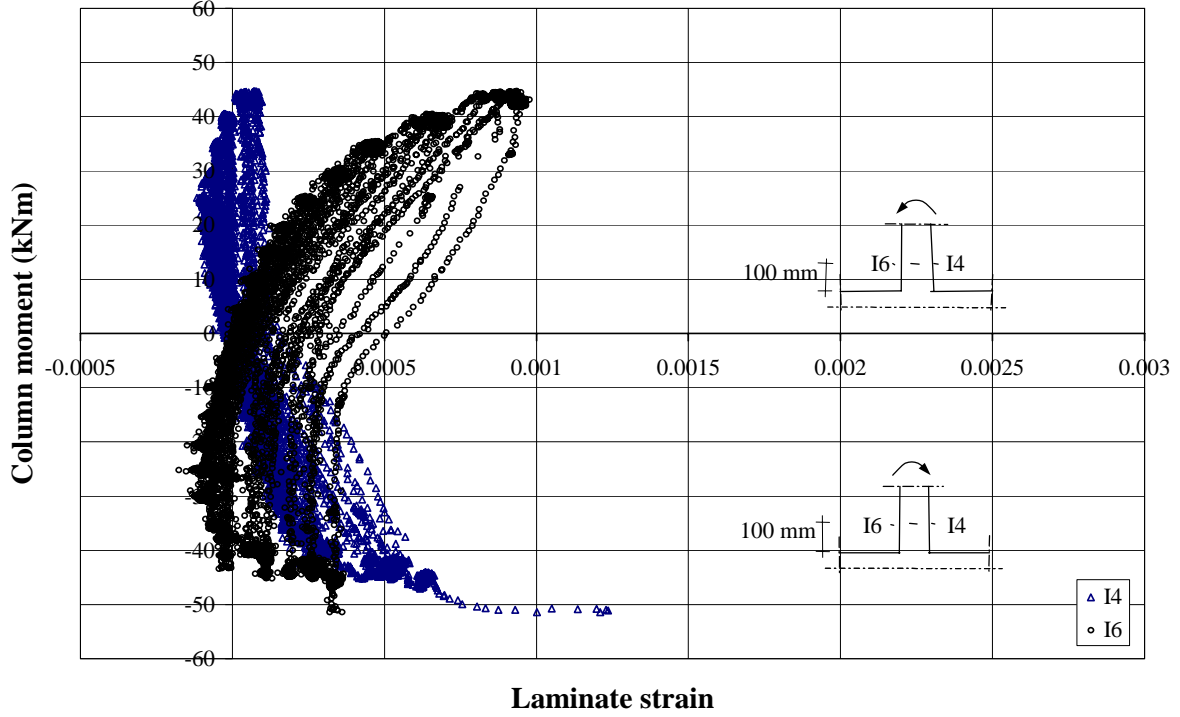


Figure C.19 Inferior column moment-laminate strain: H2U

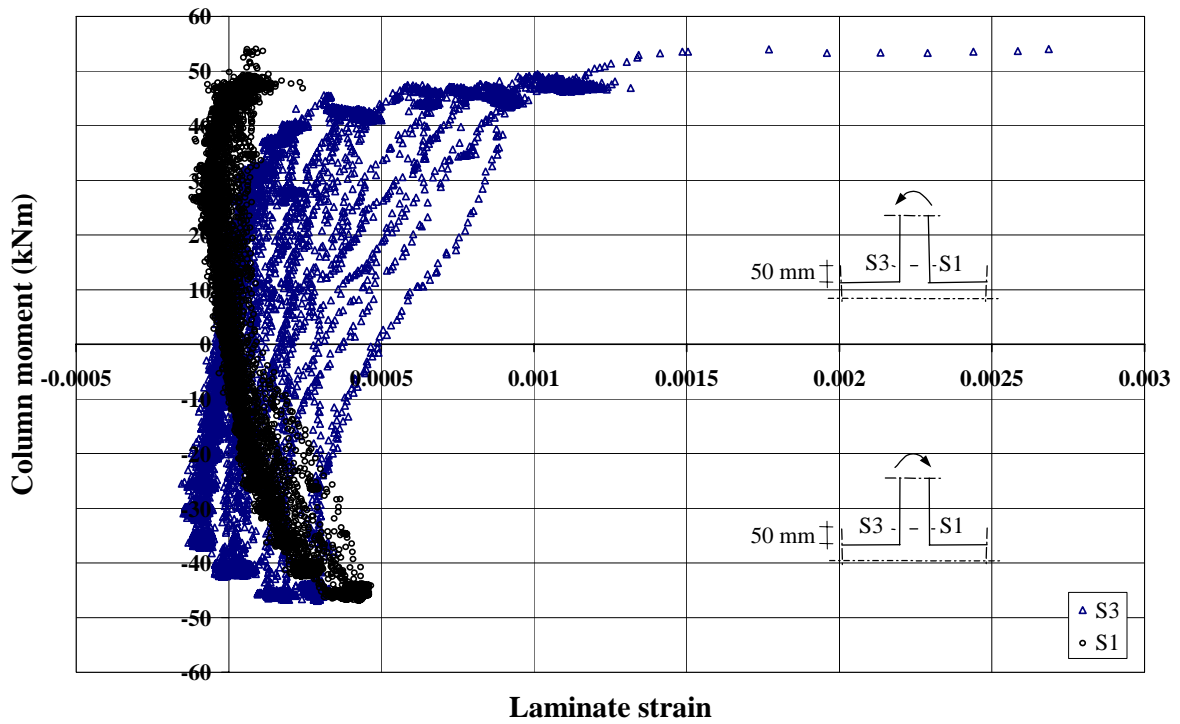


Figure C.20 Superior column moment-laminate strain: H2U

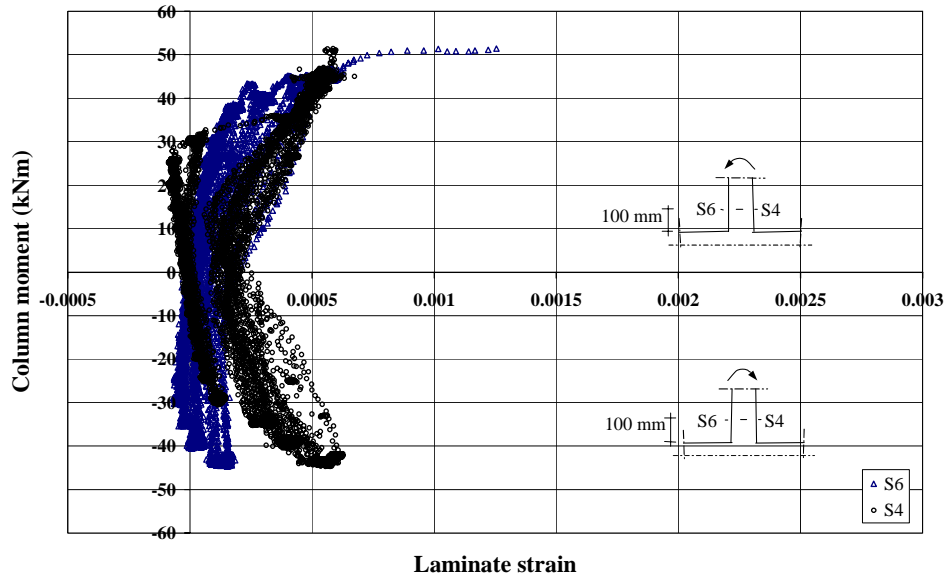


Figure C.21 Superior column moment-laminate strain: H2U

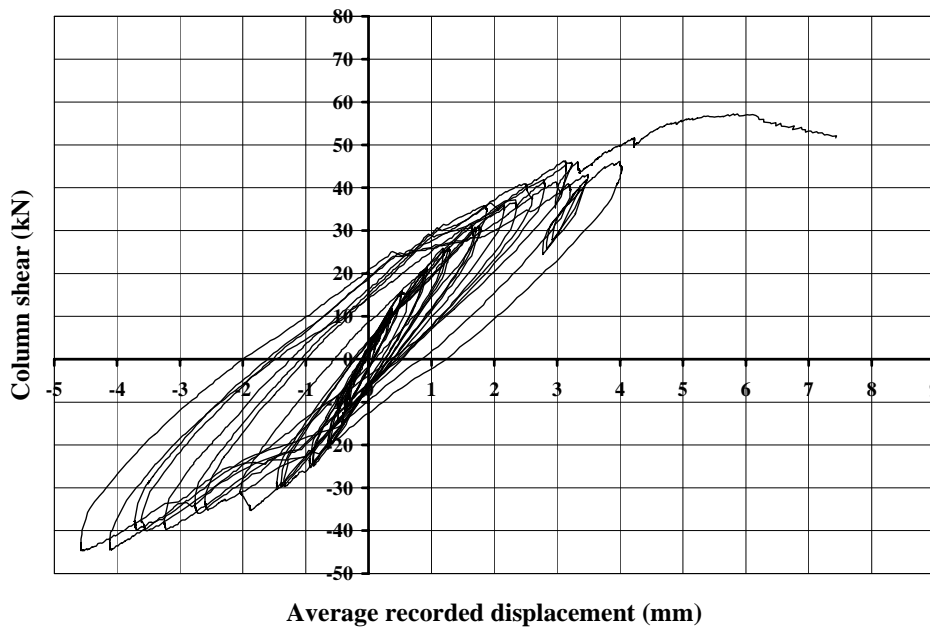


Figure C.22 Column shear-displacement: L3

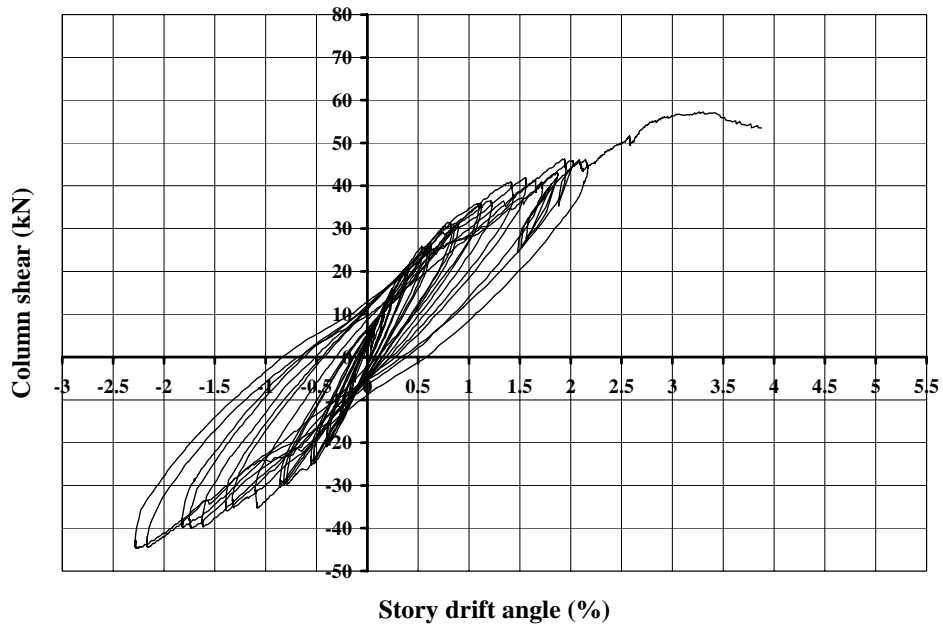


Figure C.23 Column shear-story drift: L3

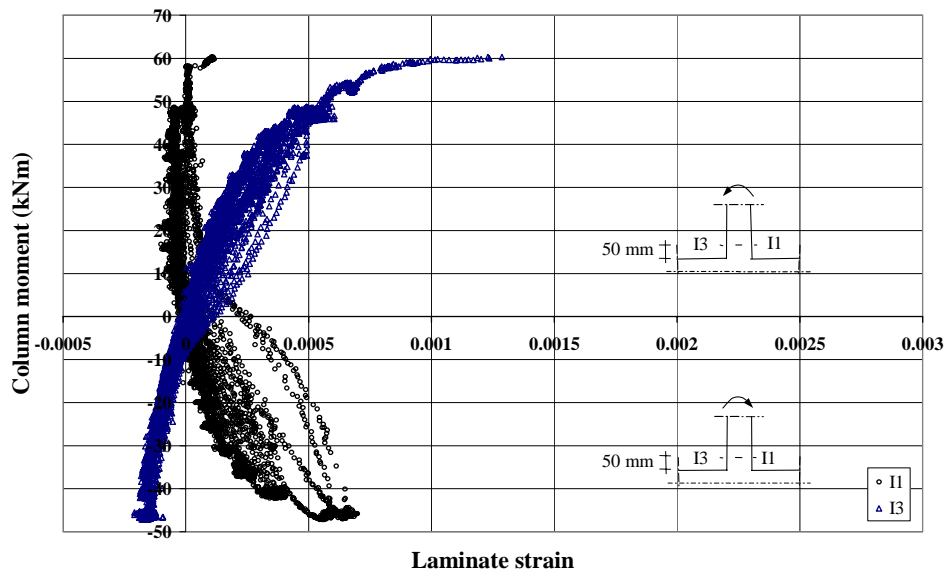


Figure C.24 Inferior column moment-laminate strain: L3

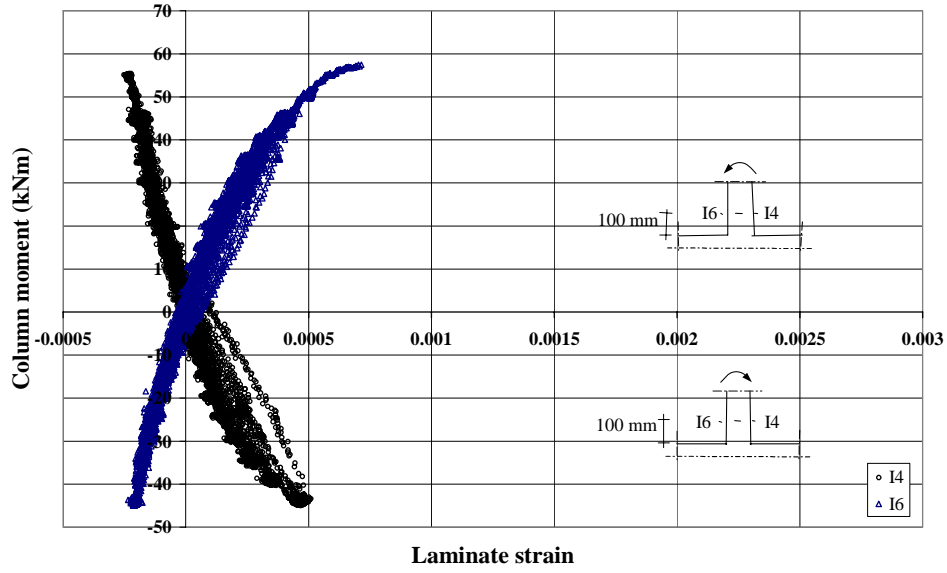


Figure C.25 Inferior column moment-laminate strain: L3

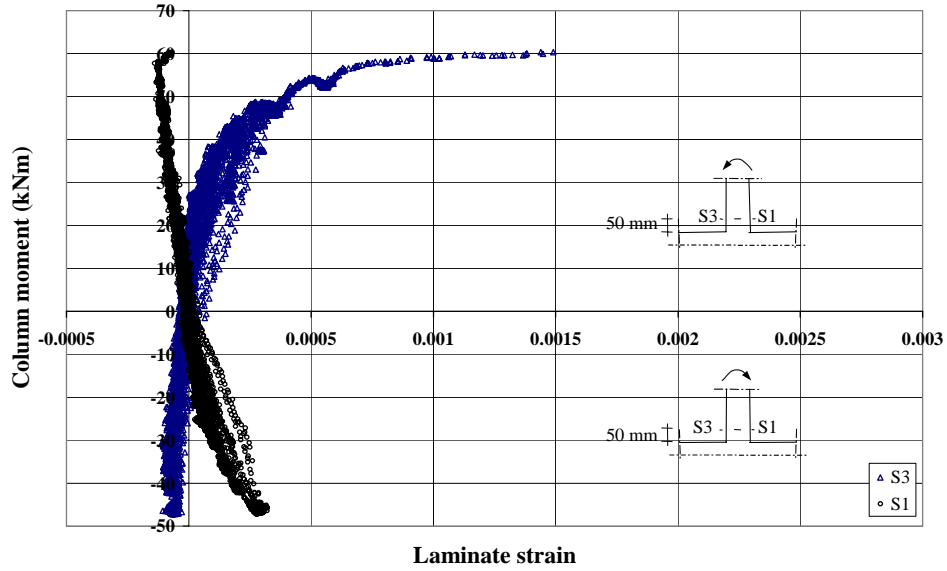


Figure C.26 Superior column moment-laminate strain: L3

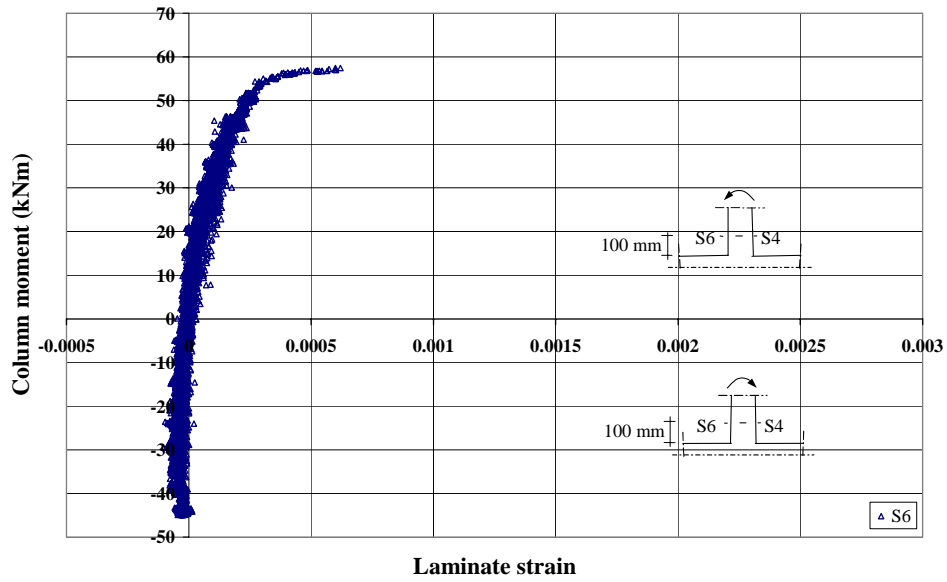


Figure C.27 Superior column moment-laminate strain: L3

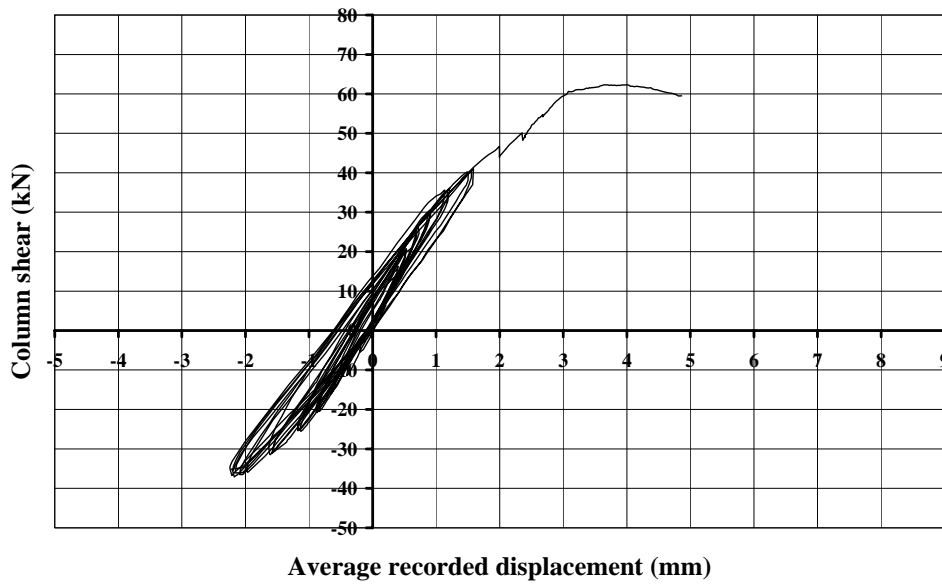


Figure C.28 Column shear-displacement: H3

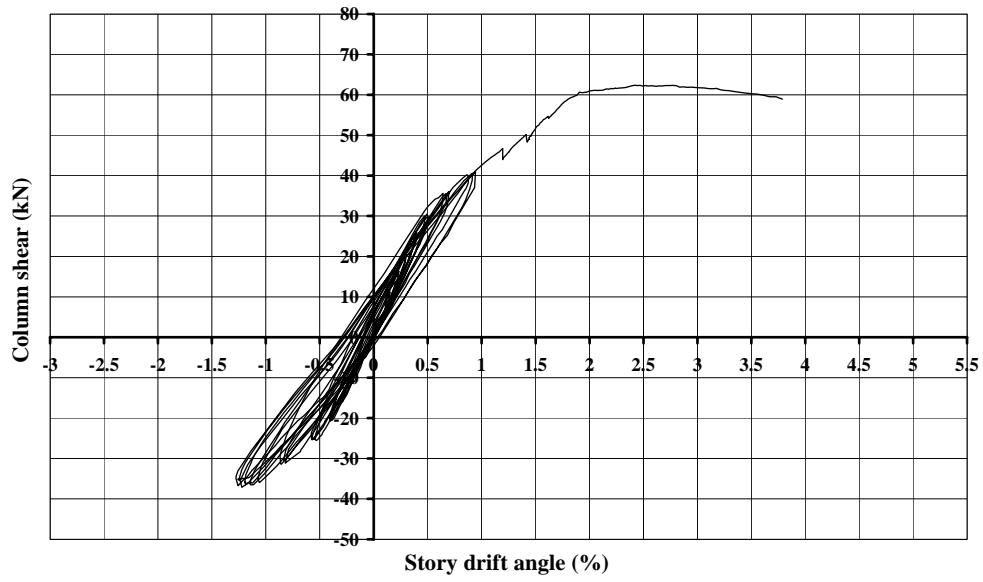


Figure C.29 Column shear-story drift: H3

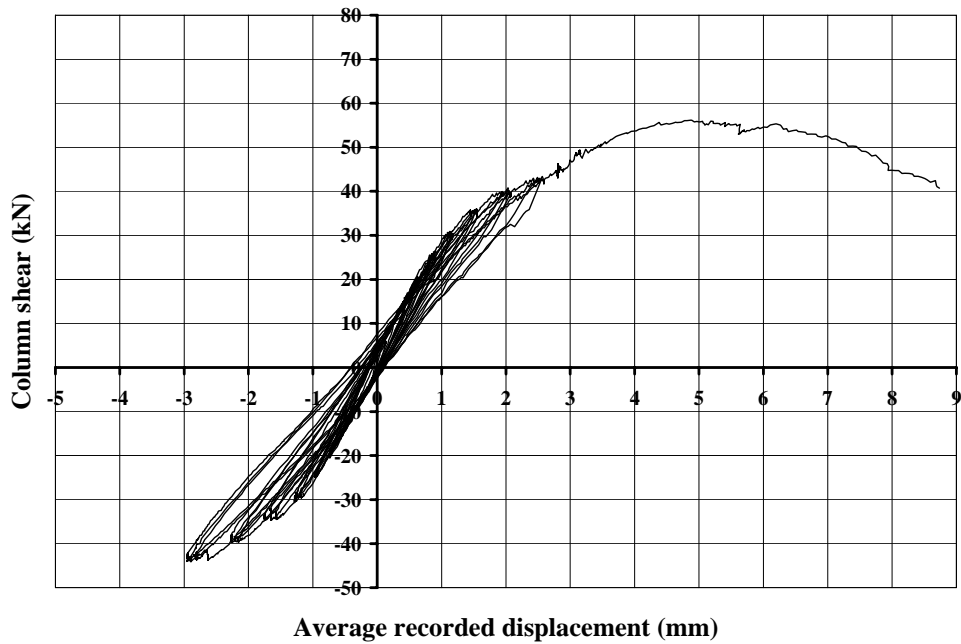


Figure C.30 Column shear-displacement: M3

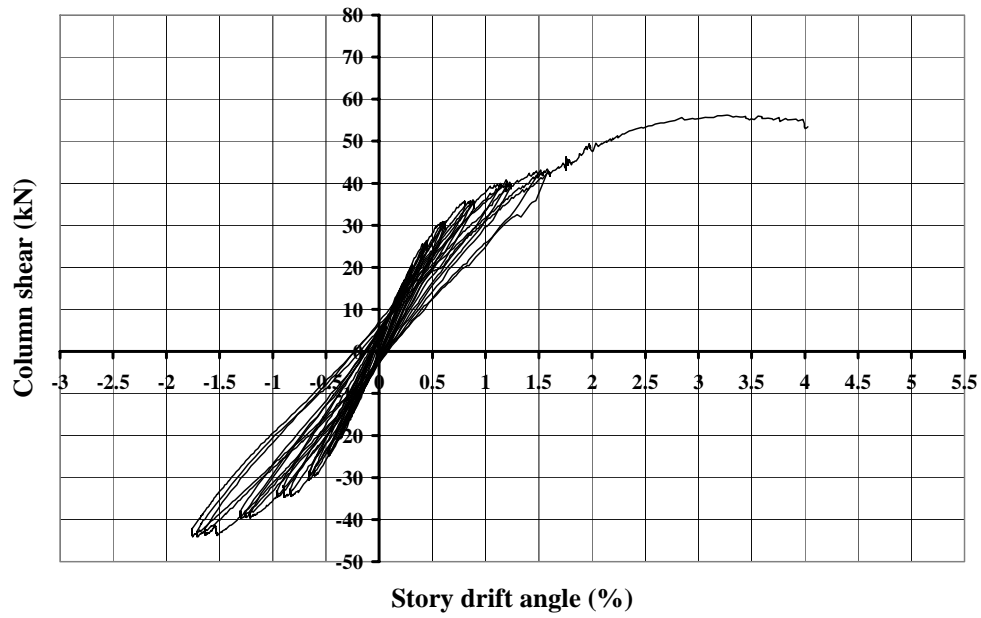


Figure C.31 Column shear-story drift: M3

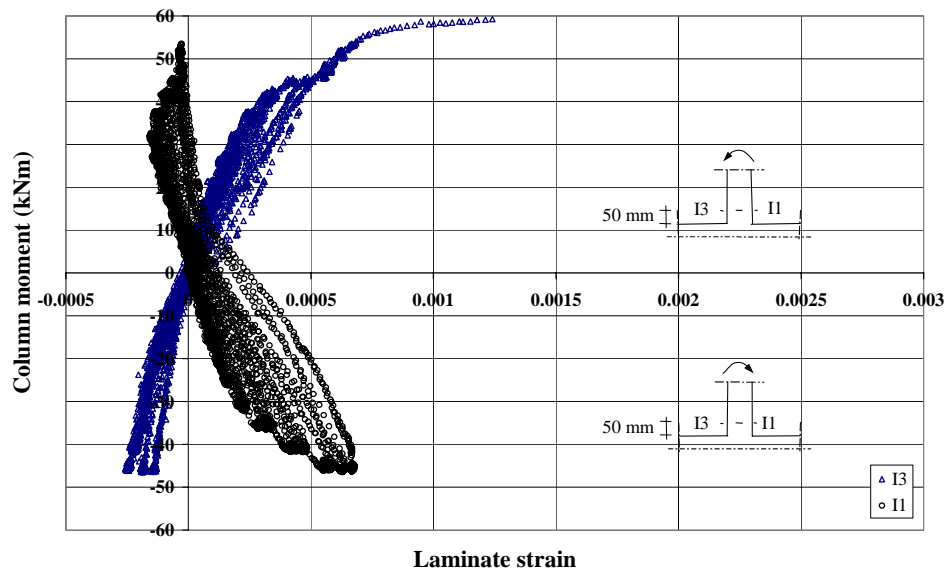


Figure C.32 Inferior column moment-laminate strain: M3

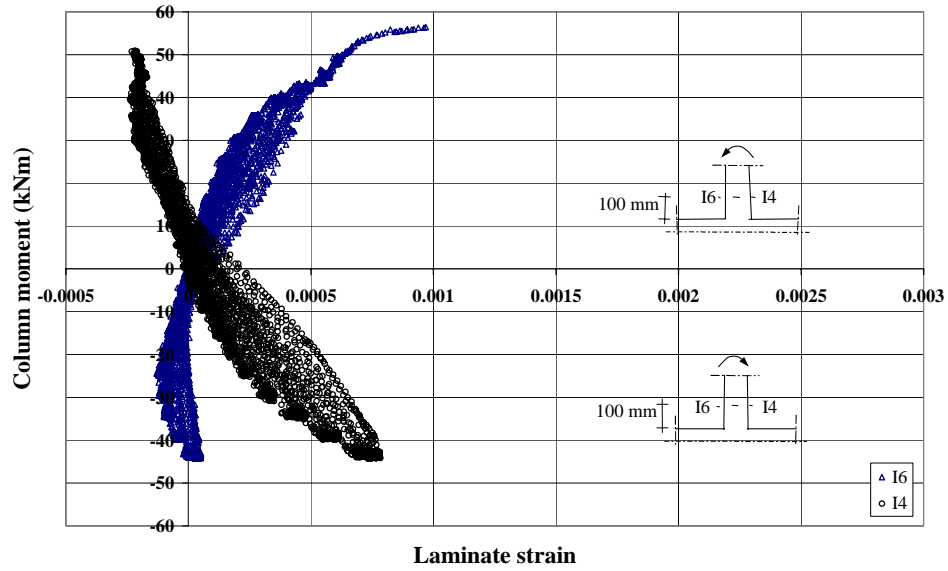


Figure C.33 Inferior column moment-laminate strain: M3

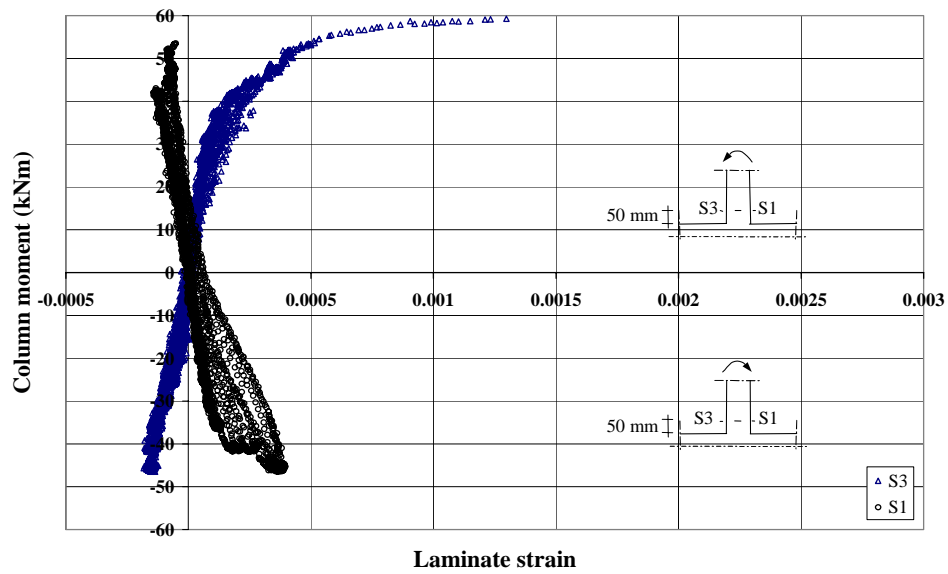


Figure C.34 Superior column moment-laminate strain: M3

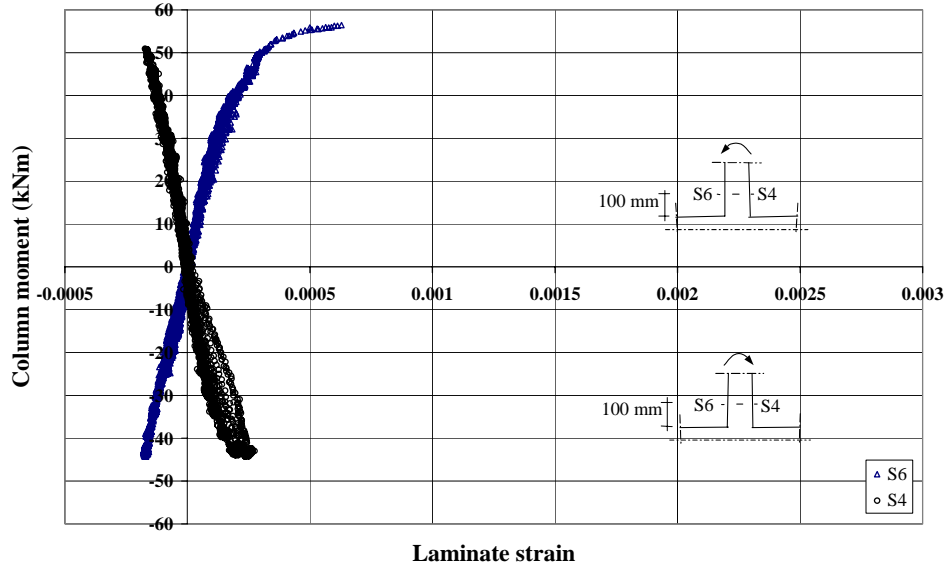


Figure C.35 Superior column moment-laminate strain: M3

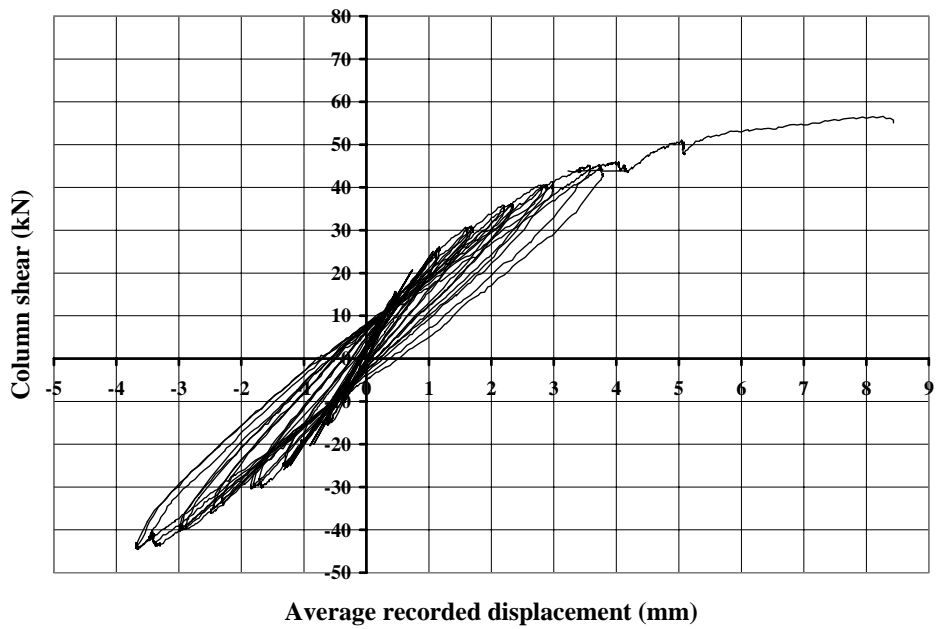


Figure C.36 Column shear-displacement: L4

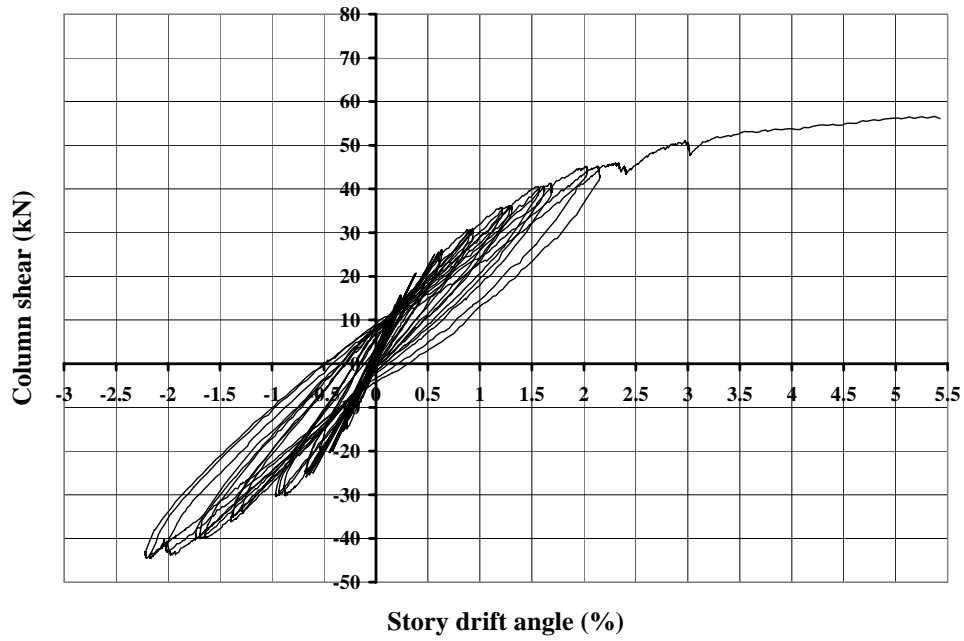


Figure C.37 Column shear-story drift: L4

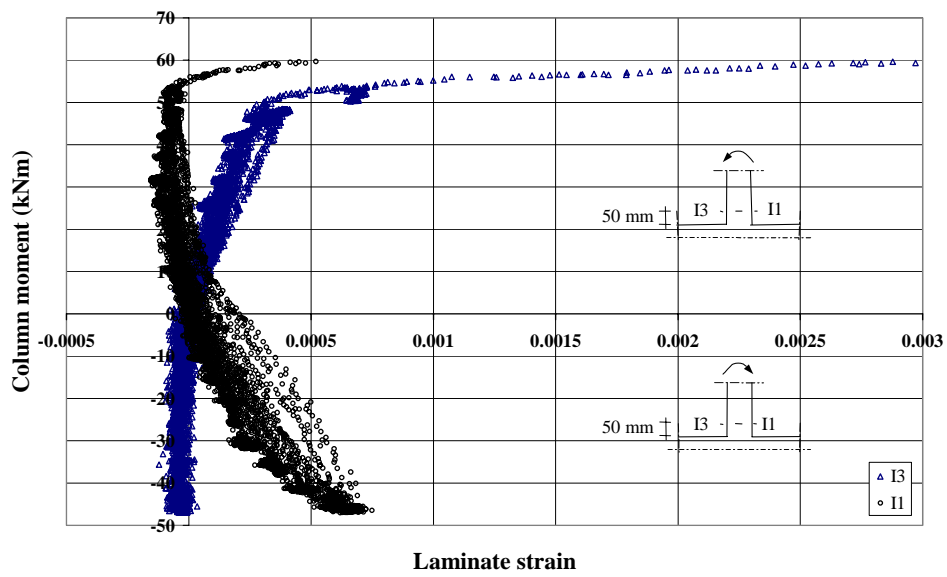


Figure C.38 Inferior column moment-laminate strain: L4

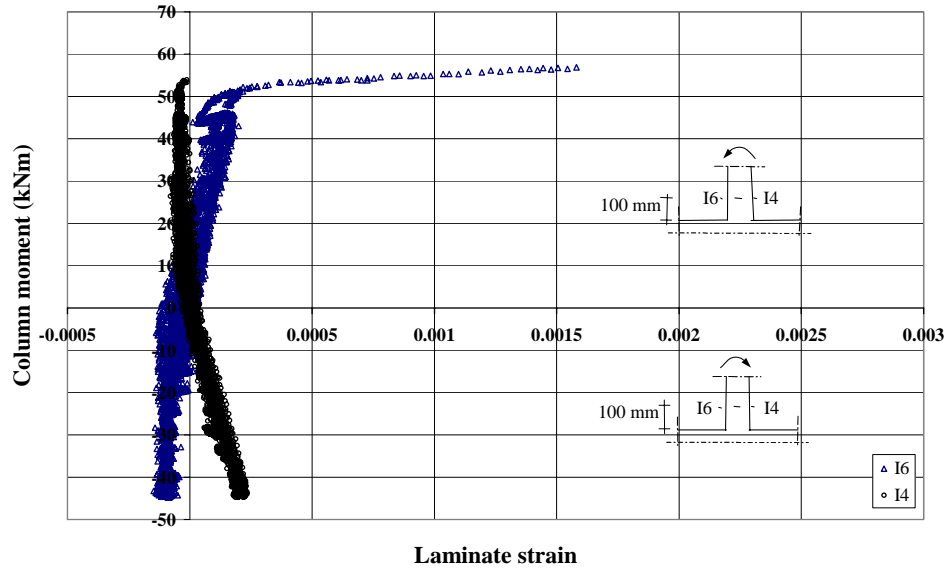


Figure C.39 Inferior column moment-laminate strain: L4

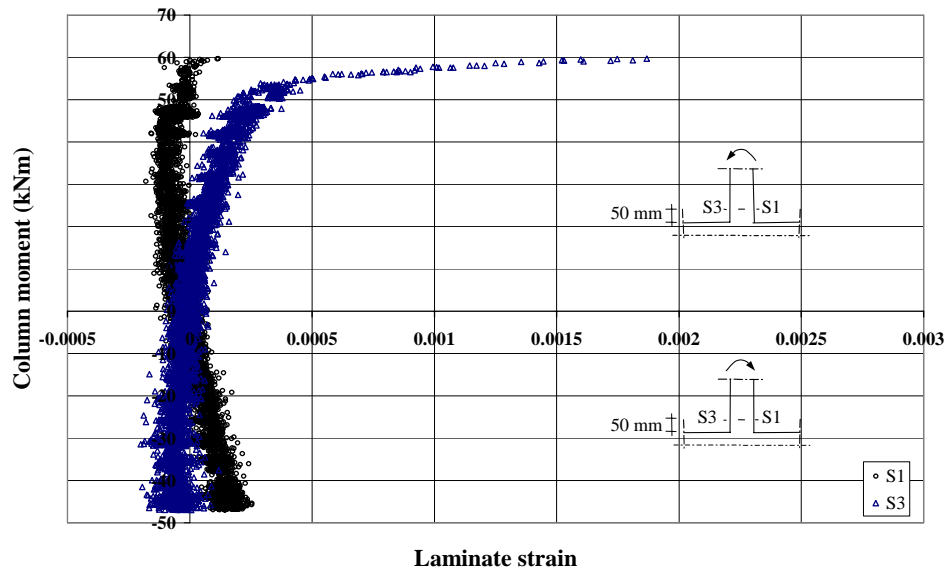


Figure C.40 Superior column moment-laminate strain: L4

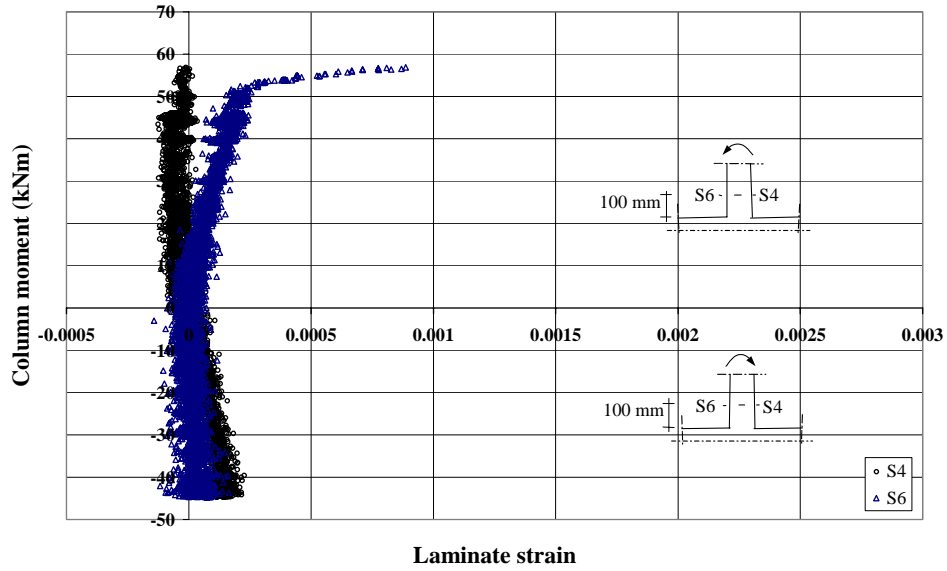


Figure C.41 Superior column moment-laminate strain: L4

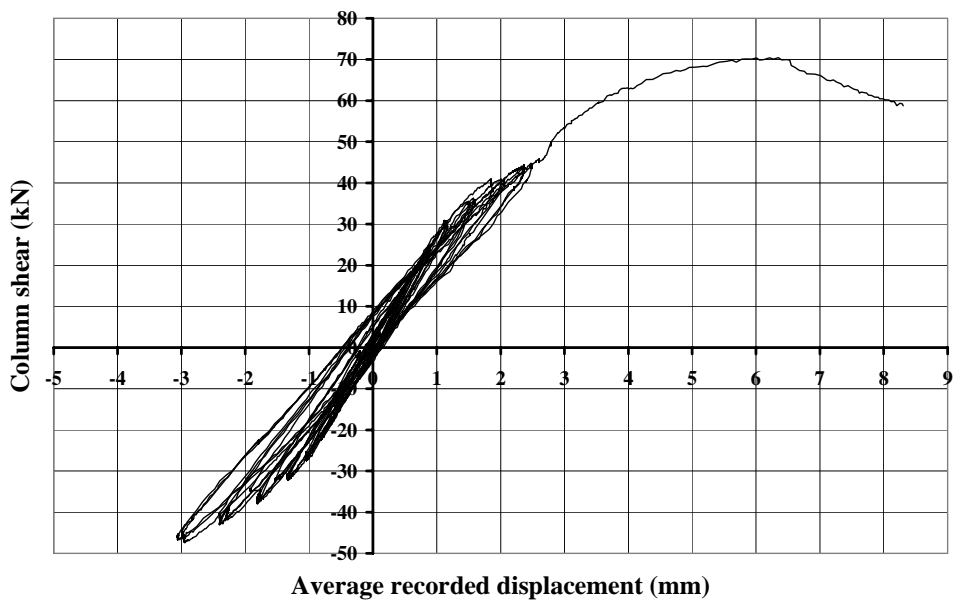


Figure C.42 Column shear-displacement: H4

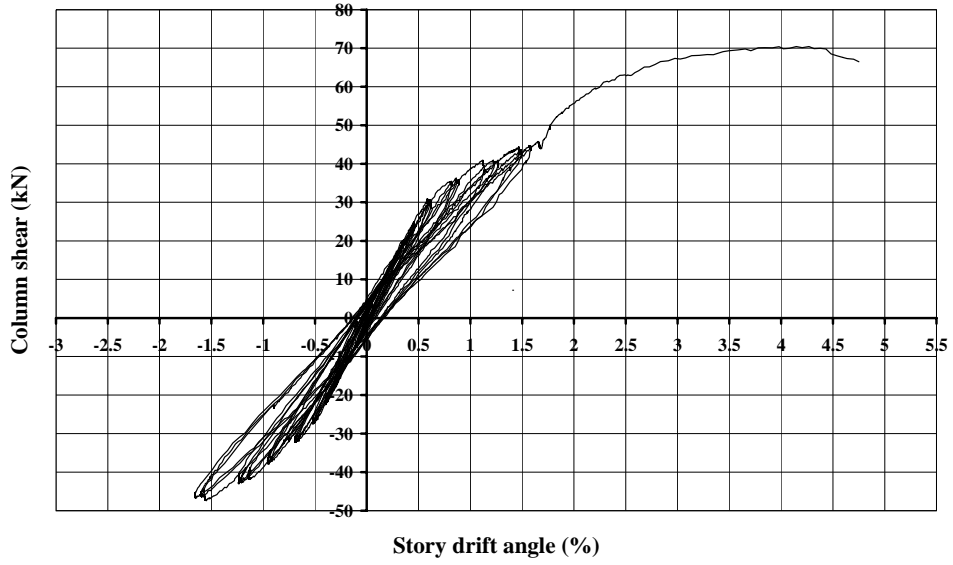


Figure C.43 Column shear-story drift: H4

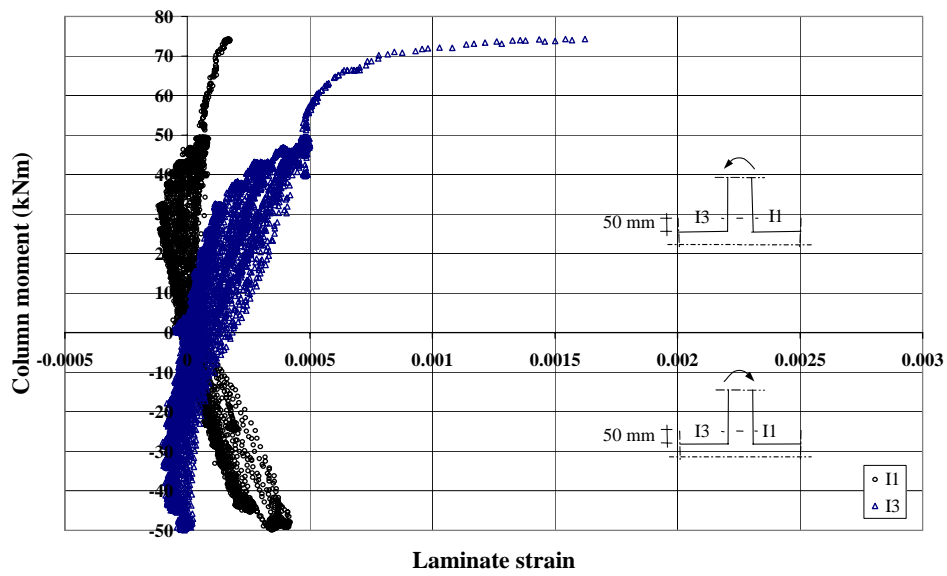


Figure C.44 Inferior column moment-laminate strain: H4

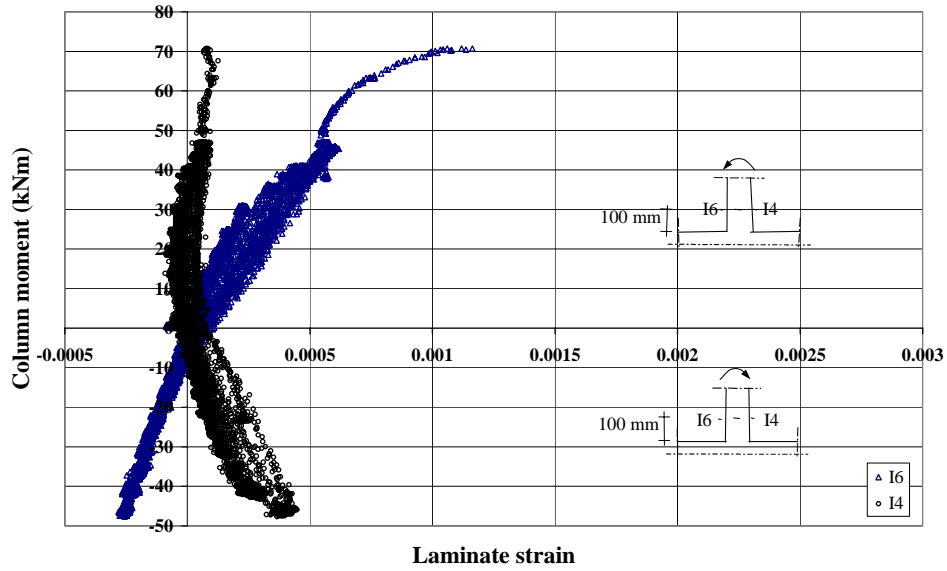


Figure C.45 Inferior column moment-laminate strain: H4

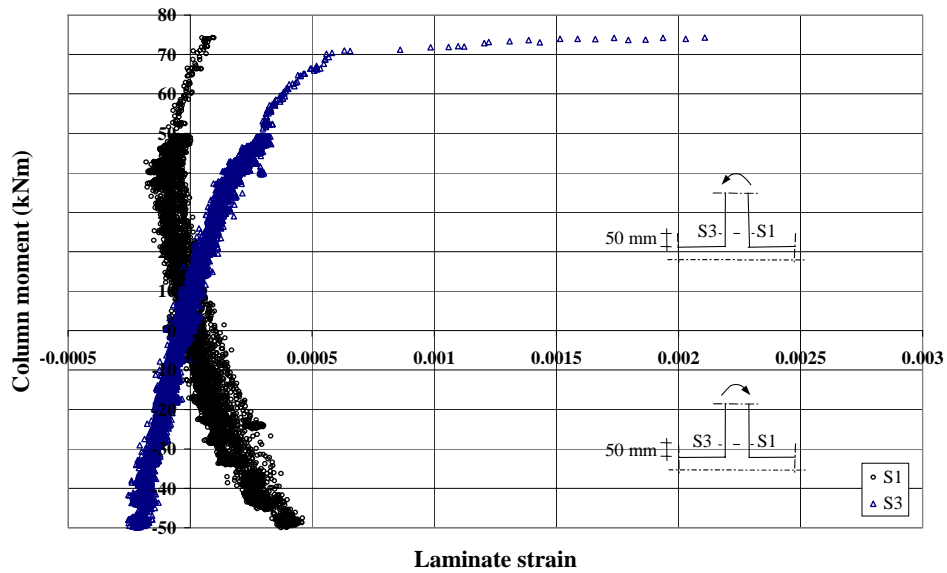


Figure C.46 Superior column moment-laminate strain: H4

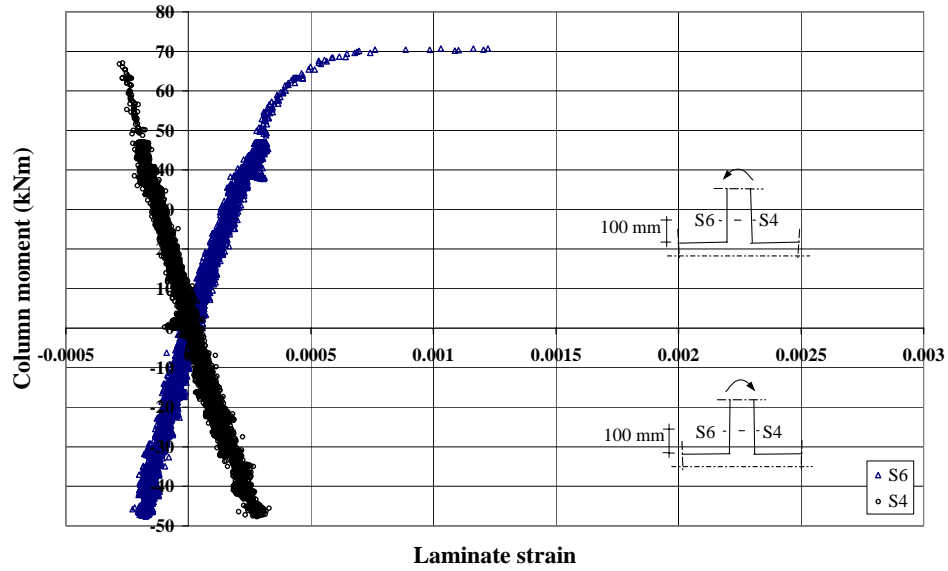


Figure C.47 Superior column moment-laminate strain: H4

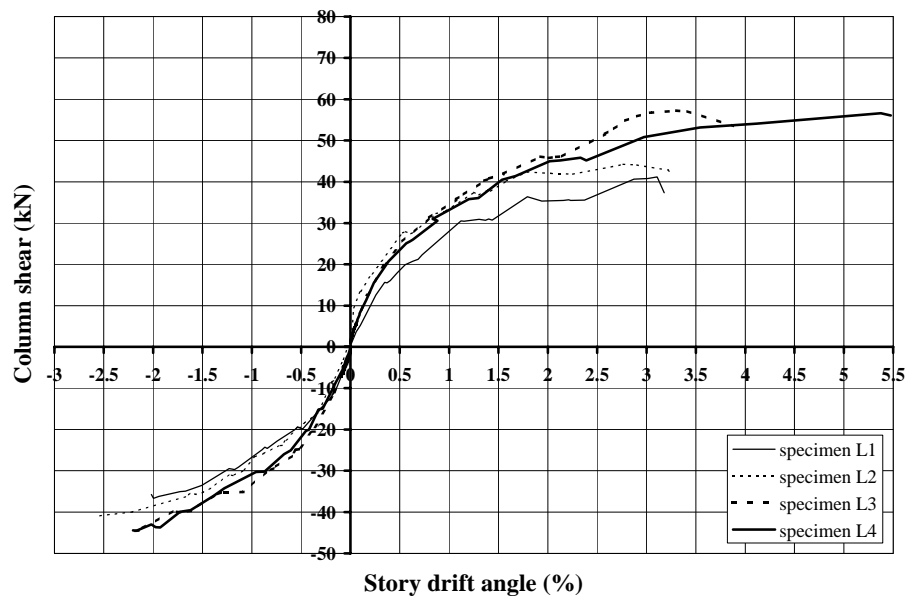


Figure C.48 Column shear-story drift: comparison for series L connections

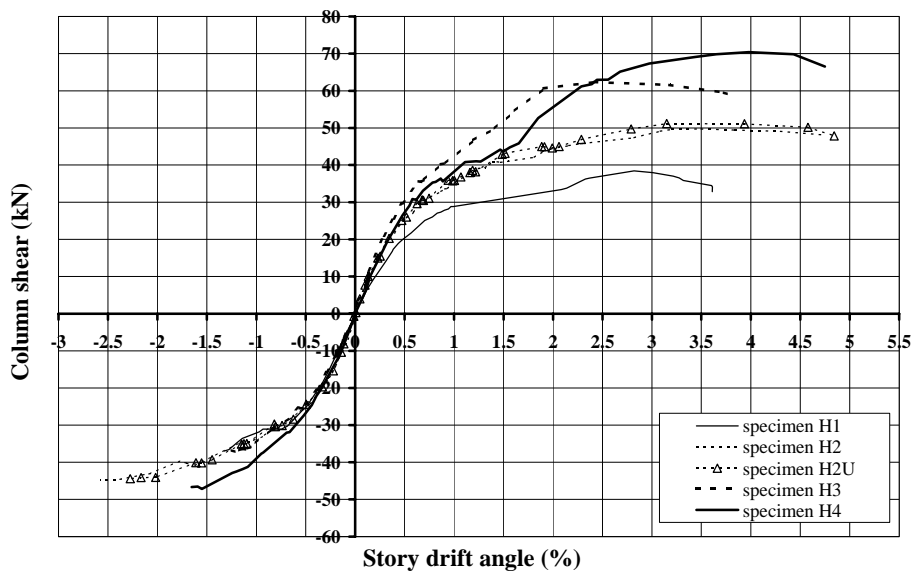


Figure C.49 Column shear-story drift: comparison for series H connections



Figure C.50 Column shear-story drift: comparison for type 1 connections

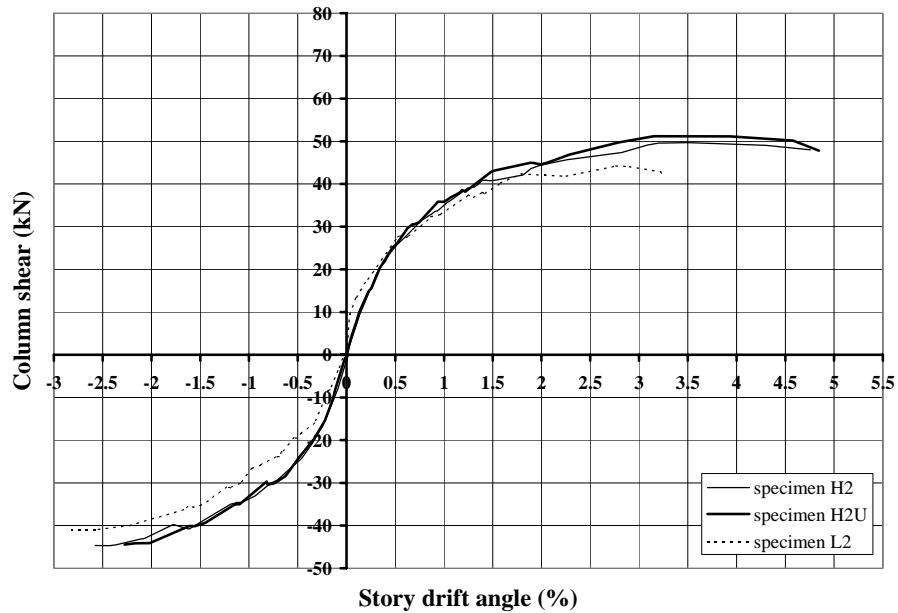


Figure C.51 Column shear-story drift: comparison for type 2 connections

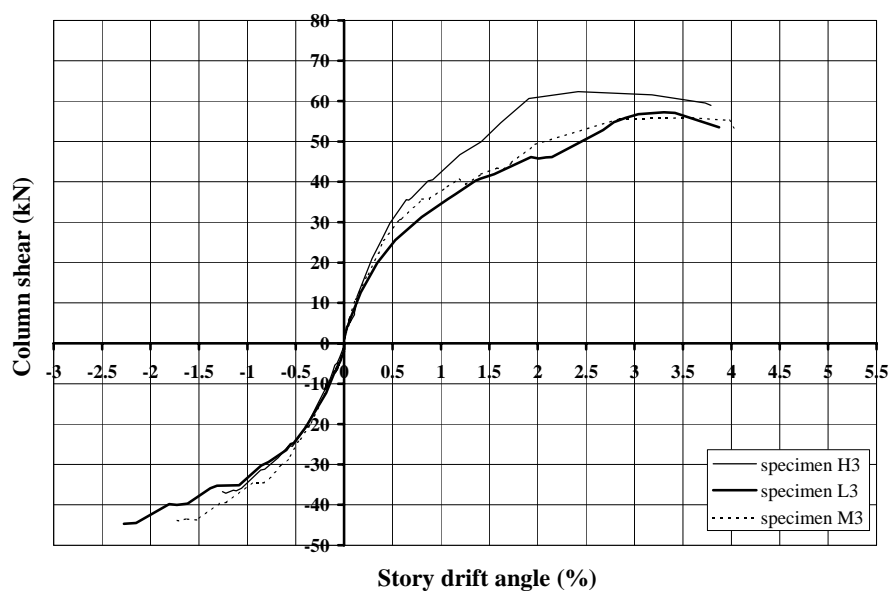


Figure C.52 Column shear-story drift: comparison for type 3 connections

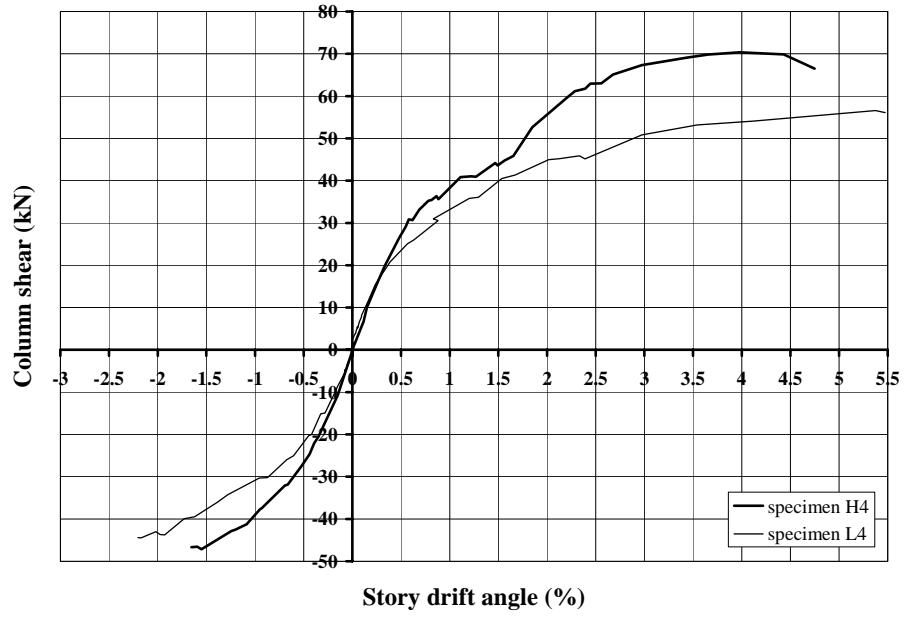
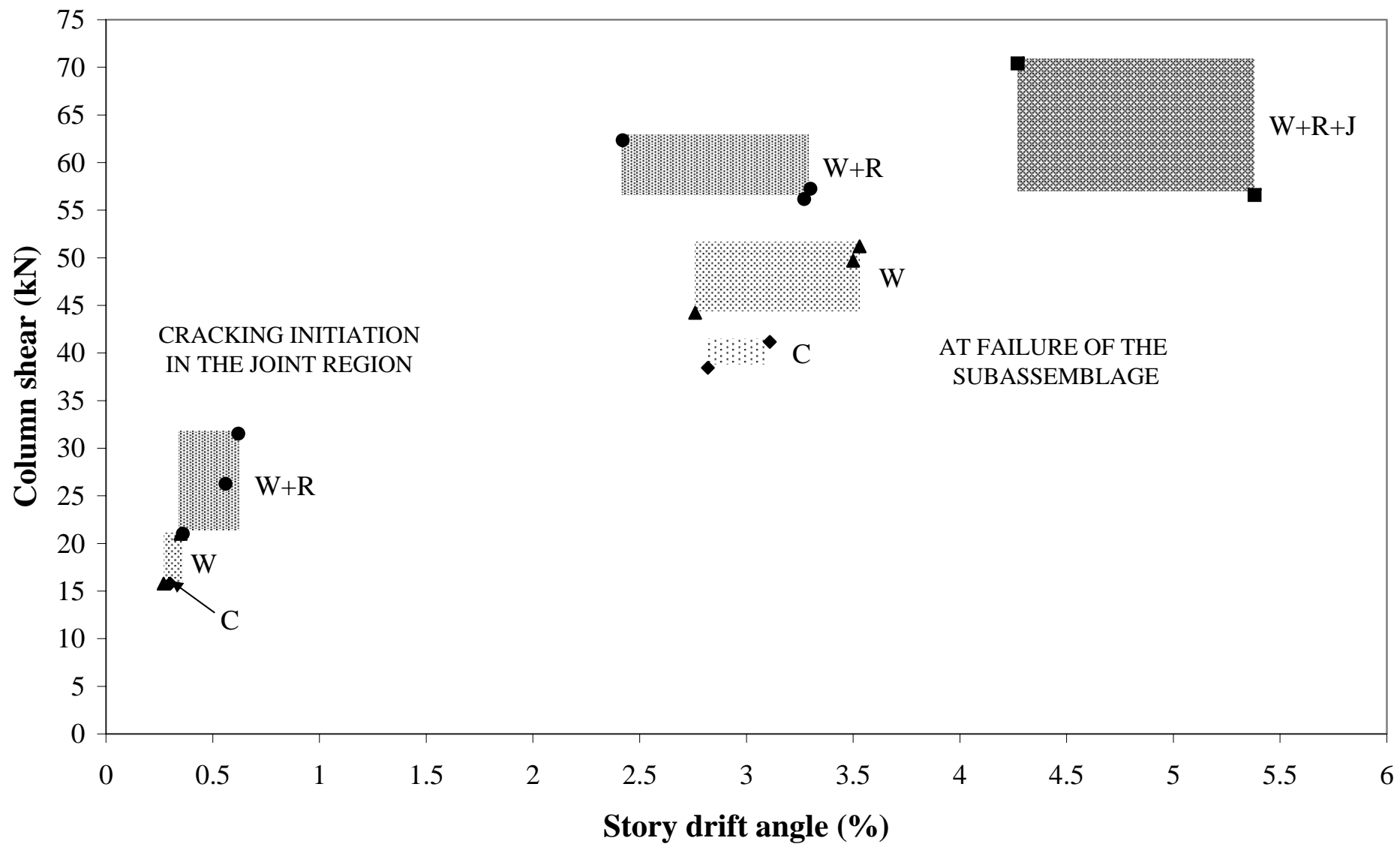
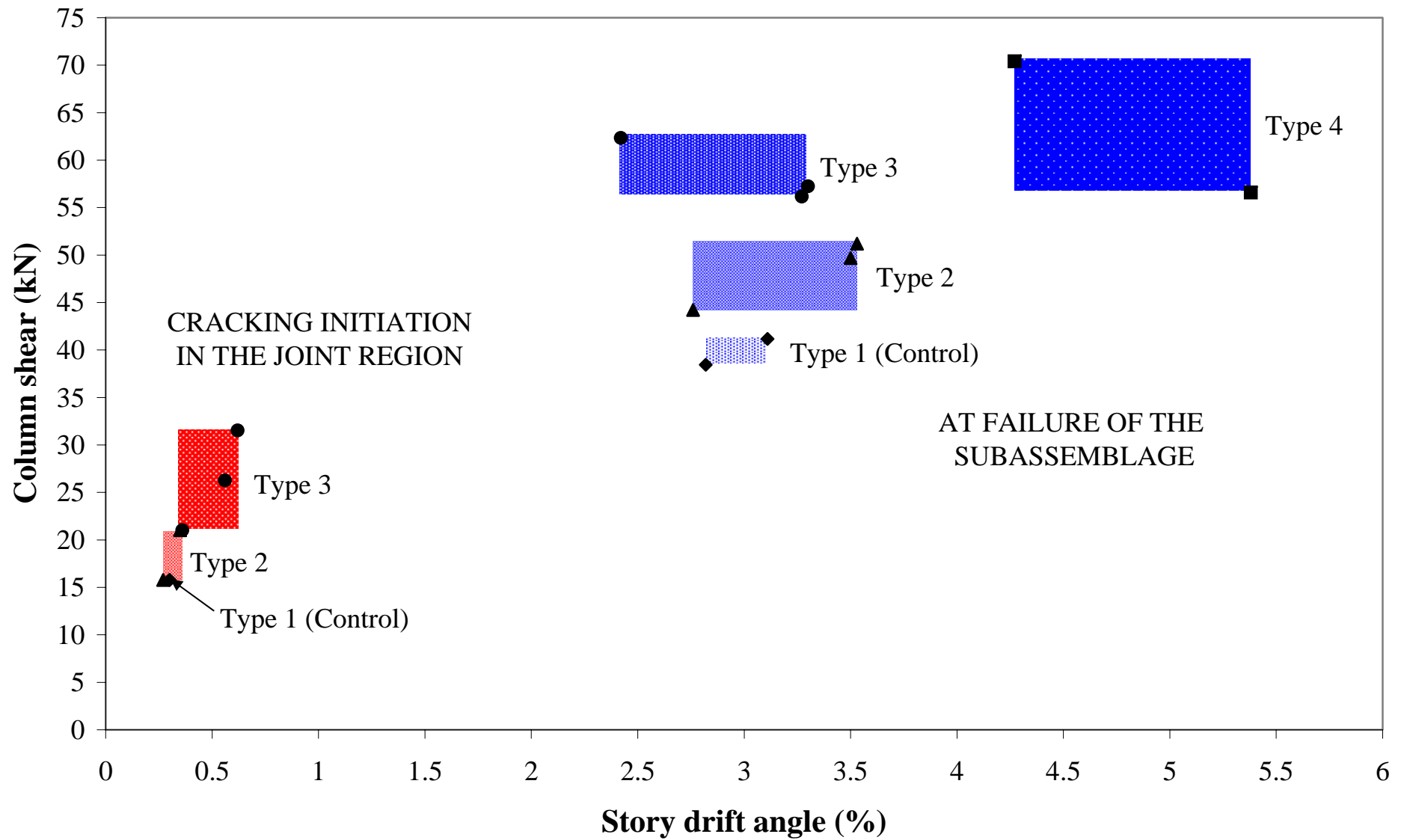


Figure C.53 Column shear-story drift: comparison for type 4 connections





7. REFERENCES

- ACI-ASCE Committee 352. (1985), "*Recommendations for Design of Beam-Column Joints in Monolithic Reinforced Concrete Structures*," ACI 352R-85, ACI Journal, V. 82, No. 3, 266-283.
- Alcocer, S.M. (1993), "*RC Frame Connections Rehabilitated by Jacketing*," Journal of Structural Engineering, V. 119, No. 5, 1413-1431.
- Alkhrdaji, T.; and Nanni, A. (2000), "*Flexural Strengthening of Bridge Piers Using FRP Composites*," ASCE Structures Congress 2000, Philadelphia, PA M. Elgaaly, Ed., May 8-10, CD version, #40492-046-008, 8 pp.
- American Concrete Institute ACI, Committee 318, (1963), "*Building Code Requirements for Reinforced Concrete*," American Concrete Institute, Detroit, Michigan.
- Antonopoulos, C.P.; Triantafillou, T.C.; and Papanicolau, C.G. (2001), "*Experimental Investigation of FRP-Strengthened RC Beam-Column Joints*," Proceedings of the Fifth International Conference on Fibre-Reinforced Plastics for Reinforced Concrete Structures, Cambridge, UK, 16-18 July 2001, 329-338.
- ATC40. (1996), "*Seismic Evaluation and Retrofit of Concrete Buildings*," California Seismic Safety Commission, Report SSC 96-01.
- Beres, A.; El-Borgi, S.; White, R.N.; and Gergely, P. (1992a), "*Experimental Results of Repaired and Retrofitted Beam-Column Joints Tests in Lightly Reinforced Concrete Frame Buildings*," Technical Report NCEER-92-0025, October.
- Beres, A.; Pessiki, S.P.; White, R.N.; and Gergely, P. (1996), "*Implications of Experiments on the Seismic Behavior of Gravity Load Designed RC Beam-to-Column Connections*," Earthquake Spectra, V. 12, No. 2, May.
- Beres, A.; White, R.N.; and Gergely, P. (1992b), "*Seismic Behavior of Reinforced Concrete Frame Structures with Nonductile Details: Part I – Summary of Experimental Findings of Full Scale Beam-Column Joint Tests*," Technical Report NCEER-92-0024, September.
- Bonacci, J.F.; and Wight, J.K. (1996), "*Displacement-Based Assessment of Reinforced Concrete Frames in Earthquake*," Mete A. Sozen Symposium, ACI publication SP 162, 117-133.

- Bracci, J.M.; Reinhorn, A.M.; and Mander, J.B. (1992), "*Evaluation of Seismic Retrofit of Reinforced Concrete Frame Structures: Part II – Experimental Performance and Analytical Study of a Retrofitted Structural Model*," Technical Report NCEER-92-0031, December.
- Calvi, G. M.; Magenes, G.; and Pampanin, S. (2001), "*Beam-Column Joint Damage and Collapse: Implications and Relevance in RC Frame Assessment*," Accepted for publication on Journal of Earthquake Engineering.
- Corazao, M.; and Durrani, A.J. (1989), "*Repair and Strengthening of Beam-to-Column Connections Subjected to Earthquake Loading*," Technical Report NCEER-89-0013, February.
- Cosenza, E.; and Manfredi, G.; (1997), "Some Remarks on the Evaluation and Strengthening of Underdesigned R.C. Frame Buildings," Technical Report, NCEER-97-0003 - State University of New York at Buffalo, 157-175.
- De Lorenzis, L. and Nanni, A. (2001), "*Bond between Near-Surface Mounted FRP Rods and Concrete in Structural Strengthening*," ACI Structural Journal, in press.
- Durrani, A. J.; and Wigth, J.K. (1985), "*Behavior of Interior Beam-to-Column Connections under Earthquake-Type Loading*," ACI Journal, 82-30, May-June, 343-349.
- FEMA 273 (1997), "*NEHRP Guidelines for the Seismic Rehabilitation of Buildings*," Prepared for the Building Seismic Safety Council (BSSC), Washington, D.C., US.
- Fu, J.; Chen, T.; Wang, Z.; and Bai, S. (2000), "*Effect of Axial Load Ratio on Seismic Behavior of Interior Beam-Column Joints*," Proceedings of the Twelfth World Conference on Earthquake Engineering, Auckland, New Zealand, January 30-February 4, 2000, Paper No. 2707.
- Ghobarah, A.; Aziz, T.S.; and Biddah, A. (1997), "*Rehabilitation of Reinforced Concrete Frame Connections using Corrugated Steel Jacketing*," ACI Structural Journal, V. 4, No. 3, May-June, 283-294.
- Hakuto, S.; Park, R.; and Tanaka, H. (2000), "*Seismic Load Tests on Interior and Exterior Beam-Column Joints with Substandard Reinforcing Details*," ACI Structural Journal, V. 97, No. 1, 11-25.
- Joh, O.; and Goto, Y. (2000), "*Beam-Column Joint Behavior after Beam Yielding in R/C Ductile Frames*," Proceedings of the Twelfth World Conference on Earthquake

- Engineering, Auckland, New Zealand, January 30-February 4, 2000, Paper No. 2196.
- Kamimura, T.; Takeda, S.; and Tochio, M. (2000), "*Influence of Joint Reinforcement on Strength and Deformation of Interior Beam-Column Subassemblages*," Proceedings of the Twelfth World Conference on Earthquake Engineering, Auckland, New Zealand, January 30-February 4, 2000, Paper No. 2267.
- Kupfer, B.H. and Gerstle K.H. (1973), "*Behavior of Concrete under Biaxial Stresses*," Journal of the Engineering Mechanics Division, V. 99, No. 4, 853-866.
- Micelli, F.; and Nanni, A. (2001), "*Mechanical Properties and Durability of CFRP Rods Galileo and Leonardo*," Center for Infrastructure Engineering Studies, University of Missouri-Rolla, Report No. 00-17, March.
- Murakami, H.; Fujii, S.; Ishiwata, Y.; and Morita, S. (2000), "*Shear Strength and Deformation Capacity of Interior R/C Beam-Column Joint Subassemblage*," Proceedings of the Twelfth World Conference on Earthquake Engineering, Auckland, New Zealand, January 30-February 4, 2000, Paper No. 679.
- Pampanin, S.; Calvi, G. M.; and Moratti, M. (2001), "*Seismic Response of Reinforced Concrete Beam-Column Joints Designed for Gravity Load*," Submitted for publication to ASCE Structural Journal.
- Pantelides, C.; Clyde, C.; and Reaveley, L.D. (2000a), "*Rehabilitation of R/C Building Joints with FRP Composites*," Proceedings of the Twelfth World Conference on Earthquake Engineering, Auckland, New Zealand, January 30-February 4, 2000, Paper No. 2306.
- Pantelides, C.; Gergely, J.; Reaveley, L.D.; and Volnyy, V. (2000b), "*Seismic Strengthening of Reinforced Concrete Bridge Pier with FRP Composites*," Proceedings of the Twelfth World Conference on Earthquake Engineering, Auckland, New Zealand, January 30-February 4, 2000, Paper No. 127.
- Park, R. (1994), "*Simulated Seismic Load Tests on Reinforced Concrete Elements and Structures*," Proceedings of the Tenth World Conference on Earthquake Engineering, 6681-6693.
- Paulay, T.; and Priestley, M.J.N. (1992), "*Seismic Design of Reinforced Concrete and Masonry Buildings*," John Wiley & Sons, Inc., New York, 744 pp.
- Priestley, M.J.N. (1997), "*Displacement-Based Seismic Assessment of Reinforced Concrete Buildings*," Journal of Earthquake Engineering, V. 1, No. 1, 157-192.

- Priestley, M.J.N.; Seible, F.; and Calvi, G.M. (1996), "Seismic Design and Retrofit of Bridges," John Wiley & Sons, Inc., New York, 686 pp.
- Raffaella, G.S.; and Wight, J.K. (1995), "*Reinforced Concrete Eccentric Beam-Column Connections Subjected to Earthquake-Type Loading*," ACI Structural Journal, V. 92, No. 1, 45-55.
- Rodriguez, M.; and Park, R. (1994), "*Seismic Load Tests on Reinforced Concrete Columns Strengthened by Jacketing*," ACI Structural Journal, V. 91, No. 2, March-April, 150-159.
- Saadatmanesh, H; Ehsani, M.R.; and Jin, L. (1997), "*Repair of Earthquake-Damaged RC Columns with FRP Wraps*," ACI Structural Journal, V. 94, No. 2, March –April.
- Stoppenhagen, D.R; Jirsa, J.O.; and Wyllie, L.A. (1995), "*Seismic Repair and Strengthening of a Severely Damaged Concrete Frame*," ACI Structural Journal, V. 92, No. 2, March –April.
- Sugano, S. (1997), "*State-of-the-art in Techniques for Rehabilitation of Buildings*," Proceedings of the Eleventh World Conference on Earthquake Engineering, Acapulco, Mexico, June 23-28, 1996, Paper No. 2175.
- Tabata, K.; and Nakachi, T. (1996), "*Repair of High-Strength Reinforced Concrete Beam-Column Joints*," Proceedings of the Eleventh World Conference on Earthquake Engineering, Acapulco, Mexico, June 23-28, 1996, Paper No. 1480.
- UNDP/UNIDO RER/79/015. (1983), "*Repair and Strengthening of Reinforced Concrete, Stone and Brick-Masonry Buildings*," United Nations Development Programme, Vienna, Austria.
- Wang, Y.C.; and Restrepo, J.I. (2001), "*Investigation of Concentrically Loaded Reinforced Concrete Columns Confined with Glass Fiber-Reinforced Polymer Jackets*," ACI Structural Journal, V. 98, No. 3, 377-385.
- Warner, J. (1994), "*Shotcrete in Seismic Repair and Retrofit*," ACI publication SP 160, 299-313.
- White, R.N.; and Mosalam, K. (1997), "*Seismic Evaluation and Rehabilitation of Concrete Buildings*", Technical Report, NCEER-97-0003 - State University of New York at Buffalo, 177-196.

Yang, X.; Nanni, A.; Haug, S.; and Sun, C.L. (2001), "*Strenght and Modulus Degradation of CFRP Laminates From Fiber Misalignment,*" accepted for publication in *Journal of Materials in Civil Engineering*.